

Georgios Maragkos<sup>1</sup>

Johan Anderson<sup>2</sup>

Tarek Beji<sup>1</sup>

David Lange<sup>2</sup>

Bart Merci<sup>1</sup>

Anders Lönnermark<sup>2</sup>

<sup>1</sup>Ghent University (UGENT)

<sup>2</sup>Technical Research Institute of Sweden (SP)

## Modelling of physics in cascading effects

Deliverable Number: D2.5

Date September 30, 2015

Due Date (according to  
Dow) September 30, 2015

Dissemination level PU

Grant Agreement No: 607665

Coordinator: Anders Lönnermark at SP Sveriges Tekniska  
Forskningsinstitut (SP Technical Research Institute of Sweden)

Project acronym: CascEff

Project title: Modelling of dependencies and cascading effects for  
emergency management in crisis situations

## Table of Contents

1	Introduction	8
1.1	Objective	8
1.2	Report outline	8
2	Physical modelling	10
2.1	Physical modelling approaches	10
2.1.1	Introduction	10
2.1.2	Computational Fluid Dynamics	10
2.1.3	Correlations / Simplified models	11
2.1.4	Choosing the right approach	12
2.2	Physical modelling of accidents	13
2.2.1	Fire modelling	13
2.2.2	Explosion modelling	13
2.2.3	Release modelling	14
3	Computational Fluid Dynamics	15
3.1	Governing equations	15
3.2	Turbulence modelling	15
3.3	Combustion modelling	16
3.4	Radiation modelling	16
3.5	Soot modelling	17
3.6	Pyrolysis modelling	17
3.7	Discretization	17
4	Scenario: Mont Blanc tunnel fire	18
4.1	Introduction	18
4.2	The accident	20
4.2.1	Description of the accident	20
4.2.2	Impacts due to the accident	24
4.2.3	Lessons learned from the accident	25
4.2.4	Possible fictitious scenario(s)	26
4.3	Modelling of the accident	27
4.4	Results	32
4.4.1	Heat release rate	32
4.4.2	Flame spread	33
4.4.3	Tenability criteria	33
4.4.4	Cascading effects	43
5	Scenario: Music festival	44
5.1	Introduction	44
5.2	The accident	44
5.2.1	Description of the accident	44
5.2.2	Impacts due to the accident	46
5.3	Modelling of the accident	46
5.4	Results	52
5.4.1	$\text{NO}_2$ dispersion	52
5.4.2	$\text{NH}_4\text{NO}_3$ aerosol	56
5.4.3	Fractional Effective Dose (FED)	59
5.4.4	Cascading effects	61



6	Scenario: Wildfire – Skatås forest fire	63
6.1	Introduction	63
6.2	Description of the initial system including more details on the initial event	64
6.3	Description of cascading effects, types of dependencies, systems involved after the spread from the initial system	65
6.4	Real consequences and possible consequences	66
6.5	Modelling of wildfires	66
6.6	WFDS model and input	67
6.7	Single burning tree model	68
6.8	A field of several burning trees	70
6.9	The wildfire scenario	72
6.10	Discussion	77
6.11	Cascading effects	78
7	Conclusions	79
8	References	81
Appendix 1: Types of accidents		85
A1.1	Introduction	85
A1.2	Accidents	86
A1.2.1	Fire accidents	86
A1.2.2	Explosion accidents	87
A1.2.3	Release accidents	87
A1.2	Cascading effects in accidents	88
Appendix 2: Correlations / simplified models		91
A2.1	Introduction	91
A2.2	Fire-related correlations	91
A2.2.1	Introduction	91
A2.2.2	Flame height	91
A2.2.3	Plume centerline temperature	92
A2.2.4	Radiant heat flux to a target	93
A2.2.5	Time to failure	95
A2.2.6	Ignition time of solid materials	95
A2.2.7	Pre-flashover temperature in an enclosure	97
A2.2.8	Prediction of flashover	98
A2.2.9	Post- flashover temperature	98
A2.2.10	Equivalent fire duration	99
A2.2.11	Smoke production rate	99
A2.2.12	Enclosure smoke filling	99
A2.2.13	Flame spread in forests	100
A2.3	Pollutant dispersion modelling	100
A2.3.1	Introduction	100
A2.3.2	Simple approach	101
A2.3.3	Gaussian dispersion model	101
A2.4	Explosion modelling	106
A2.4.1	Introduction	106
A2.4.2	Damage probability by an explosion	106
A2.4.3	Peak overpressure in an explosion	107
A2.4.4	BLEVEs	108
A2.5	Verification of correlations	109



A2.6      References      110



## Executive Summary

The objective of Task 2.5 is to investigate how computer modelling can be used as input to an Incident Evolution Tool (IET). In some situations the cascading effects depend on the physics and to fully understand the effect of incident management, also physical processes need to be modelled. Therefore, this task aims at modelling the necessary processes in order to support the simulated exercises in WP5 based on the physical effects identified in Task 2.3.

In total three scenarios are simulated within Task 2.5, two scenarios involved fire (Mont Blanc tunnel and wildland fire cases) and one scenario involved pollutant dispersion near a populated area. A detailed description of the numerical set-up used to model the scenarios is given and the results from the numerical simulations of the different test cases considered are analyzed. Based on the simulation results, valuable conclusions are drawn for each test case with regards to the viability of the use of numerical modelling as input for the IET to be developed within the project and for the simulated exercises to be performed within WP5.

An analysis of the level and complexity in which the modelling of physics in cascading effects can be included was also presented. In addition to the use of Computational Fluid Dynamics (CFD) also well known, experimentally derived, empirical correlations can serve as a valuable input to the IET to be developed or when dealing with a crisis management. Although the majority of this report focusses on the use of CFD for modelling of large scale incidents, an overview of analytical models which may be suitable in some instances is provided in Appendix 2. The (combined or not) applicability of these two different approaches has specific advantages and disadvantages which are discussed in the body of this report. Ultimately their use depends on the level of accuracy of the input required in the IET when trying to model the physics in cascading effects.

Based on the work which is reported herein, the authors conclude that the suitability of a physical modelling approach to study the different kinds of scenarios as input to the IET in CascEff is strongly dependent upon the desired level of accuracy and the time and computational resources which are available. For the three scenarios studied in detail in this report, computational methods were found to have varying applicability, largely dictated by the scale of the incident. Further, any modelling exercise will be limited by the computational capacity of the users and the size and complexity of the model which is being attempted, as evidenced by the wildfire scenario modelling reported. If the scope of the study is to have a rough estimate or outputted quantities in short time then the use of correlations or simplified models is as an attractive alternative which may yield suitably informative results.

The use of physical modelling (either simplified or CFD modelling) can provide a lot of valuable information to be used towards decision making during crisis situations and the study of cascading events. Generally, the use of physical modelling can be used in all three phases of a possible accident with cascading effects: beforehand, as a form of training exercise for prevention of future accidents; during, in order to provide valuable information about future events that might occur and help during the decision making process; and afterwards, with providing information about the consequences of the accident. It even allows first responders and other stakeholders the option to revisit the conditions and the evolution of the accident in order to learn lessons from it. During all three stages of an accident, physical modelling can play an important and valuable role during the planning, decision-making process and action phases.



# Nomenclature

## Acronyms

1D	One-dimensional
BLEVE	Boiling liquid expanding vapour explosion
CAM	Congestion Assessment Method
CFD	Computational Fluid Dynamics
CLICHE	Confined LInked CHamber Explosion
FED	Fractional Effective Dose
FDS	Fire Dynamics Simulator
FVM	Finite Volume Method
HGV	Heavy Goods Vehicle
LES	Large Eddy Simulation
RTE	Radiative Transfer Equation

## Roman symbols

A	Surface area ( $\text{m}^2$ )
A	Pre-exponential factor ( $\text{K}^{-1}\text{s}^{-1}$ )
C	Constant characteristic of the type of object being viewed through the smoke (-)
C	Volume fraction
$C_s$	Smagorinsky model constant
$C_v$	Modified Deardorff model constant
$E_A$	Activation energy (J/mol)
G	Total irradiance ( $\text{W}/\text{m}^3$ )
h	Sensible enthalpy (kJ/kg)
h	Height (m)
HV	Hyperventilation factor (-)
k	Kinetic energy ( $\text{m}^2/\text{s}^2$ )
k	Thermal conductivity ( $\text{W}/(\text{m}\cdot\text{K})$ )
K	Light extinction coefficient ( $\text{m}^{-1}$ )
$K_m$	Mass extinction coefficient ( $\text{m}^2/\text{kg}$ )
L	Flame height (m)
L	Load (kg)
m	Mass (kg)
$\dot{m}''$	Mass loss rate ( $\text{kg}/\text{m}^2$ )
N	Non-dimensional number
$N_s$	Number of chemical species
P	Total radiative power of the flame (kW)
P	Pressure (Pa)
p	Coefficient dependent upon the stability of the atmosphere
$\dot{q}'''$	Radiative source term ( $\text{kW}/\text{m}^3$ )
$\dot{Q}$	Total heat release rate (kW)
$\dot{Q}_E''$	External heat flux ( $\text{kW}/\text{m}^2$ )
$\dot{q}_r''$	Radiative heat flux ( $\text{kW}/\text{m}^2$ )
r	Distance (m)
R	Universal gas constant (8.314 J/mol·K)
s	Stoichiometric ratio
S	Strain rate ( $\text{s}^{-1}$ )
S	Visibility (m)
t	Time (s, min)
T	Temperature ( $^\circ\text{C}$ , K)



$T_s$	Activation temperature (K)
$u, v, w$	Velocity components (m/s)
$V$	Volume ( $m^3$ )
$W$	Weight (kg)
$Y$	Mass fraction (-)
$z$	Height (m)
$z_e$	Scaled distance ( $m/kg^{1/3}$ )

### Greek symbols

$\alpha$	Absorption coefficient
$\Delta$	Filter width (m)
$\Delta H_c$	Heat of combustion (kJ/kg)
$\mu$	Dynamic viscosity ( $kg/m \cdot s$ )
$\pi$	Pi number (3.14159)
$\rho$	Density ( $kg/m^3$ )
$\sigma$	Stefan-Boltzmann constant ( $5.67 \times 10^{-8} W m^{-2} K^{-4}$ )
$\tau$	Mixing time scale (s)
$\chi_r$	Radiative fraction (-)
$\dot{\omega}''$	Chemical source term ( $kg/m^3 s$ )

### Sub-scripts

0	Reference
chem	Chemical
conv	Convection
crit	Critical
d	Diffusion
eff	Effective
f	Fire
F	Fuel
fo	Flashover
g	Gravitational
k	Chemical specie
l	Layer
min	Minimum
O	Oxidizer
rms	Root mean square
s	Sensible
s	Soot
sgs	Sub-grid scale
t	Turbulent
th	Thermal
u	Advection
v	Vent

### Super-scripts

-	Time averaged quantity
$\sim$	Mass-weighted average quantity
T	Transpose

### Other symbols

$\nabla$	Divergence / Gradient operator
----------	--------------------------------



# 1 Introduction

The aim of the CascEff project is to improve our understanding of cascading effects [1] in crisis situations by identification of initiators, dependencies and key decision points. Within this framework, an Incident Evolution Tool will be developed capable of predicting past, present and future crisis evolution leading to cascading effects. An important aspect is the identification of human activities in crises, specifically in relation to emergency responder tactics and crisis communication. The developed Incident Evolution Tool will lead to improved incident management by providing an open methodology for understanding and modelling cascading effects in emerging accidents.

## 1.1 Objective

The objective of Task 2.5 is to investigate how computer modelling can be used as input to an incident evolution tool. In some situations the cascading effects depend on the physics and to fully understand the effect of incident management physical processes need to be modelled. Therefore, this task aims at modelling the necessary processes in order to:

1. evaluate the use of numerical models as possible input to the proposed IET; and
2. to provide information to allow the project consortium to perform and understand the simulated exercises in WP5 based on the physical effects identified in Task 2.3.

Examples of test cases to be simulated include: plume spread (originating from a chemical hazard or a large fire), fire development and spread, toxicity (evacuation modelling is included in WP3).

## 1.2 Report outline

This report is divided into the following chapters:

- In chapter 2, an introduction into physical modelling is presented. Additionally, some of the different methods of modelling the physics in cascading effects, the use of Computational Fluid Dynamics (CFD) and the use of correlations/simplified models are presented. The main advantages and disadvantages associated with each method are also reported.
- In chapter 3, a brief overview of the CFD code FDS, which is typically used for numerical simulations of fire-related applications and which can be used for pollutant dispersion scenarios is given. FDS version 6 is used for the numerical simulations in this report.
- In chapter 4, the first scenario considered, the Mont Blanc tunnel fire, is presented. A detailed description of the numerical set-up used to model the scenario is given and the results from the numerical simulations of the different test cases considered are analyzed.
- In chapter 5, the second scenario considered, the music festival, is presented. A detailed description of the numerical set-up used to model the scenario is given and the results from the numerical simulations of the different test cases considered are analyzed.
- In chapter 6, the third scenario considered, a wildland fire, is presented. A detailed description of the way the scenario is modelled is given and the results from the numerical simulations are analyzed.
- In chapter 7, the main conclusions of the report are presented.

In addition to the main body of the report, the report includes two appendices:

- In Appendix 1, with a classification of the different types of accidents often encountered in technological events is provided with specific reference to the process industries.



- In Appendix 2, a presentation of some of the available correlations and simplified models available in literature relevant for the modelling of physics in cascading effects of fire-related, pollutant dispersion and explosion scenarios is reported.



## 2 Physical modelling

### 2.1 Physical modelling approaches

#### 2.1.1 Introduction

The modelling of physical phenomena is an important topic in mechanical engineering and deals with the required steps necessary for translating a physical problem into a mathematical problem. There are different approaches of modelling the physics depending on the time available to solve a problem but also on the level of accuracy required. This can be particularly important in the case of modelling the physics in cascading effects where time can be an important aspect in the decision making process. The modelling of physics is here focused on fire-related applications and pollutant dispersion problems, two kinds of scenarios that are of great interest when studying cascading effects. Within this framework, two general methodologies for modelling the physics are available:

- Computational Fluid Dynamics (CFD)
- Correlations / Simplified models

It is important to note that the use of CFD is typically considered to be more accurate than the use of correlations or simplified models, however, it also generally more time consuming to use and requires greater knowledge about the specific case in question. Depending on the application and the level of accuracy needed the use of the one or the other can have advantages and disadvantages. There are also differences in how different types of models can be used in connection with an IET.

Whichever method for modeling the physics in cascading effects is selected, it should be well established the range over which it is valid, its limitations, the input information required, the valid results that can be obtained and the sensitivity of these results to the input information. All modelling approaches suffer from uncertainties that will have an impact on their output results. With a given set of input data (e.g. initial conditions, geometry, boundary conditions) it is unlikely that the output of the physical models will match exactly the result in reality with the same conditions.

#### 2.1.2 Computational Fluid Dynamics

Computational Fluid Dynamics (CFD) deals with the numerical solution of equations governing fluid flow and related problems in order to simulate these phenomena on a computer. The wide range of applicability of CFD in various disciplines has made its use appealing to engineers dealing everyday problems. In CFD, the space of study is divided into a large number of control volumes, named cells, ranging from a few thousands up to several millions, depending on the problem at study and the desired level of detail and accuracy that the engineer wants to achieve. In every cell, conservation laws of mass, momentum, chemical species and energy are solved, leading to a large set of coupled algebraic equations that are solved by appropriate numerical techniques. Such techniques involve the Reynolds-Averaged Navier Stokes (RANS) simulations, where only the mean quantities are solved, but also, the approach adopted in the current studies, the Large Eddy Simulations (LES), where only the large scale are resolved in the numerical simulations and the effect of the small scales is modelled. However, a detailed solution of the equations involved in each problem and geometry at study is not yet feasible with the current stage of computer technology and simplified models for e.g. combustion, turbulence, radiation, etc. have to be introduced. Typical CFD codes, often used for numerical simulations of various applications, include the Fire Dynamics Simulator (FDS), ANSYS Fluent, CFX, FLACS and FireFOAM.

The use of CFD has nowadays become an integral part of protection design and can provide a valuable insight towards trying to predict possible cascading effects in a crisis. The wide range of applicability of CFD models in areas such as e.g. fire modelling, design of smoke control systems, performance based design or structural fire engineering has made them a useful tool



and their use by research scientists and fire safety engineers has substantially increased over the last decades [2-3]. CFD models can be used not only to evaluate the effectiveness of current or future protection systems but also to answer “what if” questions and be used towards a cost-effective design without compromising safety.

Numerical simulations can be effectively used not only towards designing new scenarios involving cascading effects but also to study past events and evaluate the possible outcomes by altering various elements and key decision points involved in these scenarios. Within the wider context of the CascEff project, CFD could be used to help to elaborate and inform multiple timelines for scenarios as required within the IET. Of course the wide range of possible scenarios and the variation of each scenario itself could make such a database very large and time consuming to create. Additionally, the current stage of computer systems has not yet advanced to a stage where the use of CFD for real time simulation of an accident would be possible. Nevertheless, numerical simulations can be used in order to create a pre-run database containing a finite number of carefully planned and pre-defined scenarios that could involve cascading effects and would be helpful for training purposes and during crisis management situations. The models can also be used to understand the influence of different factors making it possible to increase the understanding of cascading effects.

Throughout the majority of this report we rely on CFD models to study 3 of the CascEff scenarios. The underlying physics to CFD modelling are discussed in more detail in chapter 3.

### **2.1.3 Correlations / Simplified models**

In cases or accidents where no prior information or detailed knowledge of the facility/area is known or some estimate of certain quantities is a prerequisite for crisis management then simple correlations can be used, instead of CFD models, and be applied in order to obtain a first approximation of the desired quantity. There is a wide range of correlations and simplified models reported in literature for a wide variety of applications. Such correlations and simplified models can give a rather rough but good first approximation of critical quantities in an accident and can provide the officers dealing with a crisis management with the required information in order to make key decisions.

Correlations and simplified models can be applied to predict the effects of accidents [4]; they consist of sets of equations describing the physical processes involved and can provide estimates of e.g. the thermal radiation and convective heating resulting from a fire, the peak overpressure from an explosion, the path followed and distance reached by ejected fragments or the evolution of a toxic gas concentration in the atmosphere. Their complexity varies significantly, ranging from simple models to models that are complex to use. Overly simplistic models are easy to use but often lead to significant errors in the predictions. In theory, complex models provide more accurate results but in practice they usually require the input of information that is not easily available.

Different models exist for modelling fires ranging from simple models that provide conservative results (e.g. the point source radiation model) to more complex models that provide relatively accurate predictions of fires and require a small amount of information but cannot produce very accurately the shape and size of flames (e.g. the solid flame radiation model). In accidents involving explosions of vessels, uncertainties arise from the lack of information about the energy available to create overpressure. The pressure inside the vessel before the explosion must be known, which cannot be easily predicted. Furthermore, the energy released by the explosion will also depend on the thermodynamic process responsible for the expansion of the gas. The atmospheric dispersion of toxic gases can be predicted with reasonable accuracy in the case of neutral or light substances. However, the dispersion of heavier than air gases is not yet sufficiently well studied and the existing models are relatively complex and reveal significant scattering in their predictions.



The use of physical modelling to predict accidents that could potentially lead to cascading effects should therefore be performed with caution. Reasonable assumptions must be applied and a certain safety margin must be taken into account considering that some excessively conservative approaches can lead to over-predictions of the effects and the potentially influenced areas of the accidents at study. In such cases, experience of physical modelling of accidents can play a significant role.

Within this framework, the use of such correlations and simplified models in the case of crisis management is not always straightforward and several prerequisites should be defined. Accurate application of such formulas and models, therefore, requires the following [5]:

1. Knowledge of the phenomena relevant to estimating the physical effects of an accident,
2. Knowledge of the models that have been developed to describe these phenomena,
3. Understanding of the general principles of the selection of these models, and the conditions under which these models can be applied,
4. Understanding of the procedure according to which the selected models should be applied.

A number of methodologies and software tools dealing with the assessment and/or analysis of cascading effects in industrial facilities are available in literature and an overview can be found in [6]. Although the focus of the application of these methods in this reference is industrial facilities, the models themselves are general and can be applied to many other cases.

A more detailed summary of some of the simpler analytical and empirical models is provided in Appendix 2. The remainder of this chapter focuses on a short discussion about selecting the most appropriate choice between simple and complex models for studying large scale incidents involving cascading effects.

#### **2.1.4 Choosing the right approach**

As previously described, there are different levels of modelling the physics in cascading effects depending on the desirable level of accuracy of the output. While simple models and correlations are easily applicable and the outputted result is immediate, there are still many cases of modelling scenarios involving cascading effects that will require CFD modelling. To decide which is the best approach to follow each time it is necessary to decide beforehand on:

- What is the scope of the study?
- What is the required depth of the study?
- How many scenarios will be modelled?
- Who will carry out the study?
- How much time is available?

If the scope of the study is a full investigation with great detail and accuracy of all possible cascading effects then the use CFD modelling is necessary. In this case, it will be possible to have distinct links between systems, accurate modelling of different originators but also to model the dependencies between different systems. If the scope of the study is to have a rough estimate or outputted quantities in short time then the use of correlations or simplified models is more appropriate and still acceptable.

The use of CFD modelling is, nowadays, a very valuable tool when dealing with many applications. It is important, however, to consider that CFD modelling requires significant experience and expertise in order to be used effectively. It is often the case that CFD specialists do not have the required level of expertise to model and importantly to validate models of all



possible scenarios encountered in everyday life. Therefore, depending on the scenario at hand, the CFD modelling and analysis should be assigned or consulted to CFD personnel with the required experience and expertise. It is important to remember, however, that all approaches of modelling the physics in cascading effects, whether with the use of simplified models and correlations or with CFD modelling, are inherently imperfect. The use of the different modelling approaches should be contained within their limits of applicability and with caution regarding their limitations.

## **2.2 Physical modelling of accidents**

The physical modelling approach of the different kinds of accidents will strongly depend upon the level of accuracy the user wants to achieve in the given timeline available. No universal approach exists which can be followed for every scenario at hand. The use of physical models can inherently provide a lot of valuable information to be used towards decision-making during crisis situations and the study of cascading events.

Generally, the use of physical modelling can be used in all three phases of a possible accident with cascading effects: beforehand, as a form of training exercise for prevention of future accidents, during, in order to provide valuable information about future events that might occur and help during the decision making process, and afterwards, with providing information about the consequences of the accident but also revisit the conditions and the evolution of the accident in order to learn lessons from it. In all three stages of an accident, physical modelling can play an important and valuable role during the planning, decision making process and action phases. The level of accuracy of the information required from the physical modelling will be a function of the modelling approach chosen. All the different physical modelling approaches can be useful and provide valuable information for the study of cascading effects. Depending on the conditions present, the type of accident and the actions that need to be performed the use of one approach or the other (or combination of both) can be equally appropriate.

A brief overview of the use of physical modelling using the examples of fire, explosion and release modelling is presented below. These three cases are typical examples of incidents where CFD modelling may be applied. They are typical in accidents in, for example, the process industries, and more discussion about them is provided in Appendix 1.

### **2.2.1 Fire modelling**

Modelling of fire accidents mainly deals with the determination of the thermal exposure from a fire (e.g. heat flux) to a target, and the determination of its effect on said target. Simple correlations exist in literature that can provide estimates of e.g. the heat flux from a fire source to target at a given distance and determine if these targets will be ignited by the incident heat flux. Simple formulas can further provide additional information about a fire accident such as e.g. the flame volume, the flame length and the time to ignition of different materials. However, in cases where complex geometries are present, there is a variety of materials with significantly different material properties and there can be strong interaction of the fire with its surrounding (e.g. enclosure fires with or without ventilation) then the use of CFD modelling will be more accurate and appropriate.

### **2.2.2 Explosion modelling**

The modelling of explosions can involve vapour cloud, condensed phase, dust and runaway explosions but also BLEVEs. Generally, simple approaches based on the “TNT equivalent” model have been applied in the past to model explosions, however, such models require the calculation of the explosive mass which is an output from e.g. the release modelling or hand calculations. This can often lead to uncertainties regarding the accuracy and validity of such methods. More accurate modelling of explosions can be made with the use of CFD models, which can couple the release of a substance in the atmosphere and the physics related to



explosions in a more coherent manner. Such approach, even though will be significantly more accurate, will nevertheless require more time for completion.

### 2.2.3 Release modelling

The modelling of release accidents typically deals with the determination of the rate at which the toxic substance is released (or the release of gases that could pose a risk for explosion) and the way it will be dispersed into the atmosphere due to e.g. an accident or a loss of container, together with the associated physical properties (e.g. temperature). Simple approaches of modelling such accidents assume the rate of discharge to be constant with time while more sophisticated models consider a time-dependent discharge rate. The latter approach, even though more complex, is inherently more appropriate for studying cascading effects since it can account for any possible event escalation. By considering a transient release rate of toxic substances, certain uncertainties in the modelling are avoided such as e.g. the constant rate approach can lead to over-prediction of the flammable/explosive mass in a vapour cloud.

In simple cases of gases released from a source where constant rate can be safely assumed simple formulas and simplified models exist to calculate the evolution of the toxic substances at a given downstream distance from the source. Nevertheless, if complex geometries are involved and the assumption of a constant release rate is not valid then the use of CFD modelling is more appropriate since the level of physics that can be included in numerical simulations of such accidents is higher.



### 3 Computational Fluid Dynamics

A well-known CFD code, often used for numerical simulations of fire-related applications or pollution dispersion scenarios is the Fire Dynamics Simulator (FDS) [7]. This code (version 6) has been used for the numerical simulations of the different scenarios presented in this report. In this chapter, the governing equations along with all the sub-models that were used for the numerical simulations with FDS are presented.

#### 3.1 Governing equations

FDS (<http://firemodels.github.io/fds-smv/>), developed by NIST, is a Large Eddy Simulation (LES) code written in Fortran. It is a second order accurate, finite difference code with explicit time marching that uses structured grids. The code solves for the low-Mach number form of the Navier–Stokes equations along with an equation for chemical species and energy. The ideal gas law couples temperature, density, and pressure, with the chemical species mass fraction being incorporated in the pressure term. For a detailed description of the equations and the approximations used in the FDS code, the reader can refer to [7]. The filtering process in LES introduces unclosed quantities that are not resolved, such as the sub-grid scale (sgs) stress terms, the sgs heat and mass flux, the combustion heat release rate, and the radiation loss that have to be modeled. The conservation equations for mass, momentum, chemical species and sensible enthalpy using Favre-filtered quantities (e.g.  $\tilde{\phi} = \overline{\rho\phi} / \bar{\rho}$ ) are then:

$$\text{Mass: } \frac{\partial \bar{\rho}}{\partial t} + \nabla \cdot (\bar{\rho} \tilde{u}) = 0 \quad (3.1)$$

$$\text{Momentum: } \frac{\partial(\bar{\rho}\tilde{u})}{\partial t} + \nabla \cdot (\bar{\rho}\tilde{u}\tilde{u}) = -\nabla \bar{p} + \nabla \cdot \left[ \mu_{\text{eff}} \left( \nabla \tilde{u} + (\nabla \tilde{u})^T - \frac{2}{3} (\nabla \cdot \tilde{u}) I \right) \right] + \bar{\rho}g \quad (3.2)$$

$$\text{Species: } \frac{\partial(\bar{\rho}\tilde{Y}_k)}{\partial t} + \nabla \cdot (\bar{\rho}\tilde{u}\tilde{Y}_k) = \nabla \cdot \left[ \bar{\rho} \left( D_k + \frac{\nu_{\text{sgs}}}{Sc_t} \right) \nabla \tilde{Y}_k \right] + \dot{\omega}''_k, \quad (k=1,...,N_s-1) \quad (3.3)$$

$$\text{Enthalpy: } \frac{\partial(\bar{\rho}\tilde{h}_s)}{\partial t} + \nabla \cdot (\bar{\rho}\tilde{u}\tilde{h}_s) = \frac{\bar{D}p}{Dt} + \nabla \cdot \left[ \bar{\rho} \left( D_{th} + \frac{\nu_{\text{sgs}}}{Pr_t} \right) \nabla \tilde{h}_s \right] - \nabla \cdot \bar{\dot{q}''}_r + \bar{\dot{q}'''}_c \quad (3.4)$$

where  $\bar{\rho}$  is the density,  $\tilde{u}$  is the velocity,  $\bar{p}$  is the pressure,  $\mu_{\text{eff}} = \mu + \mu_{\text{sgs}}$  is the effective dynamic viscosity,  $\mu$  is the laminar viscosity,  $\mu_{\text{sgs}} = \bar{\rho}\nu_{\text{sgs}}$  is the sub-grid scale viscosity,  $I$  is the identity tensor,  $g$  is the gravitational acceleration,  $\tilde{Y}_k$  is the species mass fraction,  $D_k$  is the species mass diffusivity,  $Sc_t$  is the turbulent Schmidt number,  $\dot{\omega}''_k$  is the species reaction rate,  $\tilde{h}_s$  is the sensible energy,  $D_{th}$  is the thermal diffusivity,  $Pr_t$  is the turbulent Prandtl number,  $\bar{\dot{q}''}_r$  is the radiative heat flux,  $\bar{\dot{q}'''}_c = \Delta H_c \bar{\omega}''_F$  is the heat release rate per unit volume due to combustion and  $\Delta H_c$  is the heat of combustion of the fuel.

#### 3.2 Turbulence modelling

Two different turbulent models are employed in the numerical simulations of the different scenarios presented in the report. First the well-known Smagorinsky model [8], originally developed for atmospheric flows, in which the sub-grid scale dynamic viscosity,  $\mu_{\text{sgs}}$ , is calculated based on the resolved strain rate as:



$$\mu_{sgs} = \bar{\rho}(c_s \Delta)^2 |\tilde{S}| \quad (3.5)$$

where  $c_s$  is a model constant,  $\Delta$  is the LES filter size (e.g. cubic root of the cell volume) and  $\tilde{S} = 0.5(\nabla \tilde{u} + \nabla \tilde{u}^T)$  is the strain rate tensor. The model constant  $c_s$  can be either constant or determined dynamically during the simulation. The constant formulation of the model was used to avoid any numerical instabilities often associated with the dynamic formulation due to the relatively coarse grids used in numerical simulations of complex or large-scale applications.

The modified Deardorff turbulence model [9] is the second model used. In this case, the sub-grid scale viscosity is calculated based on the sub-grid scale kinetic energy,  $k_{sgs}$ , and is calculated as:

$$\mu_{sgs} = \bar{\rho} C_v \Delta \sqrt{k_{sgs}} \quad (3.6)$$

### 3.3 Combustion modelling

The combustion model applied in FDS employs a one-step, infinitely fast, irreversible chemical reaction for chemical species, e.g. for n-heptane  $C_7H_{16}$ :



combined with a modified Eddy Dissipation Concept (EDC) model [10] to deal with turbulence-chemistry interactions. Within the EDC model the fuel mass re-action rate is calculated as:

$$\overline{\dot{\omega}''}_F = \bar{\rho} \frac{\min(\tilde{Y}_F, \tilde{Y}_{O_2} / r_s)}{\tau_{mix}} \quad (3.8)$$

where  $\tilde{Y}_F$  and  $\tilde{Y}_{O_2}$  are the fuel and oxygen mass fractions, respectively and  $r_s$  is the stoichiometric ratio. The  $\overline{\dot{\omega}''}_k$  for the others species are obtained through simple stoichiometric relations. The mixing time scale,  $\tau_{mix}$ , is calculated by comparing the chemical time scale with the mixing times for diffusion  $\Delta / D_F$ , where  $D_F$  is the fuel mass diffusivity), sub-grid scale advection ( $\Delta / \sqrt{2k_{sgs}}$ ) and buoyant acceleration ( $\sqrt{(2\Delta / g)}$ ). The sub-grid scale kinetic energy,  $k_{sgs}$ , is approximated based on scale similarity arguments as:

$$k_{sgs} = \frac{1}{2} \left[ (\bar{u} - \hat{u})^2 + (\bar{v} - \hat{v})^2 + (\bar{w} - \hat{w})^2 \right] \quad (3.9)$$

where  $\bar{u}, \bar{v}, \bar{w}$  are the average values of  $u, v, w$  in the cell centers and  $\hat{u}, \hat{v}, \hat{w}$  are the weighted averages of  $u, v, w$  in the adjacent cells.

### 3.4 Radiation modelling

A commonly used radiation model is adopted in this study in which the radiative intensity is treated as a function of both spatial location and angular direction and is obtained by solving the radiative transfer equation (RTE) by the finite volume discrete ordinates model (fvDOM) accounting for attenuation and augmentation of radiation by absorption and emission, respectively. Under the assumption of an optically thin flame, neglecting scattering, the radiative heat flux is then calculated as:

$$\nabla \cdot \overline{\dot{q}''}_r = \kappa_p (4\sigma T^4 - G) \quad (3.10)$$

where  $\kappa_p$  is the mean Planck absorption coefficient,  $\sigma$  is the Stefan-Boltzmann constant and  $G$  is the total irradiance. The mean Planck absorption coefficients for the chemical species are temperature-dependent and calculated by the RADCAL model [11]. However, in FDS the

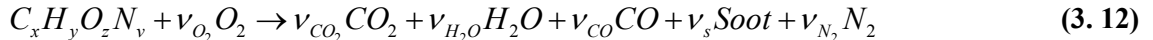


source term of the RTE is constrained in the flame region to a fraction of the total heat release rate per unit volume,  $\overline{\dot{q}''}$ , by specifying a radiative fraction,  $\chi_r$ , as:

$$\nabla \cdot \overline{\dot{q}''}_r = \chi_r \overline{\dot{q}''} \quad (3.11)$$

### 3.5 Soot modelling

A simple soot model was employed in the numerical simulations in which soot yield,  $y_s$ , is prescribed, specifying the amount of fuel that is converted into smoke particulate. This approach is adopted when simple chemistry is used in the numerical simulations with the chemical reaction to take the generic form:



### 3.6 Pyrolysis modelling

A one-dimensional, heat conduction equation is solved for temperature within a solid material which has the form:

$$\rho_s c_s \frac{\partial T_s}{\partial t} = \frac{\partial}{\partial x} \left( k_s \frac{\partial T_s}{\partial x} \right) + \dot{q}_s''' \quad (3.13)$$

where  $k_s$ ,  $\rho_s$ ,  $c_s$  are the heat conductivity, the density and the heat capacity of the solid material and the source term,  $\dot{q}_s''' = \dot{q}_{s,c}''' + \dot{q}_{s,r}'''$ , which consists of chemical reactions and radiative absorption. The term  $\dot{q}_{s,c}'''$  is effectively the heat production (loss) rate, calculated by the pyrolysis model, while the term  $\dot{q}_{s,r}'''$  describes the absorption and emission in depth or radiation.

The density of a solid material is then evolving in time according to a conservation equation in which the reaction rates (source term) are functions of the solid and gas phase conditions and are obtained as a combination of Arrhenius and power functions. For a more comprehensive and detailed presentation of the pyrolysis model used in FDS the reader is referred to [7].

### 3.7 Discretization

In FDS, the governing equations are advanced in time by using a second order explicit Runge–Kutta scheme. Spatial derivatives are estimated with second-order finite differences on a rectangular grid, with scalar quantities assigned to the cell center and velocities assigned to the cell faces. Convective terms are upwind biased, based on a Courant–Friedrichs–Lewy condition, in the predictor step and downwind biased in the corrector step. If the Courant number is near unity, this corresponds to a nearly fully upwind scheme, while for a Courant number much less than unity, the scheme is more centralized. This second-order finite differencing scheme of FDS cannot, however, fully resolve sharp gradients on a relatively coarse grid. Steep gradients can cause local over-shoots and under-shoots in quantities like density and species mass fraction. For this reason, a flux correction scheme is performed in both the predictor and corrector steps to ensure that the quantities stay bounded. The second-order TVD scheme, “SuperBee,” is used for scalar transport and the diffusive terms are central differenced. A fast Fourier transform-based solver solves the Poisson equation.



## 4 Scenario: Mont Blanc tunnel fire

### 4.1 Introduction

The Mont Blanc tunnel (Figure 4.1) is one of Europe's longest road tunnels, located underneath the Mont Blanc mountain in the Alps, connecting Chamonix of France and Courmayeur of Italy via European route E25. The tunnel is managed by two public companies (organizations), ATMB (Autorout et Tunnel du Mont Blanc) in France and SITMB (Societa Italiana del Trafono di Monte Bianco) in Italy, each responsible for approximately half of the tunnel length. The tunnel is used mainly for tourism and regional trade purposes by automobiles and Heavy Goods Vehicles (HGV) and is of one of the major trans-Alpine routes for transporting freight from Italy to northern Europe.



**Figure 4.1** Entrance of the Mont Blanc tunnel on the (a) French side and (b) Italian side.

The Mont Blanc tunnel is a single-bore, two-lane tunnel which is 11.6 kilometres long, 8.6 meters wide and 6.0 meters high, having a  $50 \text{ m}^2$  cross-section [12]. The entrance elevation on the French side is 1,274 m and 1,381 m in Italy, with a maximum of 1,395 m near the centre, a maximum difference of 121 m (Figure 4.2). At the point prior to the 1999 fire incident, the roadway slab and the ducts beneath were reinforced concrete structures, however, the 0.5 m thick tunnel lining was pure concrete without reinforcement. The horseshoe shaped profile of the tunnel has a 7 m wide roadway with two 0.8 walkways on each side and has a clearance of 4.5 m in height (Figure 4.3). Every 300 m, there are vehicle rest areas (Garages), 3.15 m wide by 30 m long, situated on alternating sides of the roadway and numbered from 1 to 36 in the France-Italy direction.

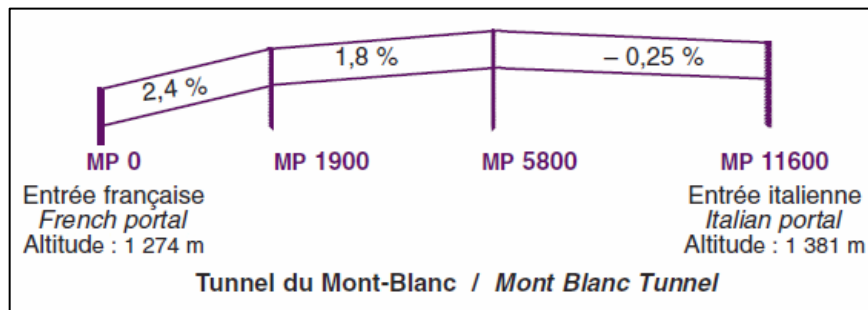


**Figure 4.2** Longitudinal profile of the Mont Blanc tunnel. Figure reproduced from [13].

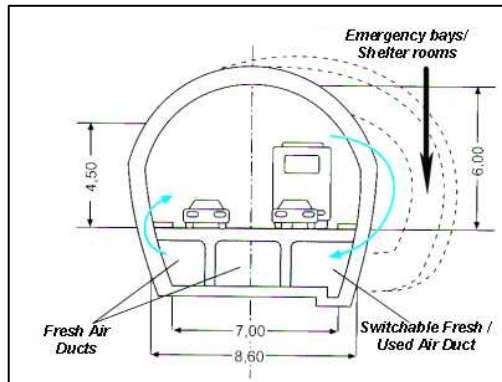


**Figure 4.3 Cross-sectional area of the Mont Blanc tunnel. Figure reproduced from [14].**

Four ducts supplying fresh air, starting at each of the portals, are positioned underneath the roadway. Each duct serves a quarter of the half length of the tunnel (1,450 m) by ventilation slots located every 10 m at the bottom of the lateral wall in the Italy-France direction, providing 75 m<sup>3</sup>/s of fresh air in the tunnel [12]. Consequently, a maximum of 300 m<sup>3</sup>/s of fresh air can be supplied from each portal or 600 m<sup>3</sup>/s in the entire tunnel. A fifth duct was originally built for removal of smoke, through openings positioned in the ceiling, with an extraction capacity of 150 m<sup>3</sup>/s. The exhaust duct was later modified to work as both a supplemental air supply duct and an exhaust duct. This enabled a total of 450 (300 + 100) m<sup>3</sup>/s of fresh air to be supplied from each portal or 900 m<sup>3</sup>/s to the entire tunnel. Additionally, in the French side, the exhaust duct was further modified to enable concentration of the exhaust capacity in any of the one-, two- or three-thirds of the half-length. On the Italian side, motorized dampers were built at each exhaust opening to focus the exhaust on any of the two to four openings. All these modifications resulted in a reduction of the tunnel's exhaust capacity. Approximately 65-85 m<sup>3</sup>/s of smoke could be extracted over a single third of the tunnel half on the French side and 70-90 m<sup>3</sup>/s by four openings on the Italian side instead of 150 m<sup>3</sup>/s for the whole half of the tunnel as was originally designed [15].

At its opening year in 1965 approximately 350,000 vehicles passed through the Mont Blanc tunnel. Already in 1980 the tunnel was used by 1.4 million vehicles per year and reached a high peak in 1998 with a traffic log of approximately 2 million vehicles. Following the 1999 fire accident, traffic levels a decade after the re-opening in 2002, had reached almost the same levels as before the accident. In 2013 the Mont Blanc tunnel had a traffic log of about 1.8 million vehicles (Table 4.1). This is five times more than during its first year of operation in 1965.

**Table 4.1 Evolution of traffic in the Mont Blanc tunnel.**

Year	Cars & Motorcycles	Coaches	Trucks	Total
1965	334,326	5,409	5,337	345,072
1970	605,978	10,364	138,176	754,518
1980	850,334	21,632	537,214	1,409,180
1990	1,117,635	30,903	746,523	1,895,061
1998	1,192,615	28,370	776,604	1,997,689
2003	1,126,912	12,597	274,327	1,413,836
2013	1,220,223	14,566	549,175	1,783,964

## 4.2 The accident

### 4.2.1 Description of the accident

On the morning of 24 March 1999 a Belgian HGV with a refrigerated trailer entered the tunnel from the French side. The truck had traveled several kilometers inside the tunnel when oncoming vehicles noticed the first signs of smoke coming out of the truck. The driver eventually stopped at kilometer 6.7 in the France-Italy direction and left his vehicle close to Garage 21 (Figure 4.4), which eventually caught fire. The fire quickly spread to the vehicles behind the truck. It is believed that the fast growth of the fire was due to the large fuel load of the HGV which included 550 liters of diesel in the truck's fuel tank, 9 tons of margarine, 12 tons of flour and the shell of the refrigerated trailer which was made of a combustible isothermal foam. At the time of the fire, there was a weak air flow [12] (1 to 1.5 m/s) in the Italy-France direction, forcing the smoke and flame spread mainly in the direction of the French entrance. As a result, many vehicles stopped behind the truck were trapped and caught in the fire. Fire fighters were dispatched at both ends of the tunnel in order to suppress and control the fire. However, the intense heat and smoke filled the entire tunnel section preventing emergency rescue and firefighting operations. The result was a mega fire, which burned for approximately 53 hours reaching temperatures of 1000 °C and resulted in 39 human casualties, mainly the drivers trapped in the tunnel during the fire. Most of the drivers stayed in or near their vehicles and those who tried to escape could manage to make only 100 - 500 m before collapsing due to smoke. This indicated that the smoke was very toxic. The CO content was reported to raise quickly over 150 ppm within minutes. In addition to the huge human loss, 23 HGV, 11 cars, 1 motorcycle and 2 fire engines were also destroyed [16], making the Mont Blanc tunnel fire one of the worst road tunnel accidents ever recorded (Table 4.2). All these vehicles were between the rest areas 19 and 23, over a distance of 1.2 km.

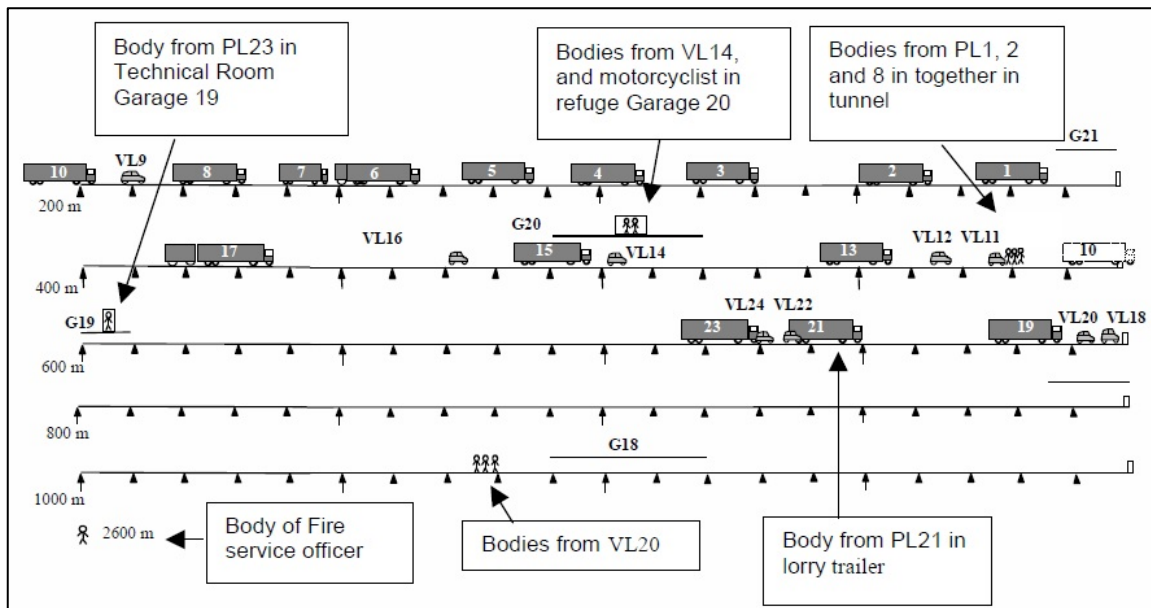


**Figure 4.4 Final locations of vehicles on the French side (distance from the burning HGV) and of decedents who left their vehicles. Locations are to scale, in 200-meter sections. Arrows are at 10 meters. Figure reproduced from [17].**

**Table 4.2 List of important road tunnel fires.**

Year	Tunnel	Country	Tunnel length (m)	Fire duration	People	Vehicles	Structure
1949	Holland	USA	2,550	4	66 injured	10 trucks, 13 cars	Serious
1978	Velsen	Nederland	770	1h 20min	5 dead, 5 injured	4 trucks, 2 cars	Serious
1979	Nihonzaka	Japan	2,045	159	7 dead, 2 injured	127 trucks, 46 cars	Serious
1982	Caldecott	USA	1,028	2h 40 min	7 dead, 2 injured	3 trucks, 1 bus, 4 cars	Serious
1983	Pecorila Galleria	Italy	662	-	9 dead, 22 injured	10 cars	Limited
1993	Serra Ripoli	Italy	442	2h 30 min	4 dead, 4 injured	5 trucks, 11 cars	Limited
1995	Pfander	Austria	6719	1h	3 dead, 4 injured	1 truck, 1 van, 1 car	Serious
1999	Mont Blanc	France/Italy	11,600	53h	39 dead	23 trucks, 11 cars, 1 motorcycle, 2 fire engines	Serious (closed for 3 years)
1999	Tauren	Austria	6,401	15h	12 dead, 49 injured	14 trucks, 26 cars	Serious (closed for 3 months)
2001	St. Gottard	Switzerland	16,900	Over 2 days	11 dead	2 trucks, 23 vehicles	Serious
2003	Baregg	Switzerland	1,390	-	2 dead, 21 injured	4 trucks, 3 fire engines	Serious
2006	Viamala	Switzerland	760	-	9 dead, 6 injured	1 bus, 2 cars	-



Based on the longitudinal air flow at the time of the fire (1 to 1.5 m/s) and on the assumption that no more than half of the oxygen from the air that passed the fire was burned, it was estimated that the maximum heat release rate from the fire was between 75 and 110 MW. Under these conditions, the fire duration of the HGV was estimated to be between 1.5 to 2 hours, having a calorific potential value of about 600 GJ. It was also reported that the air supply through duct no. 5 at the ceiling of Garage 21 did not have a significant impact on the fire, because it was upstream of the truck and had a flow of up to 10 m<sup>3</sup>/s, compared to 50-70 m<sup>3</sup>/s, brought in by the longitudinal air flow [12]. A more detailed presentation of the ventilation regimes inside the tunnel before and after the fire accident as well as a detailed chronology of the events that occurred during the tunnel fire is presented in Table 4.3 and Table 4.4, respectively. A full description and more details about the 1999 Mont Blanc tunnel fire are given in the public investigation report [12] of the accident.

**Table 4.3 Ventilation regimes before and after the alarm [18].**

Duct No.	French side			Italian side	
	Portal gallery	1-4	5	1-4	5
Before 10:55	Exhaust 2/4	Supply 2/4	Exhaust 2/4	Supply 2/3	Supply 1/3
After 10:55	Exhaust 4/4	Supply 4/4	Exhaust 3/4	Supply 3/3	Supply 3/3

**Table 4.4 Chronology of the 1999 Mont Blanc tunnel fire [18].**

Time	Time after alarm (min)	Chronology of the incident
10:46	-6	A truck stopped at French toll plaza.
10:52	0	An opacimeter in rest area 18 detected smoke from the HGV and raised alarm.
10:53	+1	The HGV stopped at the location 6500 m away from French portal. A French tunnel operator realized that a fire had happened.
10:54	+2	An Italian tunnel operator received a call from lay-by 22 (about 300 m away from the incident).
10:55	+3	The French and Italian regulators closed the toll. An ATMB agent enters the tunnel and is stopped shortly after rest area 18 (about 750 m from the originally-caught-fire truck).
10:57	+5	ATMB light fire engine entered the tunnel with 4 men from French portal. There was an alarm from lay-by 21 (use of a fire alarm push button).
10:57 ~ 11:01	+5 ~ +9	The employees of Italian toll companies entered the tunnel.
10:58	+6	There was an alarm showing the lifting of a fire extinguisher from rest area 21. The French tunnel control centre alerted the public rescue services.
10:59	+7	ATMB rescue vehicle with 2 men entered the tunnel from French portal.
11:02	+10	The fire rescue vehicle of Chamonix left its base. The Italian tunnel control centre alerted the Courmayeur (Italian) fire brigade.
11:04	+12	The first Italian firefighting vehicle of Courmayeur left its station.
11:05	+13	A French patrolman came within some 10m of the HGV on fire from Italian portal.
11:08	+16	ATMB light fire engine could not advance further after 5400 m due to



		smoke. They went into shelter located at lay-by 17 (5100 m away from the French portal).
11:09	+17	ATMB rescue vehicle was blocked by the smoke after 5100 m. They went into the shelter located at lay-by 17.
11:10	+18	The first high power fire engine on Chamonix (French) reached the tunnel portal.
11:11	+19	The first Italian fire engine entered the tunnel.
11:16	+24	The Italian firemen were stopped by smoke at lay0-by 22 (about 300 m away from the incident). They had to retreat to lay-by 24 (900 m away from the vehicle) with another 2 Italian firemen and wait rescuers for about 3 hours.
11:15 – 11:18	+23-26	The French fire engine was stopped by dense smoke at 3700 m of the French portal. The firefighter had to escape to lay-by 12 (3600 m away from the French portal) and wait for rescuers for 5 hours.
11:32 – 11:36	+40-44	A second French fire engine entered the tunnel to rescue trapped French firemen. However, rescuers failed to reach lay-by 12 and were forced to stay at lay-by 5 (1500 m from the French portal).
12:55	+2h 3	A rescue operation started from the French side.
13:04	+2h 12	The Specialized Rescue Plan for the tunnel was activated on the French side.
About 14:16	+3h 24	5 Italian firefighters were evacuated through the ventilation duct.
15:00	+4h 8	The 5 Italian firefighters were evacuated.
18:35	+7h 43	All the trapped fire and rescue teams from the French side were rescued.
	+53 h	The fire was extinguished.

It has been estimated that the total energy released in the accident was in the order of 5000-7000 GJ with a peak heat release rate of 380 MW [19]. The tunnel remained closed for 3 years undergoing repair and safety improvement works, after the severe infrastructure damages it had sustained due to the fire (Figure 4.5), only to re-open in 2002. A series of additional fire protection systems (see Table 4.5) were included in the refurbished Mont Blanc tunnel in order to improve its fire safety.



Figure 4.5 Aftermath of the Mont Blanc tunnel fire (1999).

**Table 4.5 Fire protection systems in the Mont Blanc tunnel before and after its refurbishment [20].**

At time of fire (1999)	After refurbishment (2002)
Safety niches every 100 m containing a fire pull-box and two fire extinguishers.	Fire-resistant stainless steel cladding fitted to walls.
Fire niches every 150 m with water supply for firefighting.	Concrete-lined pressurised emergency shelters every 300 m (37 in total), fitted with fire doors and connected to a safety corridor parallel to the tunnel.
Alarm and fire detection system.	A total of 116 smoke extractors every 100 m.
Pressurised safe refuge or emergency shelter every 600 m with 2h fire rating (18 in total) without a safety.	Heat sensors at both ends of the tunnel to detect overheated trucks before they enter the tunnel.
Outdated ventilation system with ducts underneath the roadway and limited smoke extraction capacity.	Three command and control centres; the newly added central centre has a round the clock firefighting team.
Two command and control centres at both ends with a firefighting team at the French entrance.	More traffic lights and flashing warning signs.
Traffic signals every 1.2 km.	

#### 4.2.2 Impacts due to the accident

Accidents in tunnels have typically limited possibilities of evacuation that constitutes a special risk, especially if it is combined with the risk of explosion of dangerous goods [21]. The consequences of such incidents can be severe in terms of victims, damage to the structure and impact on the transport economy. The 1999 Mont Blanc tunnel fire resulted both in human casualties and long-term economic and social disruptions due to its ensuing closure for 3 years that impacted an area with a radius of over 300 km in central Europe from a traffic congestion point of view [22].

The 1999 Mont Blanc tunnel fire accident is a historic event and presents an interesting and challenging case for simulation within the CascEff project framework for several reasons:

- It is a *historic* and *international event* (France and Italy) with *cross-border effects* (traffic congestion due to the tunnel's closure).
- There were two *interdependent key decision points*, mostly at operational level, that had to be taken regarding the ventilation and the evacuation of the tunnel.
- It resulted in *severe impacts* (both short-term and long-term).

A brief overview of the impacts caused by the Mont Blanc tunnel fire is presented below:

1. **Technical:** Damages in the tunnel infrastructure, material losses, legal costs and liabilities). The cost for repairing and renovating the Mont Blanc tunnel was approximately 350 million euros [23].
2. **Organizational:** The fire accident resulted in a closer collaboration of ATMB and SITMB and the introduction of a third control and command centre.
3. **Social:** 39 deaths. Increased traffic congestion due to the tunnel's closing for 3 years.
4. **Economic:** The estimates of the effects on the local Italian economy around the area of the Mont Blanc Tunnel were estimated at €1.75 billion [24].
5. **Environmental:** High pollution levels in the valley surrounding the Mont Blanc tunnel.

Strictly speaking these aspects (e.g. cross-border effects, key decision points, interdependency and severe impacts), this historic scenario, does not fully comply with all the requirements



defined within the CascEff project regarding cascading effects such as the interdependency between several systems. Therefore, the proposed Mont Blanc tunnel fire scenario will serve as a basis for the development of fictitious scenario(s) involving interdependency between multiple systems in which cascading effects will be more clearly studied. The simulation of the base scenario, however, is still considered very valuable within the framework of the CascEff project because of its significance and the severe consequences associated with it.

#### **4.2.3 Lessons learned from the accident**

From the various tunnel accidents that have occurred in the past, valuable information has been collected and presented in the reports of the PIARC Committee on Road Tunnels. These reports not only present statistics of breakdowns, accidents and fires in tunnels, but also guidelines related to the geometric design of tunnels, the fire safety equipment and operating procedures needed by engineers and decision-makers involved in tunnel design and operation [25].

The severity of the Mont Blanc tunnel fire (1999), along with the fires in the Tauern (1999) and St. Gotthard (2001) tunnels, has increased the awareness of the possible impact of accidents in tunnel. Even though the possibility of such tunnel fires to escalate into major events is low, they still are considered severe due to the impact in human lives, infrastructure damages and economy.

After the official investigation of the Mont Blanc tunnel fire, it was concluded that the fatal consequences could had been greatly reduced by [25]:

- A more efficient organisation of operational and emergency services (harmonised, safer and more efficient emergency procedures, specifically for cross-border operation)
- More skilled personnel
- More effective safety systems
- Greater awareness among users (car and truck drivers) on how to behave in emergency situations

It was concluded that the a serious HGV fire in the Mont Blanc tunnel could lead to different consequences, depending on the [26]:

- Fire rescue and the actions of the tunnel users
- Ventilation system capacities
- Ventilation system operation

In order for the ventilation network of the tunnel to work in an efficient way, the tunnel operators must locate the fire precisely and as soon as possible after an accident has occurred. It has been calculated that the response of the fire rescue forces during the Mont Blanc tunnel fire was in the order of 15 min. This means that the safety of the people trapped within the tunnel in the first stages of the fire development mostly dependents on their ability to self-evacuate and the selection of the appropriate ventilation conditions during this early stage of the fire is of great importance. It is, therefore, important not only to educate tunnel users on optimising their ability to self-evacuate, but also to have such a fire safety procedure in the early stages of a fire that the ventilation conditions will both aid the tunnel users to evacuate and the fire rescue services to reach the fire source [26].



#### **4.2.4 Possible fictitious scenario(s)**

Using the historic accident of the Mont Blanc tunnel fire as a base, various fictitious scenario(s) can be developed and simulated where the influence of cascading effects will be more profound and the initial event will propagate into a chain of events affecting more than one systems.

- **Fictitious scenario 1: Tunnel fire involving dangerous goods**

Starting from one of the previously described basic scenario (e.g. Scenario 1), different HGV's can be considered which carry dangerous goods, e.g. explosive substances (Class 1), toxic substances (Class 6.1) and/or radioactive material (Class 7). A HGV vehicle carrying one of the aforementioned dangerous goods is waiting to enter the Mont Blanc tunnel from the French side where there is big traffic congestion. Upon its entrance in the tunnel (within 50-100 m), the driver notices heavy smoke coming out of his engine and stops the HGV in the middle of the road. Tunnel operators didn't notice the incident immediately allowing a few more vehicles to enter the tunnel where they stop behind the HGV. Within minutes there is a fire burning the HGV (similar to the real Mont Blanc tunnel accident) that quickly spreads from one vehicle to another. There is a release of toxic and radioactive materials within the tunnel and in the atmosphere where wind is blowing them towards the city of Chamonix. In addition, as the fire spreads from one vehicle to another (fire has spread outside the tunnel entrance) the radiation emitted from the flame and the direction of wind are such that a fire in the Mont Blanc mountain starts and spreads towards the city of Chamonix.

Starting from the initial event (fire of the HGV inside the tunnel) there is a chain of events (fire spread from one vehicle to another) with increasing severity which propagates into a first system, the small forest above the Mont Blanc tunnel entrance (fire spread results in forest fire) which now affects a third system, the town of Chamonix which needs to be evacuated (evacuation due to fire and toxic-radioactive danger).

- **Fictitious scenario 2: Tunnel fire within a city**

A similar tunnel in dimensions as the one taken for the base scenario (e.g. Scenario 1) can be considered within a populated area (e.g. underground tunnel within a city) which will involve a fire in a HGV carrying dangerous goods. Fire will again spread from one vehicle to another, releasing of a toxic cloud towards the centre of the city that will endanger the health being of the inhabitants, resulting in the evacuation of a big part of the city.

The initial event (fire of the HGV inside the tunnel) causes a chain of events (fire spread from one vehicle to another) with increasing severity that propagates into another system, the city center that needs to be evacuated (evacuation due to toxic-radioactive danger).



### 4.3 Modelling of the accident

The Mont Blanc tunnel fire can serve as a basis of a computational fluid dynamics (CFD) study in which several scenarios of accidental fires in a tunnel can be performed. A sensitivity study on a wide range of parameters can be conducted in order to examine their influence in the fire development within the tunnel but also on the safety of the people trapped within it. Such fire scenarios can include variations in the tunnel dimensions, initial fire source, ventilation conditions, number of trapped vehicles, etc. All scenarios will involve coupled physical processes, such as combustion and radiation in the gas phase and pyrolysis in the solid phase, that have to be modeled in order to accurately perform the CFD study.

The current investigation of the Mont Blanc tunnel fire proposes the numerical simulation of a given length of the tunnel that includes the main burning area of the accident (around Garage 21). Within this main burning area, the initial fire source (burning HGV) will be modelled in order to study the flame spread from one vehicle to another but also the evolution of smoke and the consequences on the evacuation of the people trapped within the tunnel. A sensitivity analysis will be made on the ventilation conditions within the tunnel (Table 4.6), starting from 1 m/s that was reported at the place where the fire started [12] to 2-4 m/s and even 0 m/s (no ventilation) in order to examine its influence on flame spread and evacuation. All scenarios are simulated for 1 hour of real time.

**Table 4.6 Base scenarios to be simulated based on the Mont Blanc tunnel fire (1999).**

Scenario	Ventilation velocity (Italy – France direction) (m/s)
Scenario 1	0
Scenario 2	1
Scenario 3	2
Scenario 4	4

It is suggested that the following hazardous criteria are adopted in order to determine whether the conditions inside the tunnel are safe for the occupants to evacuate [27]:

- Gas temperatures  $\leq 60^{\circ}\text{C}$ .
- Radiative fluxes  $\leq 2 \text{ kW/m}^2$ .
- Visibility  $\geq 10 \text{ m}$ .
- Fractional Effective Dose index (FED) [28], a commonly used measure of human incapacitation due to the combustion gases,  $< 1$ .

An estimate of the visibility,  $S$ , within the tunnel in the numerical simulations is given as [29]:

$$S = C / K \quad (4.1)$$

where  $C$  is a non-dimensional constant dependent on the type of object being viewed through the smoke;  $C = 8$  for light-emitting signs [30], and  $K$  is the light extinction coefficient. The light extinction coefficient,  $K$ , depends on the soot concentration and a fuel-dependent mass specific extinction coefficient,  $K_m$ , and is calculated as  $K = K_m \rho Y_s$  with  $K_m = 8700 \text{ m}^2 / \text{kg}$ .

The Fractional Effective Dose (FED) is calculated as [29]:

$$FED_{total} = FED_{CO} \times HV_{CO_2} + FED_{O_2} \quad (4.2)$$

The FED dose of CO is calculated as:



$$FED_{CO} = \int_0^t 2.764 \times 10^{-5} (C_{CO}(t))^{1.036} dt \quad (4.3)$$

where  $t$  is time (min) and  $C_{CO}$  is the CO concentration (ppm).

The hyperventilation factor caused by carbon dioxide is calculated as:

$$HV_{CO_2} = \frac{\exp(0.1903C_{CO_2}(t) + 2.0004)}{7.1} \quad (4.4)$$

where  $t$  is time (min) and  $C_{CO_2}$  is the CO<sub>2</sub> concentration (percent).

The fraction of an incapacitating dose of O<sub>2</sub> hypoxia is calculated as:

$$FED_{O_2} = \int_0^t \frac{dt}{\exp[8.13 - 0.54(20.9 - C_{O_2}(t))] \quad (4.5)}$$

where  $t$  is time (min) and  $C_{O_2}$  is the O<sub>2</sub> concentration (volume percent).

In the modelling of the accident, the actual dimensions of the Mont Blanc tunnel are considered but with a reduced tunnel length of 900 m (red box in Figure 4.6). This length covers the main burning area around the HGV that caught fire and is sufficient in order to study the evacuation of the people trapped in their vehicles and the flame spread that occurred from one vehicle to another. In addition, 50 m on each side of the tunnel are considered for outflow. A longitudinal velocity of 1 m/s is considered in the numerical simulation in the Italy – France direction. The initial lower vents, placed every 10 m within the tunnel, are modelled as a continuous vent set to blow air at a total of 40 m<sup>3</sup>/s while the vitiated ducts above Garages 20 - 22 to bring fresh air at a rate of 10 m<sup>3</sup>/s each [12].

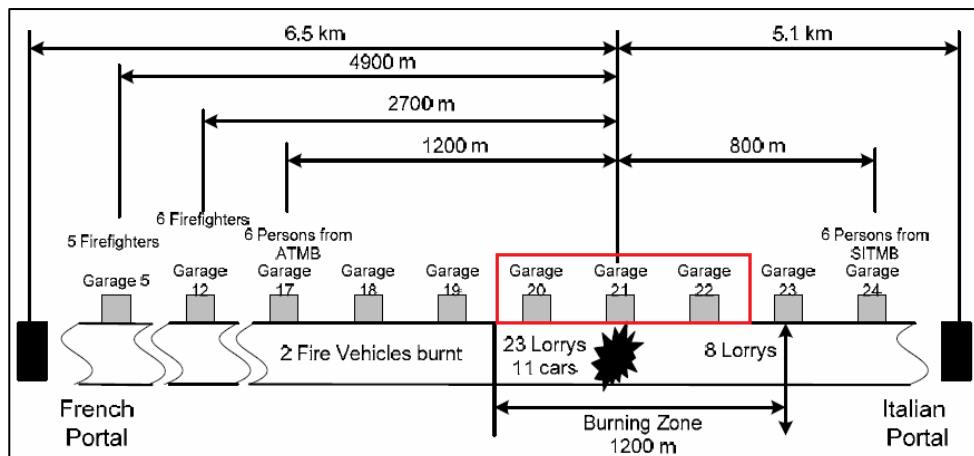


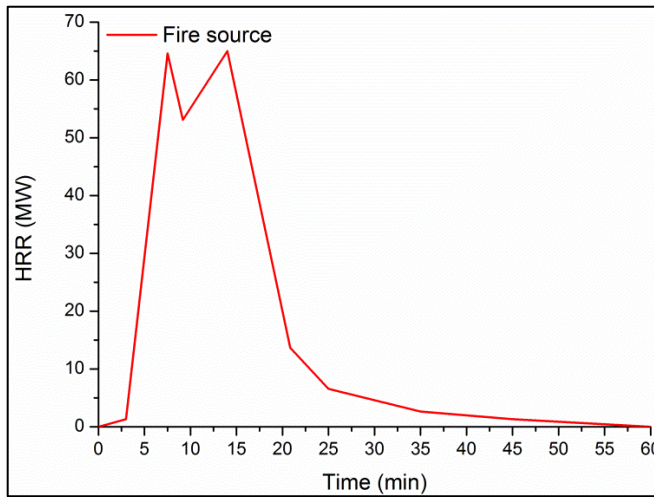
**Figure 4.6 Tunnel length (shown as red box) considered in the numerical simulations.**  
Figure reproduced from [16].

The prescribed fire source (Table 4.7) is chosen such that it emulates a burning HGV load with a pick HRR of approximately 65 MW (Figure 4.7). The curve corresponds to the obtained HRR from burning cartons and PS cups in Test 4 of the large-scale fire tests in the Runehamar tunnel [31]. This value corresponds well with the assumed lower limit of the HRR ( $\approx 75$  MW) of the burning HGV in the accident [12].



**Table 4.7 Fire source used in the numerical simulations.**

<b>Fire source</b>	<b>Value</b>
Dimensions (m x m)	5 x 2.5
Fuel	n-Heptane (n-C <sub>7</sub> H <sub>16</sub> )
Duration (min)	60
Peak heat release rate (MW)	65
Time to peak heat release rate (min)	8

**Figure 4.7 Prescribed heat release rate used in the numerical simulations [31-32].**

The numerical simulations are performed with the Fire Dynamics Simulator (FDS version 6.1.1), previously presented in Chapter 3. An overview of the numerical details and the models chosen in the numerical simulations is presented in Table 4.8.

**Table 4.8 Numerical simulations and models used in the numerical simulations.**

<b>Fire Dynamics Simulator (FDS) 6.1.1</b>	
Dimensions (m x m x m)	1,000 x 9 x 6
Number of cells	520,000
Cell type	Uniform
Cell size (m)	0.5
Turbulence model	Modified Deardorff model $\mu_{sgs} = \bar{\rho} C_v \Delta \sqrt{k_{sgs}}$ $k_{sgs} = \frac{1}{2} \left[ (\bar{u} - \hat{u})^2 + (\bar{v} - \hat{v})^2 + (\bar{w} - \hat{w})^2 \right]$ $C_v = 0.1 [33]$
Combustion model	Modified Eddy Dissipation Concept $\dot{\omega}''' = \bar{\rho} \frac{\min(\bar{Y}_F, \bar{Y}_O / s)}{\tau_{\min}}$ $\tau_{\min} = \max \left[ \tau_{chem}, \min(\tau_d, \tau_u, \tau_g, \tau_{flame}) \right]$ $\tau_d = \Delta^2 / D_F; \quad \tau_u = \Delta / \sqrt{2k_{sgs}}; \quad \tau_g = \sqrt{2\Delta / g}$
Radiation model	Radiative Transfer Equation (RTE) Finite Volume Method (FVM) – 100 angles $\nabla \cdot \dot{q}_r'' = \chi_r \dot{q}''' : \text{Inside flame zone}$



	$\nabla \cdot \dot{q}_r'' = \alpha(4\sigma T^4 - G)$ : Outside flame zone $\chi_r = 0.3$ [21]
Pyrolysis model	1D Arrhenius model $\dot{m}'' = A\rho \exp\left(-\frac{E_A}{RT_s}\right)$

In total 26 vehicles (17 HGV and 9 cars) are considered within the tunnel, based on the positions depicted in Figure 2.1 [17]. From these, 15 HGV and 9 cars are positioned downstream from the fire source, starting from 13 m away, while 2 HGV are positioned at 290 m and 315 m upstream of the fire, respectively (Table 4.9). The dimensions (L x W x H) for the each car and HGV is set to 4.5 m x 1.5 m x 1.5 m and 15 m x 2.5 m x 4 m, respectively (Figure 4.8). Each HGV is set to carry a 26t load [34] (material properties taken as plywood) with a total theoretical calorific energy of 520 GJ each.

**Table 4.9 Distance of the vehicles from the fire source in the numerical simulations.**

Name	Type	Distance from fire source (m)	Position relative to fire source	Dimensions: L x W x H (m x m x m)
Vehicle 1	HGV	13	Downstream	15 x 2.5 x 4
Vehicle 2	HGV	36	Downstream	15 x 2.5 x 4
Vehicle 3	HGV	69	Downstream	15 x 2.5 x 4
Vehicle 4	HGV	90	Downstream	15 x 2.5 x 4
Vehicle 5	HGV	113	Downstream	15 x 2.5 x 4
Vehicle 6	HGV	135	Downstream	15 x 2.5 x 4
Vehicle 7	HGV	153	Downstream	10 x 2.5 x 4
Vehicle 8	HGV	168	Downstream	15 x 2.5 x 4
Vehicle 9	Car	187	Downstream	4.5 x 1.5 x 1.5
Vehicle 10	HGV	197	Downstream	15 x 2.5 x 4
Vehicle 11	Car	220	Downstream	4.5 x 1.5 x 1.5
Vehicle 12	Car	232	Downstream	4.5 x 1.5 x 1.5
Vehicle 13	HGV	244	Downstream	15 x 2.5 x 4
Vehicle 14	Car	295	Downstream	4.5 x 1.5 x 1.5
Vehicle 15	HGV	302	Downstream	15 x 2.5 x 4
Vehicle 16	Car	325	Downstream	4.5 x 1.5 x 1.5
Vehicle 17	HGV	362	Downstream	15 x 2.5 x 4
Vehicle 18	Car	400	Downstream	4.5 x 1.5 x 1.5
Vehicle 19	Car	405	Downstream	4.5 x 1.5 x 1.5
Vehicle 20	HGV	412	Downstream	15 x 2.5 x 4
Vehicle 21	HGV	450	Downstream	15 x 2.5 x 4
Vehicle 22	Car	460	Downstream	4.5 x 1.5 x 1.5
Vehicle 23	Car	467	Downstream	4.5 x 1.5 x 1.5
Vehicle 24	HGV	472	Downstream	15 x 2.5 x 4
Vehicle 25	HGV	290	Upstream	15 x 2.5 x 4
Vehicle 26	HGV	315	Upstream	15 x 2.5 x 4



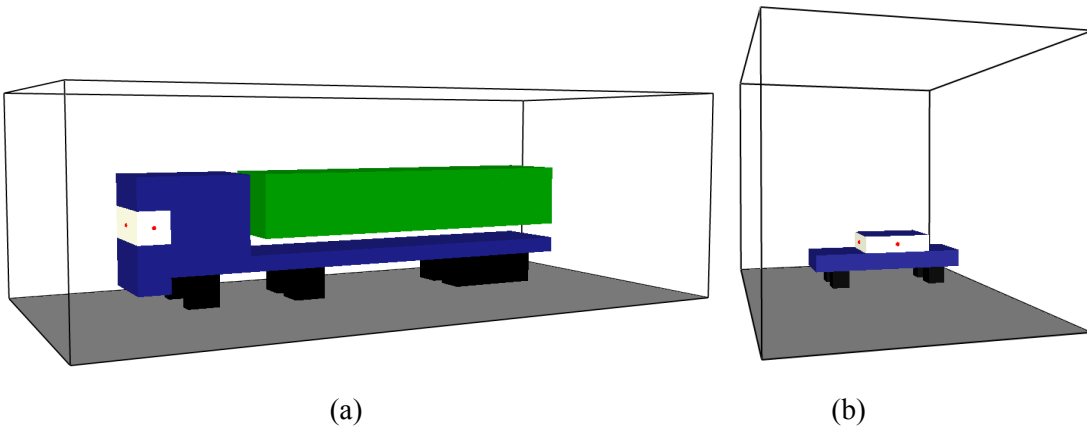


**Figure 4.8 Representation of a (a) HGV and (b) car in the numerical simulations.**

Various materials, presented in Table 4.10, were used for the interior of the vehicles and the tunnel in the numerical simulations. Concrete was used for the walls and ground of the tunnel, steel for the frame of the vehicles, rubber for the tyres of the vehicles, polyurethane for the plastics within the vehicles, polyurethane and leather as foam and cover of the vehicle's seats, respectively, laminated glass for the glasses of the vehicles and plywood was used to represent the load carried by the HGV. The glasses of all vehicles are set to break at 400 K [35].

**Table 4.10 Material properties [36-40] used in the numerical simulations.**

	Density (kg/m <sup>3</sup> )	Thermal conductivity (W/m·K)	Heat capacity (kJ/kg·K)	Emissivity	Heat of reaction (kJ/kg)	Heat of combustion (kJ/kg)
Concrete	2,280	1.04	0.88	0.95	-	-
Steel	7,850	45.80	0.46	0.25	-	-
Rubber	910	0.13	1.88	0.97	257	32,600
Polypropylene	900	0.16	1.90	0.97	2,540	43,230
Polyurethane	40	0.05	1.00	0.90	1,300	25,000
Laminated glass	2,200	0.20	1.66	0.92	-	-
Leather	100	0.10	1.00	0.95	881	18,000
Plywood	545	0.12	1.21	0.86	1,700	20,000

Combustion is modelled by a single-step reaction for heptane, a relatively simple, hydrocarbon fuel that produces a lot of soot, making it suitable for use when modelling this scenario. Apart from the main combustion products (CO<sub>2</sub> and H<sub>2</sub>O), also CO and soot are also considered by prescribing a CO and soot yield, respectively, corresponding to burning polypropylene. The details of the fire chemistry are given in Table 4.11.

**Table 4.11 Chemical reaction properties [41] used in the numerical simulations.**

Fire source	Value
Fuel	n-Heptane (n-C <sub>7</sub> H <sub>16</sub> )
Reaction	C <sub>7</sub> H <sub>16</sub> + 11(O <sub>2</sub> + 3.76) → 7CO <sub>2</sub> + 8H <sub>2</sub> O + 41.36N <sub>2</sub>
Heat of Combustion (MJ/kg)	43.74
CO yield (kg/kg)	0.024
Soot yield (kg/kg)	0.059

## 4.4 Results

### 4.4.1 Heat release rate

The results of the predicted heat release rates for the four different scenarios examined are presented in Figure 4.9. The prescribed HRR of the fire source, previously given in Figure 4.7, is also presented here for completeness.

A direct observation that can be made by looking at Figure 4.9 is that the use of ventilation or not inside the tunnel during a fire accident has a significant effect in the predicted heat release rate. For the test cases examined, if no ventilation is used ( $u=0$  m/s) the peak heat release rate obtained is in the order of 110 MW approximately 47 min after the initiating event. On the other hand, if ventilation is used ( $u=1-3$  m/s) then the predicted HRR reaches approximately 250-275 MW after 1 hour with increasing tendencies. However, this effect is not surprising. When no ventilation is used during a fire accident in a tunnel, heat is freely radiated and convected towards both ends of the tunnel. As such, the incident heat fluxes on the surfaces of the vehicles in this case are expected to be less. This will lead to a slower heating rate of the materials, therefore, resulting in a longer time to ignition and slower flame spread from one vehicle to another. On the other hand, when ventilation is used, heat is forced towards a certain direction, in this case towards France where most of the immobilized vehicles were present. This effect is certainly enhancing the incident heat fluxes on the vehicles surfaces and the resulting flame spread from the fire source towards the first vehicle but also from one vehicle to another. It is not surprising, therefore, to see that the predicted HRR when no ventilation is used inside the tunnel is much lower compared to the cases where ventilation was used. What is also evident is that the increasing ventilation speed (from 1 m/s to 3 m/s), enhances the burning of the vehicles inside the tunnel, since more  $O_2$  is now present inside the tunnel, and additionally increases the predicted HRR as well (max HRR is obtained in Scenario 4 with  $u=3$  m/s).

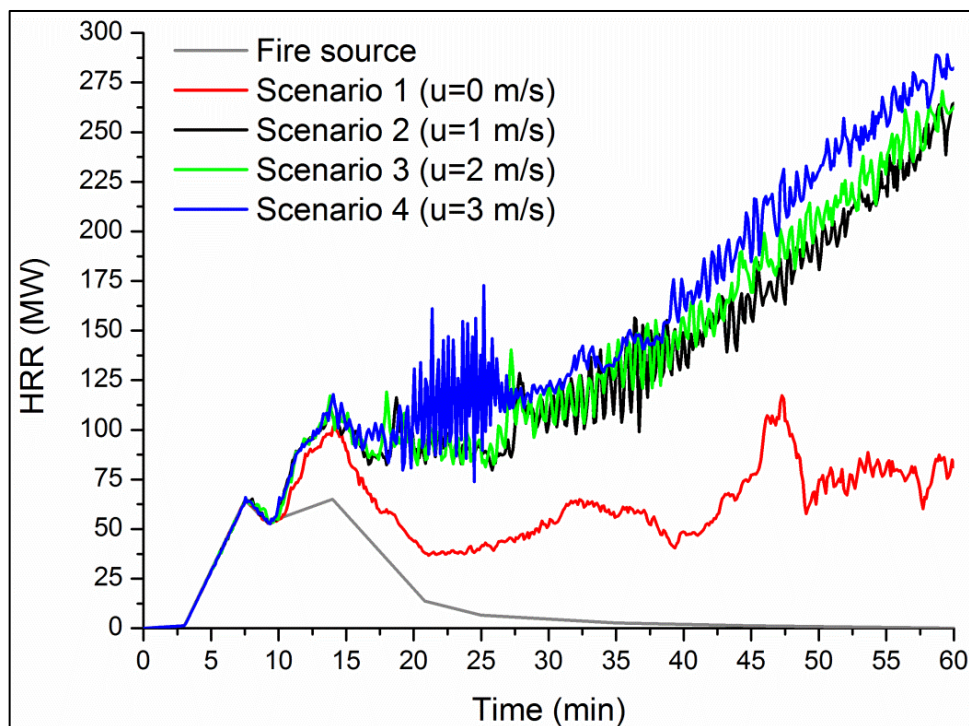


**Figure 4.9** Predicted heat release rates inside the tunnel from the numerical simulations. The grey line represents the prescribed fire source.

What is also interesting to note is that after approximately 15 min, when the prescribed HRR at the fire source is decreasing, there is sustained combustion in the scenarios involving ventilation and the incident heat fluxes on the vehicles are high enough to cause ignition, leading to flame spread from one vehicle to another and the HRR to increase with time. However, in Scenario 1 (no ventilation) when the intensity of the fire source starts decreasing ( $t>15$  min) the conditions are not appropriate to sustain burning inside the tunnel, since a greater amount of heat is lost and less oxygen is present, leading to the decrease of the HRR with time. After approximately 10 min ( $t=25$  min), the third vehicle was ignited, burned for a few minutes until the fire burned out, only to re-ignite at about time  $t=41$  min, causing the HRR to increase again.

#### 4.4.2 Flame spread

The predicted times to ignition of the different vehicles inside the tunnel for the four different scenarios examined are presented in Table 4.12. For scenario 1 ( $u=0$  m/s) only 3 vehicles ignited within the simulation of 1 hour of real time while 12 vehicles were ignited for Scenarios 2-4 involving the use of ventilation inside the tunnel. The number of cars ignited in each scenario is also reflected in the previously presented Figure 4.9. Once a vehicle is ignited then the HRR is increasing since heat is released from the additional materials burning. What is evident is that by increasing the ventilation speed inside the tunnel the time to ignition of the same vehicle is decreasing since more heat is incident on the vehicle and more oxygen is also available for combustion. If no ventilation is used inside the tunnel then a great amount of heat is lost towards the free end of the tunnel while on a different case it would had been convected towards the stopped vehicles. This effect causes a much slower heat up of the vehicles but also a slower flame spread from the fire source towards Vehicle 1 and from one vehicle to another.

**Table 4.12 Time to ignition of vehicles in the numerical simulations.**

Vehicle	Type	Scenario 1 ( $u=0$ m/s): Time to ignition ( $\approx$ min)	Scenario 2 ( $u=1$ m/s): Time to ignition ( $\approx$ min)	Scenario 3 ( $u=2$ m/s): Time to ignition ( $\approx$ min)	Scenario 4 ( $u=3$ m/s): Time to Ignition ( $\approx$ min)
Vehicle 1	HGV	11	10	10	10
Vehicle 2	HGV	12	11	11	11
Vehicle 3	HGV	1 <sup>st</sup> :25, 2 <sup>nd</sup> :41	28	27	21
Vehicle 4	HGV	-	36	35	31
Vehicle 5	HGV	-	41	39	33
Vehicle 6	HGV	-	45	43	38
Vehicle 7	HGV	-	46	45	39
Vehicle 8	HGV	-	49	47	42
Vehicle 9	Car	-	53	49	44
Vehicle 10	HGV	-	55	50	47
Vehicle 11	Car	-	56	53	49
Vehicle 12	Car	-	59	56	52
Vehicle 13	HGV	-	-	-	-
Vehicle 14	Car	-	-	-	-
Vehicle 15	HGV	-	-	-	-

#### 4.4.3 Tenability criteria

An important aspect in case of tunnel fires is the fast evacuation of the people trapped in their vehicles before the fire becomes big enough to hinder their escape route. A good way to evaluate the available evacuation time of trapped people is to check the tenability criteria, previously presented in section 5.3.



The results for the four different scenarios considered are presented in Figures 4.10-4.25. The numerical predictions for temperature, heat fluxes, FED and visibility are presented on the center of the tunnel at different locations away from the initiating event (e.g. HGV fire). The tenability criteria, denoting the appropriate safe conditions, are also presented in order to examine whether and when the conditions inside the tunnel become dangerous for the trapped people. An important aspect in the numerical simulations is the accurate prediction of the actual time the people have for safe evacuation.

Figures 4.10-4.13 present the predicted results at location  $x=-50$  m from the fire source (towards Italy) for Scenarios 1-4. This location is outside the area of the burning vehicles so naturally relatively low temperatures are predicted. It is observed that for Scenario 1, with no ventilation, higher temperatures are obtained when compared to the rest of the scenarios with activated ventilation. Additionally, there is no visibility inside the tunnel at this location after approximately 8 min while it takes approximately 50% longer (e.g. 12 min) for the visibility to diminish for the scenarios with ventilation. It is worth noting that, even though the predicted HRR for Scenario 1 is significantly lower, it used it does not necessarily represent the best strategy to follow in case of a fire accident inside the tunnel. In this case, the transport of heat, combustion products (e.g.  $\text{CO}_2$ ) and smoke towards both ends of the tunnel hinder the visibility and the access of the fire fighters (e.g. higher temperatures and heat fluxes) to the fire source in order to control and suppress it.

Figures 4.14-4.17 present the predicted results at location  $x=50$  m from the fire source (towards France) for Scenarios 1-4. This location is inside the area of the burning vehicles so naturally higher temperatures are obtained compared to the temperatures predicted at location  $x=-50$  m. In fact, this location is not only close to the initiating event but there was also sustained flaming and combustion throughout the course of all numerical simulations examined (e.g. Table 4.12). The temperatures for all scenarios exceed the tenability limit of  $60^\circ\text{C}$  after only 7.5 min and reach  $700^\circ\text{C}$  after 15 min for Scenarios 2-4 while remain significantly lower for Scenario 1. The visibility is good inside the tunnel only for 7.5 min in Scenarios 2-4 and about 6 min in Scenario 1. The heat fluxes follow the temperature pattern and become important mostly for Scenarios 2-4 after approximately 10 min. The FED dose exceeds the tenability limit of 1 after 20 min for Scenarios 2-4 while it only becomes high enough after 45 min in Scenario 1. The main observable difference between the cases with ventilation is that the increase of the ventilation speed (e.g. from 1 m/s to 3 m/s) had an impact mostly on the predicted FED starting from about 40 min onwards.

Similar observations are drawn by analyzing Figures 4.18-4.25 presenting the predicted results at the two other locations examined,  $x=100$  and  $200$  m (towards France). In this case the temperatures, heat fluxes and FED are initially (e.g. in the first minutes) significantly lower compared to the values obtained at location  $x=50$  m since it took some time for the flames to spread between one vehicle to another towards this location and the burning of the vehicles to start. Once it happens, though, the temperatures, heat fluxes and FED show a constantly increasing tendency until the end of the simulation.



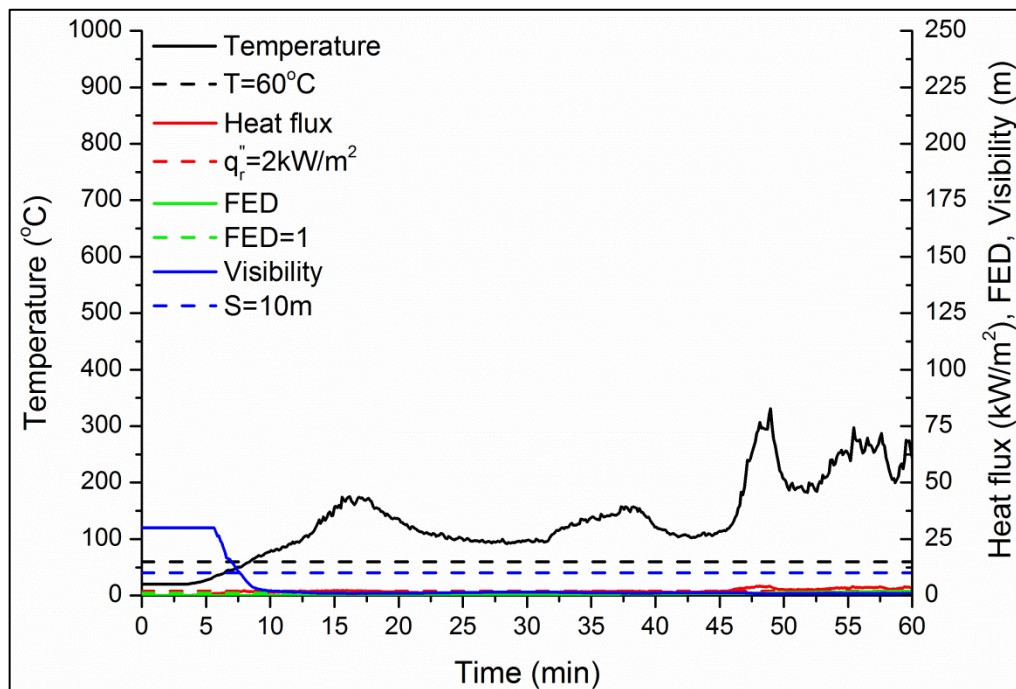


**Figure 4.10** Evolution of temperature, heat flux, FED and visibility at location  $x = -50$  m from the fire source (towards Italy) in the centre of the tunnel for Scenario 1. The dashed lines represent the tenability criteria.

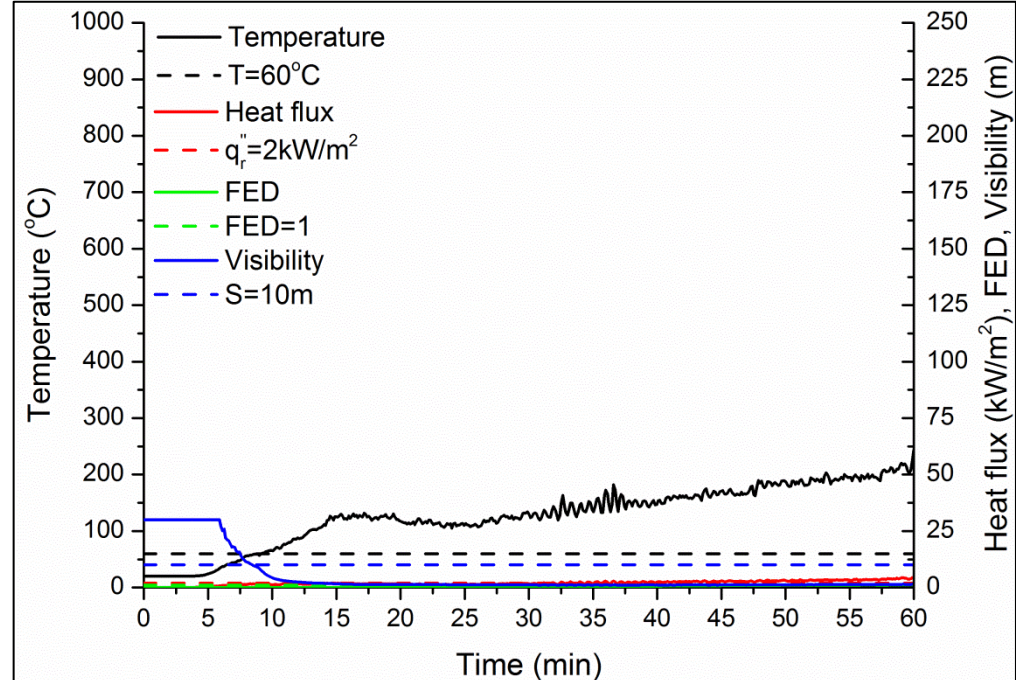


**Figure 4.11** Evolution of temperature, heat flux, FED and visibility at location  $x = -50$  m from the fire source (towards Italy) in the centre of the tunnel for Scenario 2. The dashed lines represent the tenability criteria.

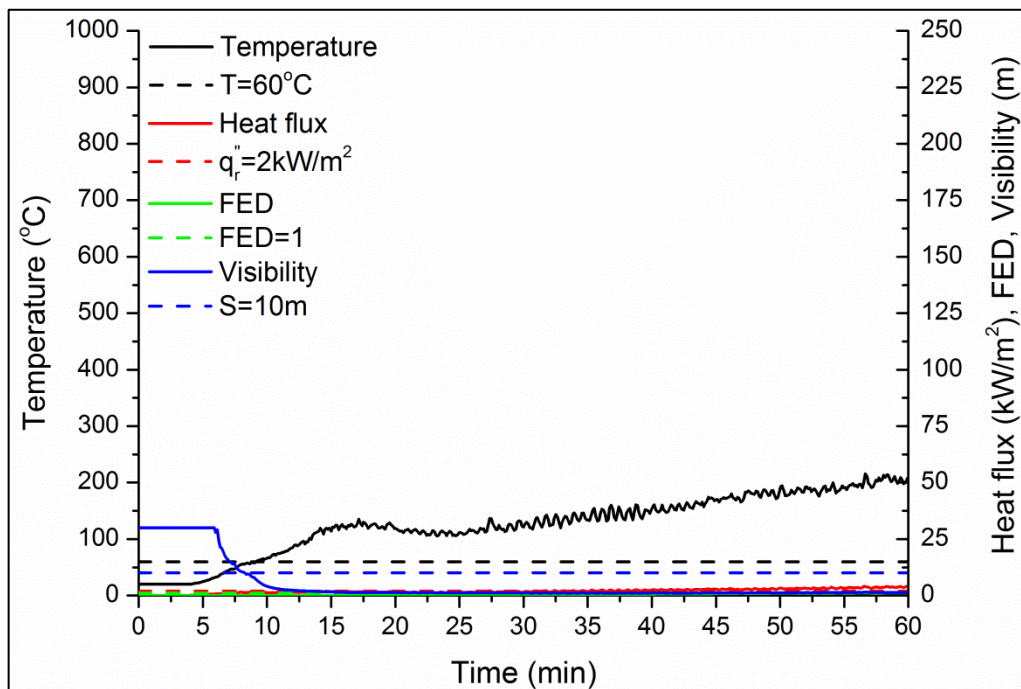


**Figure 4.12** Evolution of temperature, heat flux, FED and visibility at location  $x = -50\text{ m}$  from the fire source (towards Italy) in the centre of the tunnel for Scenario 3. The dashed lines represent the tenability criteria.

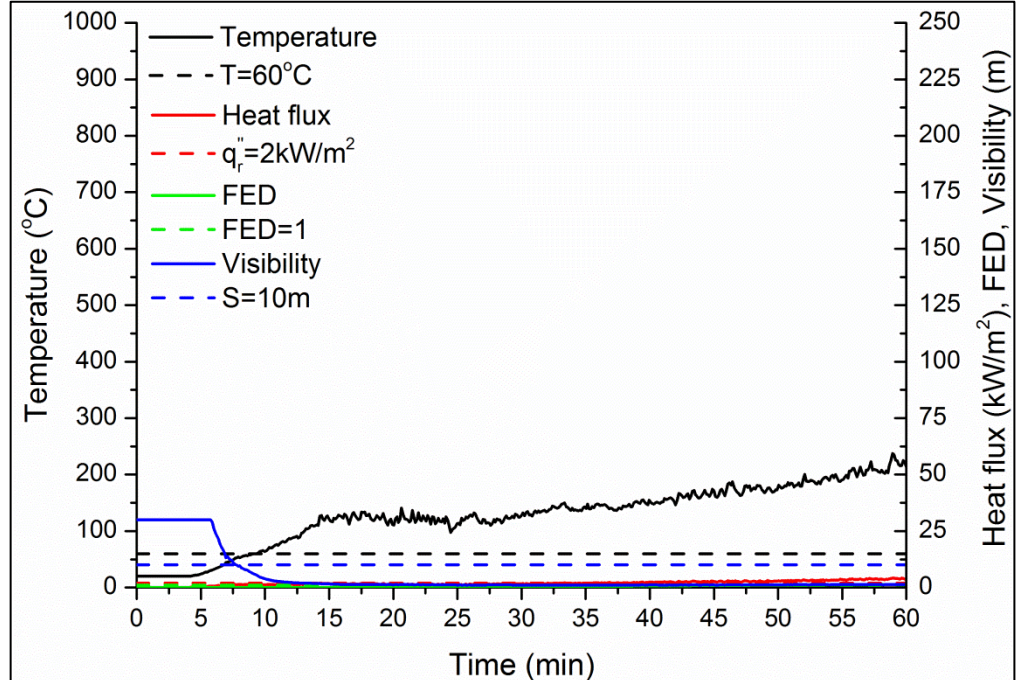


**Figure 4.13** Evolution of temperature, heat flux, FED and visibility at location  $x = -50\text{ m}$  from the fire source (towards Italy) in the centre of the tunnel for Scenario 4. The dashed lines represent the tenability criteria.

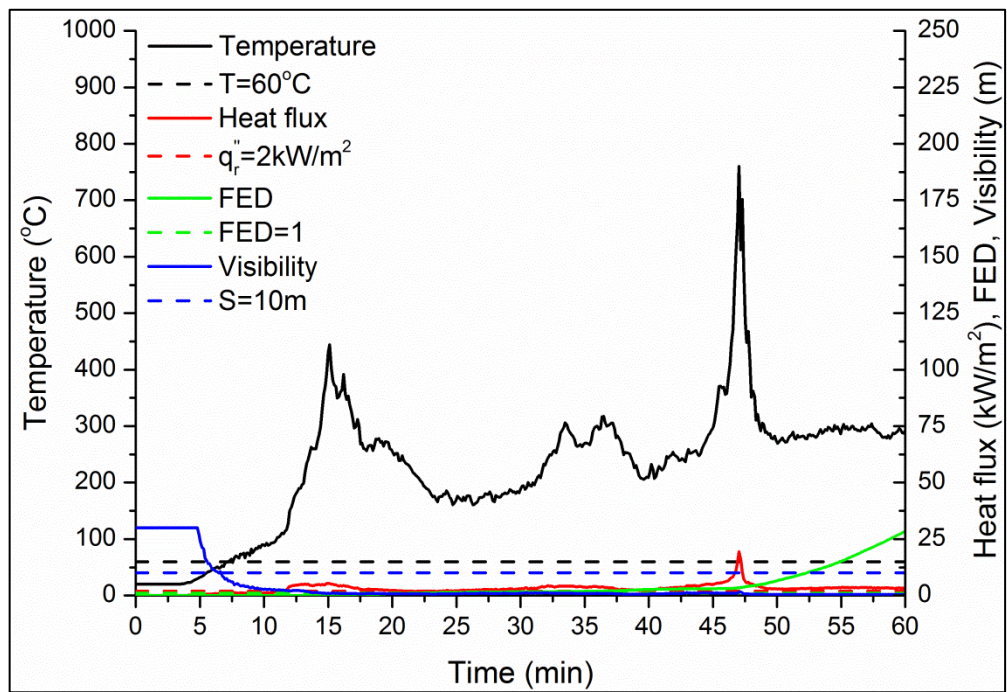


**Figure 4.14** Evolution of temperature, heat flux, FED and visibility at location  $x = +50$  m from the fire source (towards France) in the centre of the tunnel for Scenario 1. The dashed lines represent the tenability criteria.

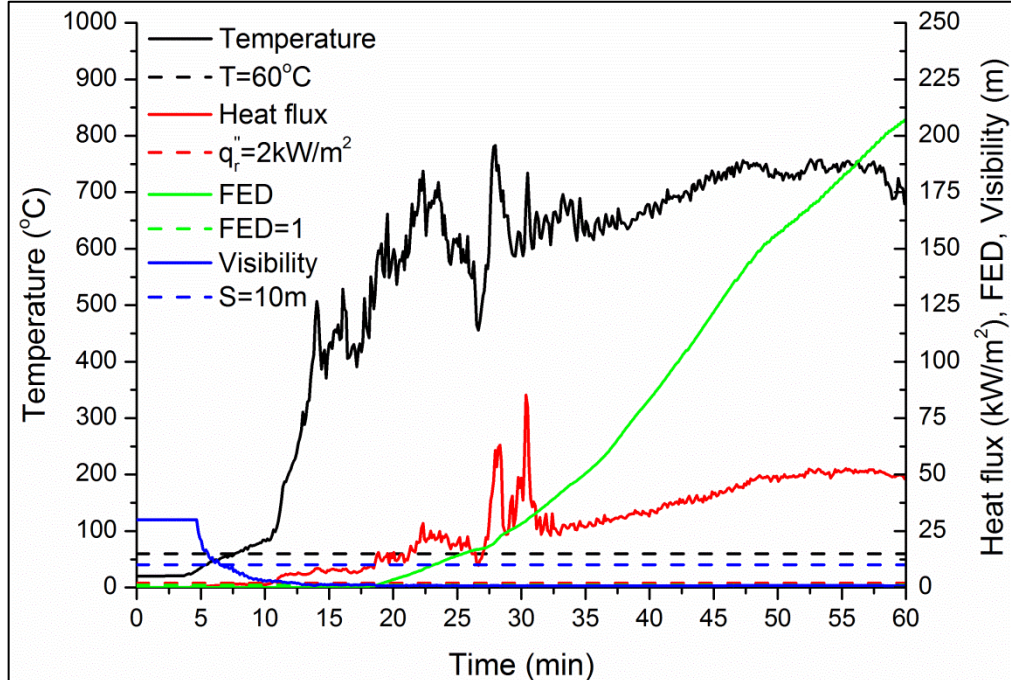


**Figure 4.15** Evolution of temperature, heat flux, FED and visibility at location  $x = +50$  m from the fire source (towards France) in the centre of the tunnel for Scenario 2. The dashed lines represent the tenability criteria.

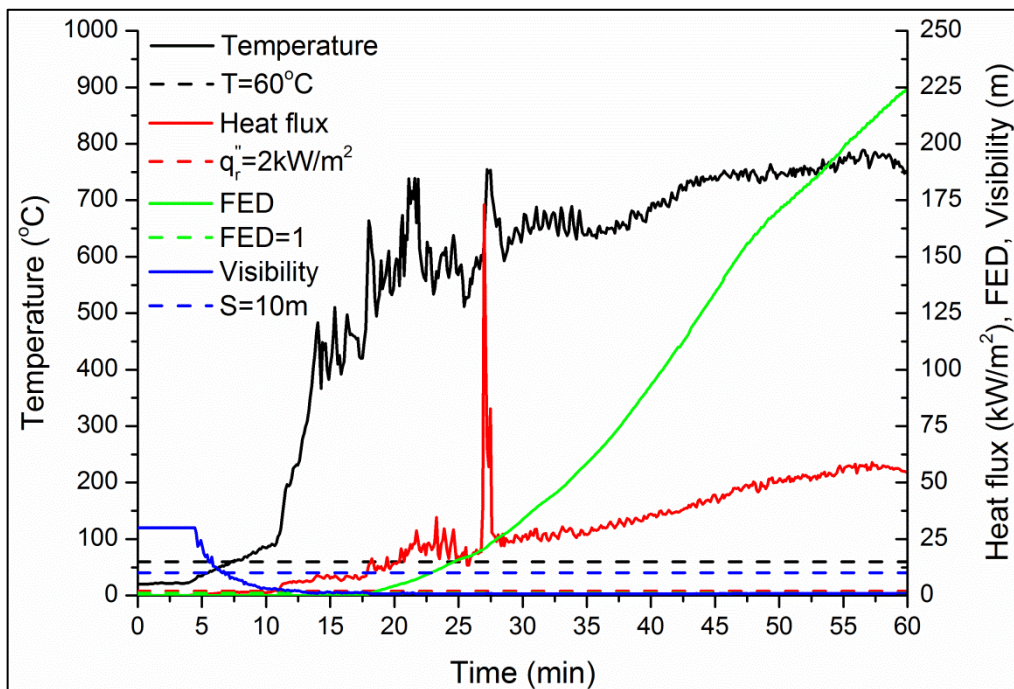


**Figure 4.16** Evolution of temperature, heat flux, FED and visibility at location  $x = +50\text{ m}$  from the fire source (towards France) in the centre of the tunnel for Scenario 3. The dashed lines represent the tenability criteria.

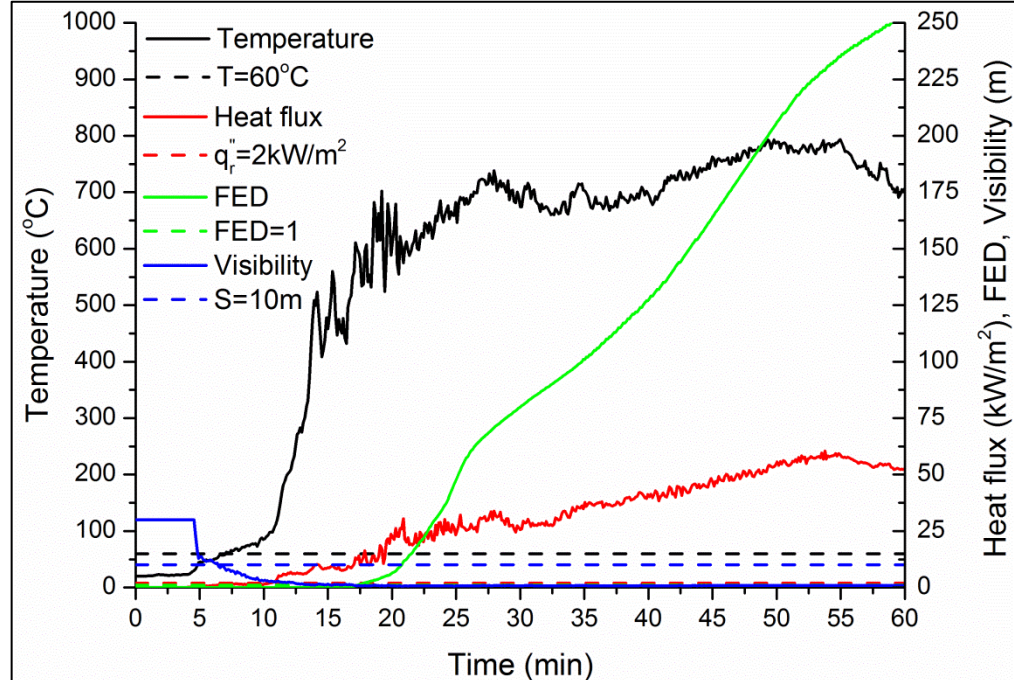


**Figure 4.17** Evolution of temperature, heat flux, FED and visibility at location  $x = +50\text{ m}$  from the fire source (towards France) in the centre of the tunnel for Scenario 2. The dashed lines represent the tenability criteria.

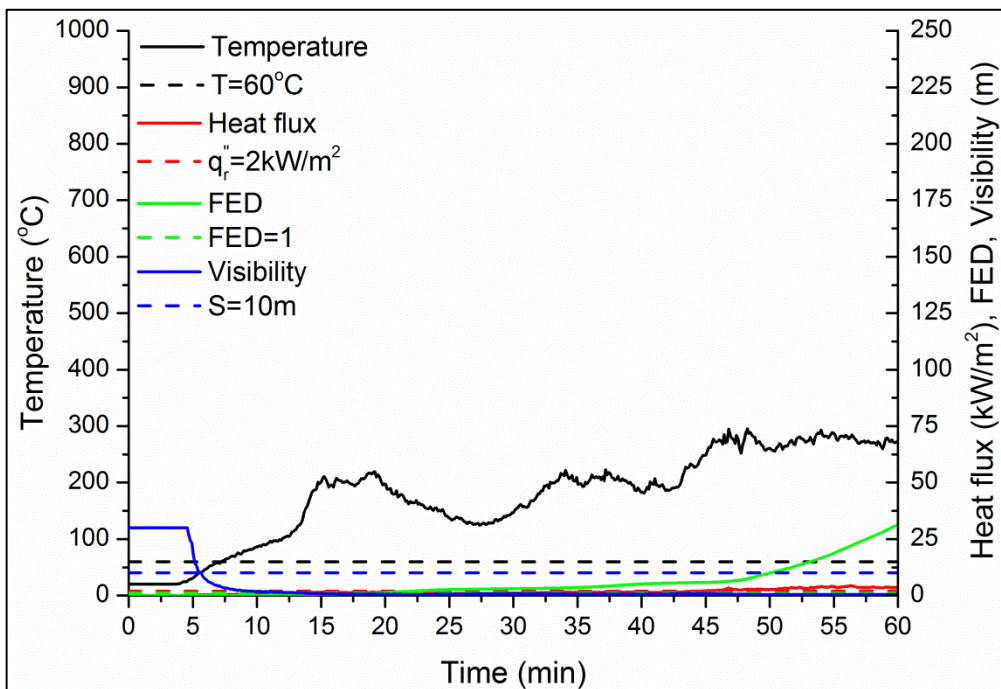


**Figure 4.18** Evolution of temperature, heat flux, FED and visibility at location  $x = +100\text{ m}$  from the fire source (towards France) in the centre of the tunnel for Scenario 1. The dashed lines represent the tenability criteria.

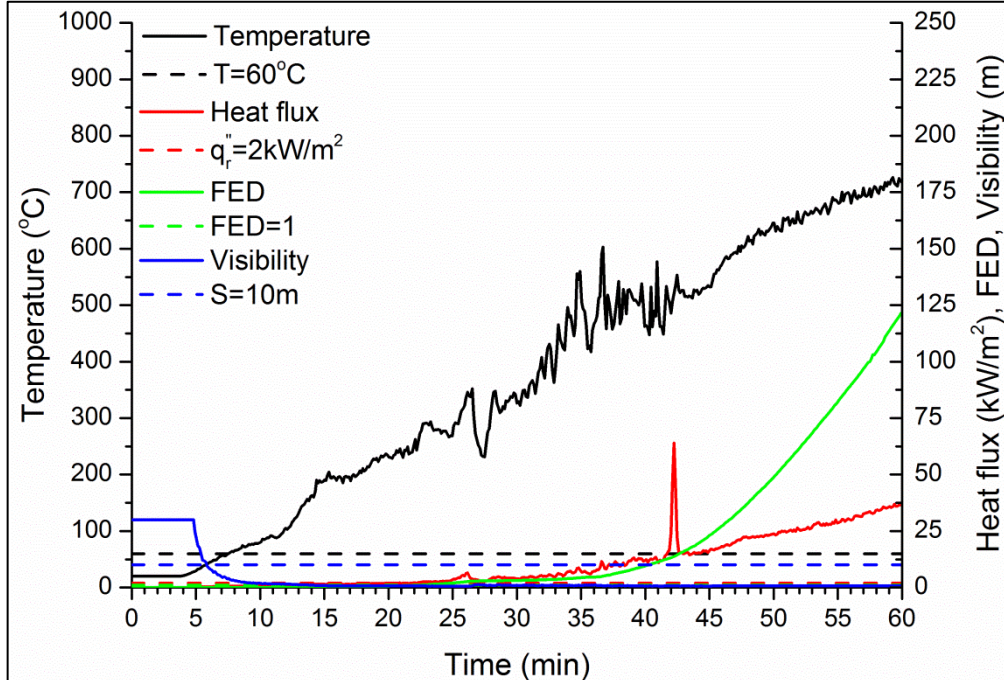


**Figure 4.19** Evolution of temperature, heat flux, FED and visibility at location  $x = +100\text{ m}$  from the fire source (towards France) in the centre of the tunnel for Scenario 2. The dashed lines represent the tenability criteria.

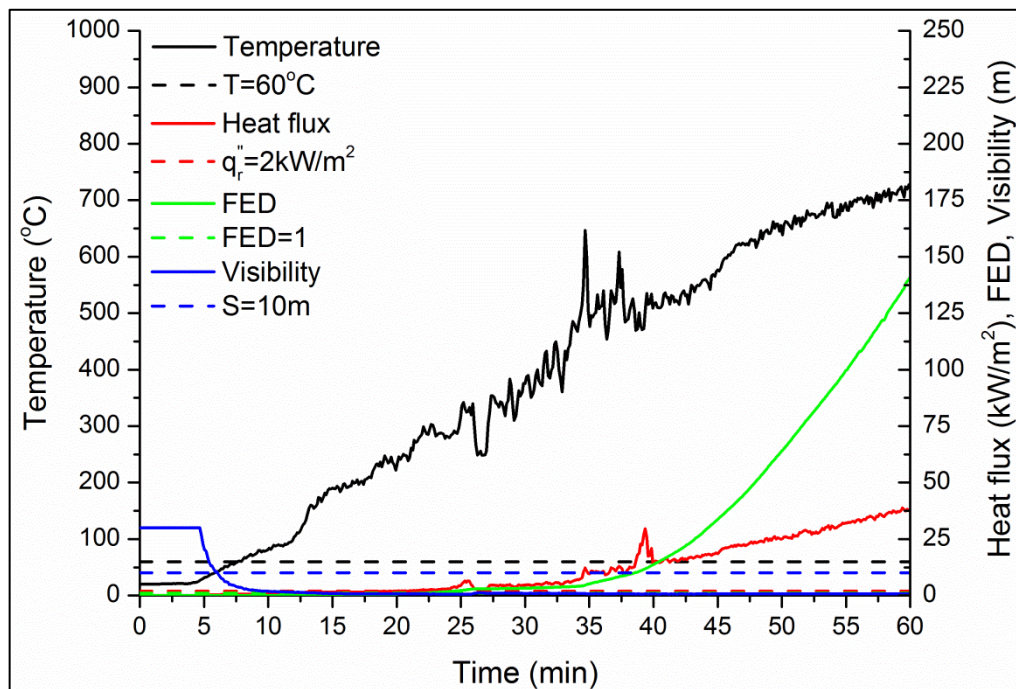


**Figure 4.20** Evolution of temperature, heat flux, FED and visibility at location  $x = +100$  m from the fire source (towards France) in the centre of the tunnel for Scenario 3. The dashed lines represent the tenability criteria.

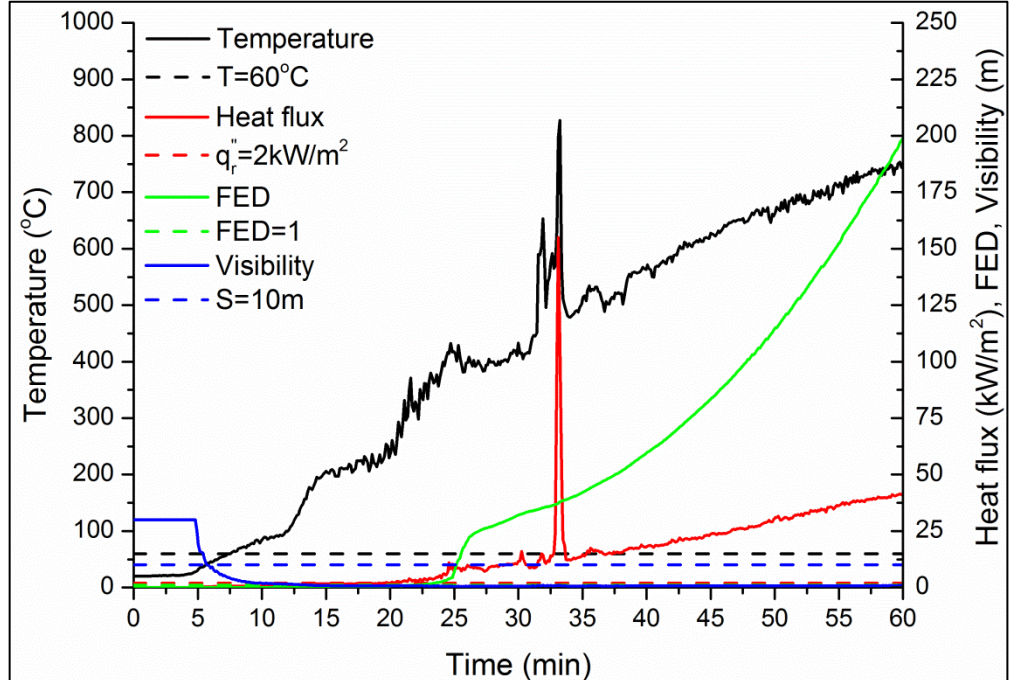


**Figure 4.21** Evolution of temperature, heat flux, FED and visibility at location  $x = +100$  m from the fire source (towards France) in the centre of the tunnel for Scenario 4. The dashed lines represent the tenability criteria.

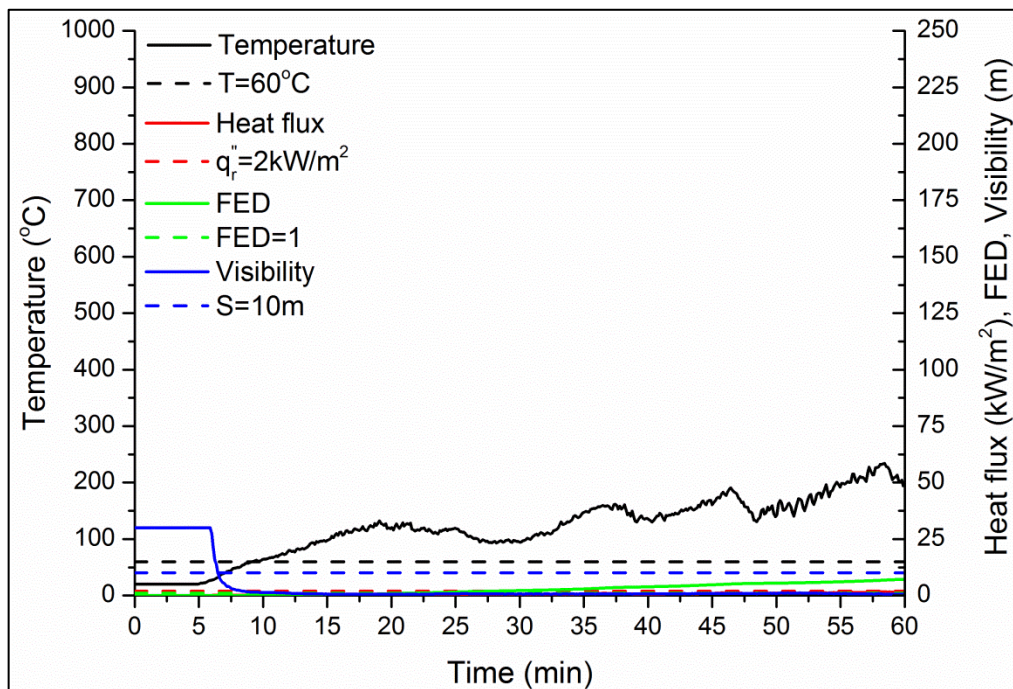


**Figure 4.22** Evolution of temperature, heat flux, FED and visibility at location  $x = +200$  m from the fire source (towards France) in the centre of the tunnel for Scenario 1. The dashed lines represent the tenability criteria.

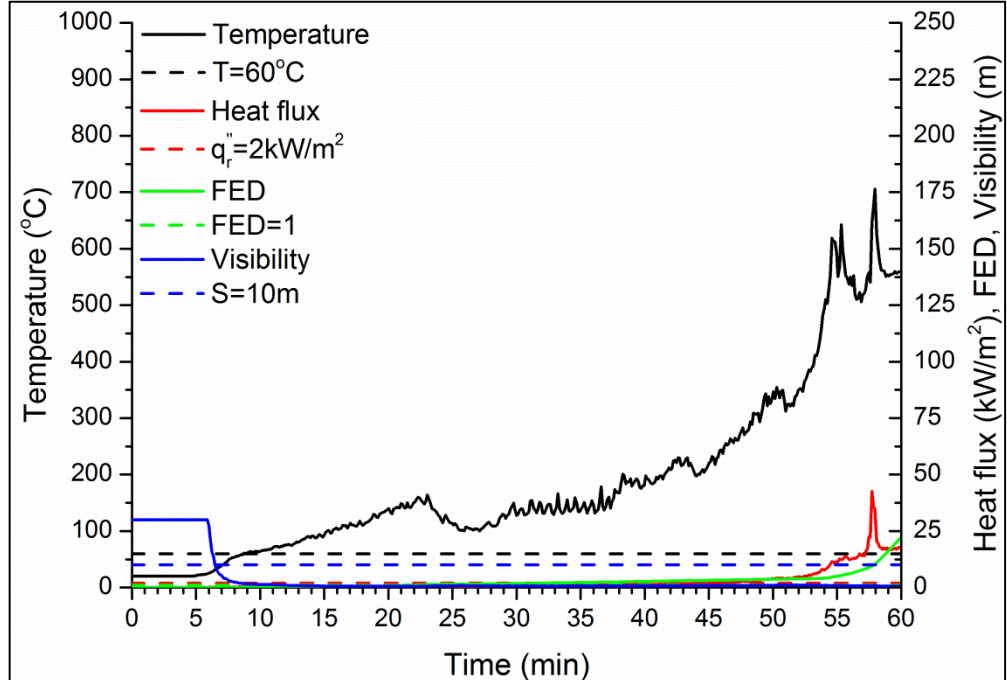


**Figure 4.23** Evolution of temperature, heat flux, FED and visibility at location  $x = +200$  m from the fire source (towards France) in the centre of the tunnel for Scenario 2. The dashed lines represent the tenability criteria.

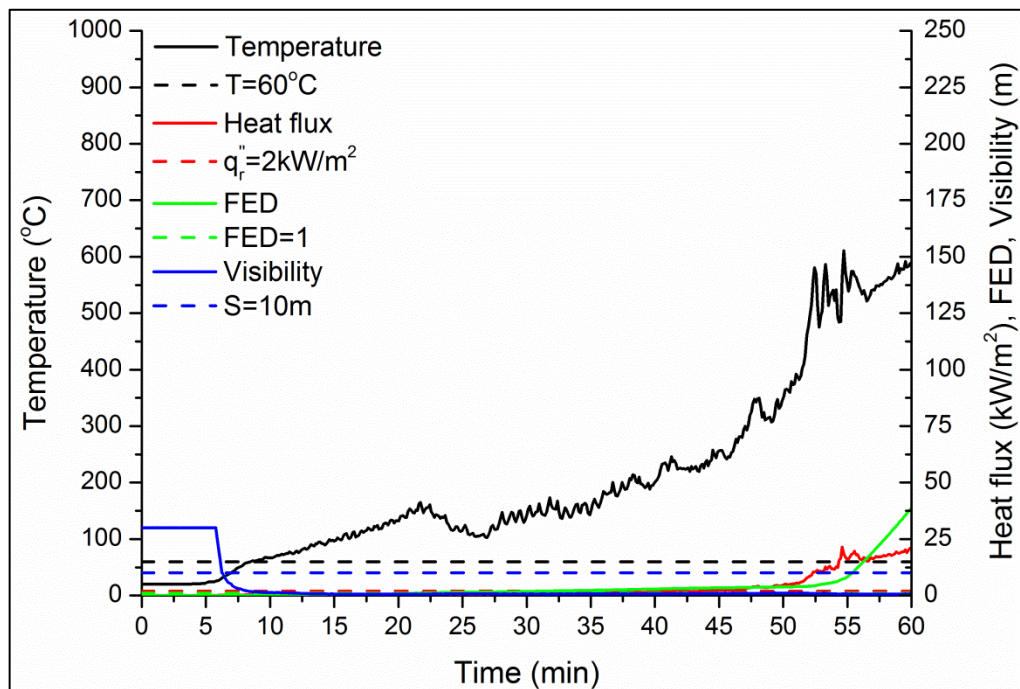


**Figure 4.24** Evolution of temperature, heat flux, FED and visibility at location  $x = +200$  m from the fire source (towards France) in the centre of the tunnel for Scenario 3. The dashed lines represent the tenability criteria.

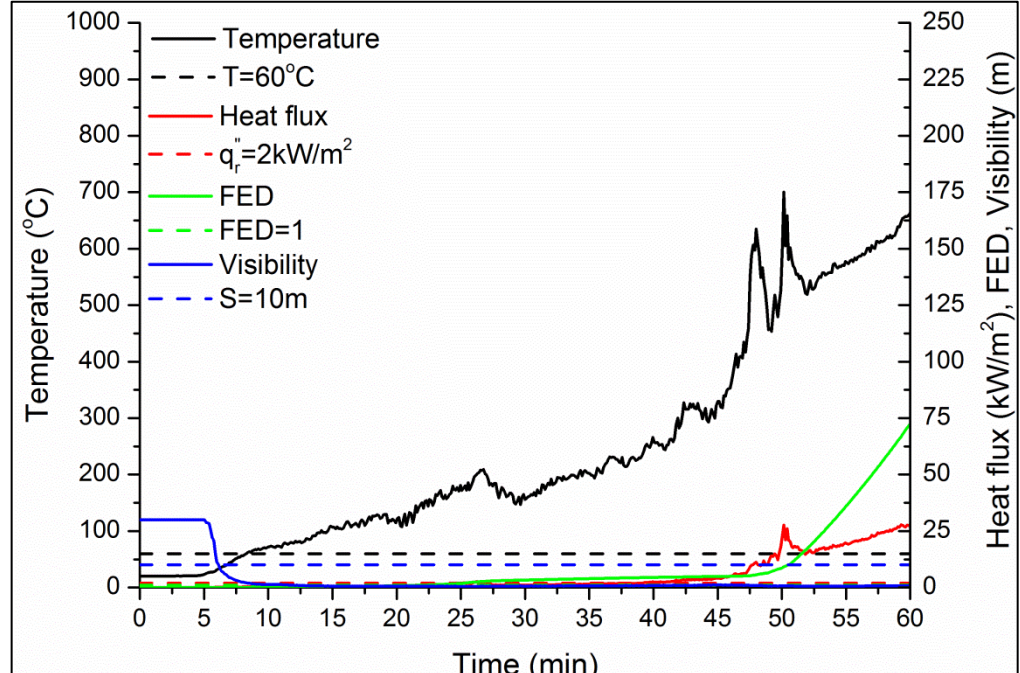


**Figure 4.25** Evolution of temperature, heat flux, FED and visibility at location  $x = +200$  m from the fire source (towards France) in the centre of the tunnel for Scenario 4. The dashed lines represent the tenability criteria.

#### 4.4.4 Cascading effects

An overview of the initiating event, the different systems affected, their interdependency and the key decision points for the Mont Blanc tunnel fire scenario considered is presented below. Additionally, a qualitative presentation of the possibility of having cascading effects and the magnitude of the impact of the different scenarios considered in the numerical simulations is given in Table 4.13.

**Initiating event:** Accidental (fire in a tunnel).

**Originating system:** A Heavy Goods Vehicle (HGV).

**Dependent/Impacted system:** Human people (deaths, evacuation), tunnel infrastructure (severe damage), traffic control (blocked traffic of a main highway connecting Italy and France).

**Interdependencies:** Physical (HGV), geographical (proximity of the human people and the tunnel infrastructure) and logical (traffic congestion due to the closing of the tunnel).

**Key decision points:** Determination of the ventilation velocity within the tunnel, evacuation of people.

**Table 4.13 Possibility of cascading effects and magnitude of impact in the different scenarios considered in the numerical simulations. Critical response time is  $\approx 10$  min.**

Scenario	Ventilation velocity (m/s)	Possibility of cascading effects		Magnitude of impact	
		$t < t_{crit}$	$t > t_{crit}$	$t < t_{crit}$	$t > t_{crit}$
Scenario 1	0	Minimum	Average	Minimum	Average
Scenario 2	1	Minimum	High	Minimum	High
Scenario 3	2	Minimum	High	Minimum	High
Scenario 4	4	Minimum	High	Minimum	High

Possibility of cascading events - Magnitude of impact: Minimum, Average, High.

For all scenarios considered in the numerical simulations, it was concluded that it is crucial for the tunnel operators, fire services and local authorities to have a fast response to the accident. It is important to immediately organize a plan for the evacuation of people trapped within the tunnel and to deal with the fire at its early stages before it grows in magnitude and results in a mega fire. Based on the numerical simulation results, the critical time of response is found to be approximately 10 min. If response occurs before this critical time limit then the possibility of having cascading effects is minimum, however, if the response occurs after this time limit then the possibility of having cascading effects is average for Scenario 1 and high for Scenarios 2-4.



## 5 Scenario: Music festival

### 5.1 Introduction

This scenario is located south of the city of Antwerp in Belgium, between river Scheldt and a main highway and tunnel (Figure 5.1). An outdoor dance festival in an area (marked in a red box) bordering a residential area of the city of Antwerp, the river Scheldt and a main road transport infrastructure (highway and secondary roads) is considered. Approximately 65.000 people attend the festival each year with ages varying mainly between 16 and 35 years old.

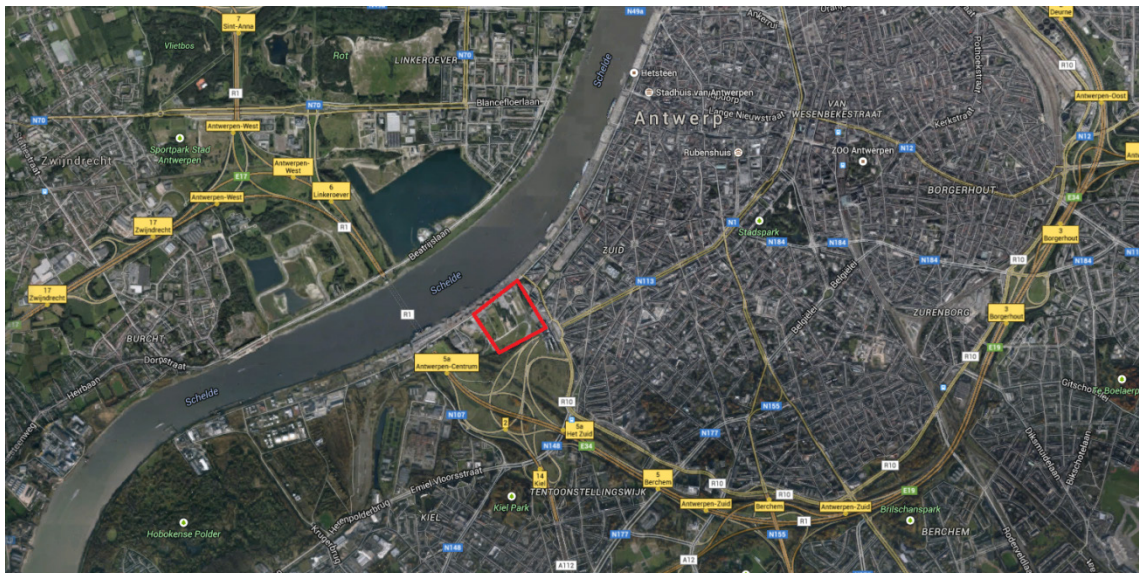


**Figure 5.1 Location (red box) of the considered music festival in Antwerp, Belgium.**

### 5.2 The accident

#### 5.2.1 Description of the accident

It is a Friday afternoon in September with warm and sunny weather where people are shopping in the city and sitting outside on terraces. At the same time, 65.000 youngsters are partying at a music festival at the south border of the city.

A ship transporting 4000 ton Ammonium nitrate ( $\text{NH}_4 \text{NO}_3$ , UN 2067) navigates on the river Scheldt. The captain notices white fumes coming from the hold. He is distracted, makes a navigation error and collides with a buoy near the quay next to the music festival. The cargo starts a self-sustained decomposition and the captain calls marine traffic control for help.

The wind blows white fumes (e.g. Figure 5.2) towards the northern corner of the festival area (Figure 5.3). The festival attendees see the white smoke coming towards them. Some people start to move towards exits while others hold ground and want to listen to the concert.

Fireworks in the production village of the festival detonate prematurely. People think it is part of the festival but some start to panic.

The fire brigade orders preventive evacuation of the production village, which is in the effect zone of the ship fire. The fire brigade uses thermal cameras and measure the temperature of the cargo is at  $180^\circ\text{C}$ . They decide to use lances to cool the cargo with water.





**Figure 5.2 Plume evolution on the 5<sup>th</sup> day of the Ostedijk ship fire accident carrying 6000 ton of NPK fertilizer [42-43].**



**Figure 5.3 Plume evolution towards the northern corner of the festival area.**

### 5.2.2 Impacts due to the accident

There is a wide range of impacts associated with the current music festival scenario, which are summarized below:

1. **Technical:** Quai infrastructure, vicinity of buildings (palace of justice) and highways + tunnels in effect area.
2. **Organizational:** Complex coordination of local authorities, fire brigade, health workers, police, port authorities and environment agency. Evacuation of potentially 60.000 -100.000 people.
3. **Social:** Panic in crowds, social unrest when people realize such hazardous material transports are organized so close to a city of  $\frac{1}{2}$  million people. Should the product detonate serious damage would be caused in a big part of the city with thousands of casualties. Thousands of people suffering from chest pain and acute breathing problems, panic in crowds.
4. **Economic:** Blockage of the traffic of the river.
5. **Environmental:** Impact on the river fauna and flora when Ammonium nitrate dissolves in water.

### 5.3 Modelling of the accident

The numerical simulations are performed with the Fire Dynamics Simulator (FDS version 6.1.2), previously presented in Chapter 3. An overview of the numerical details and the models chosen in the numerical simulations is presented in Table 5.1.

**Table 5.1 Numerical simulations and models used in the numerical simulations.**

Fire Dynamics Simulator (FDS) 6.1.2	
Dimensions (m x m x m)	650 x 600 x 160
Number of cells	7,776,000
Cell type	Uniform
Cell size (m)	2.0
Turbulence model	Smagorinsky model $\mu_{sgs} = \overline{\rho} (\Delta C_s)^2  \tilde{S} $ $C_s = 0.1 [44]$

An overview of the music festival area along with the location of the main stages that are considered in the study is presented in Figure 5.4. The scenario considered involves a preventive evacuation of a section of the festival area (Figure 5.5) containing approximately 15,000 people due to a fire breaking out on a ship close to the festival site.





**Figure 5.4** Top view of the music festival scenario and the different stages considered in the numerical simulations.



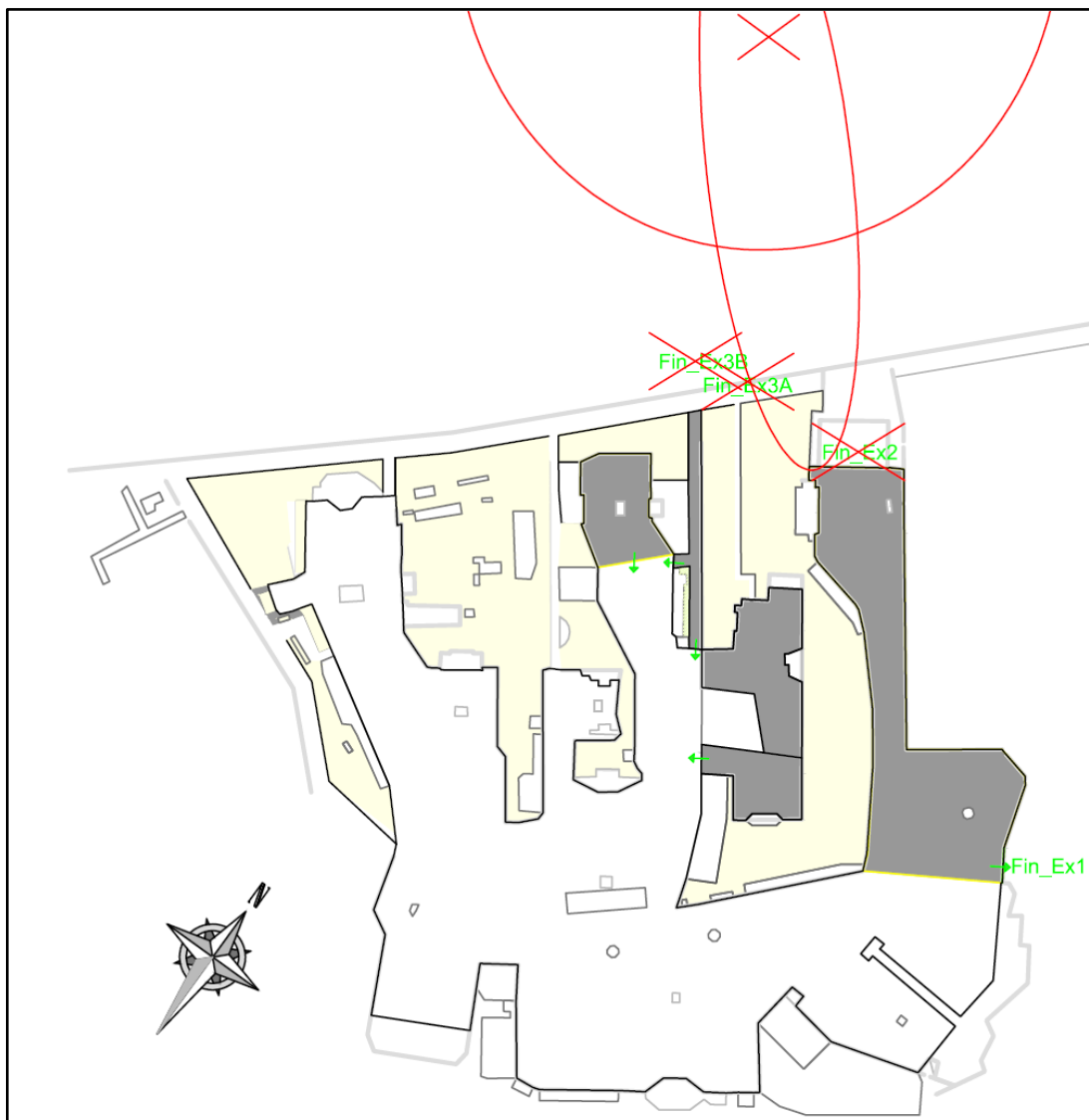


**Figure 5.5 Graphic representation of the considered pollutant dispersion and the possible exits in the music festival scenario.**

The area of the considered music festival scenario was simplified and mainly the structures that would have an effect on the flow field (buildings, stages, etc.) were considered in the numerical simulations. The computational domain (Figure 5.6) used in the numerical simulations is 650 m long, 600 m wide and 160 m high comprised of uniform cell sizes of 2 m. Similar grid sizes have been used in the past in other numerical studies of pollutant dispersion scenarios of the same size [45-46] and was shown to be sufficiently small enough to accurately capture the dispersion of toxic gasses. It is worth noting that the boundaries of the computational domain had to be extended far enough from the considered buildings of the festival in order to minimize any effects of the boundary conditions used at these boundaries.

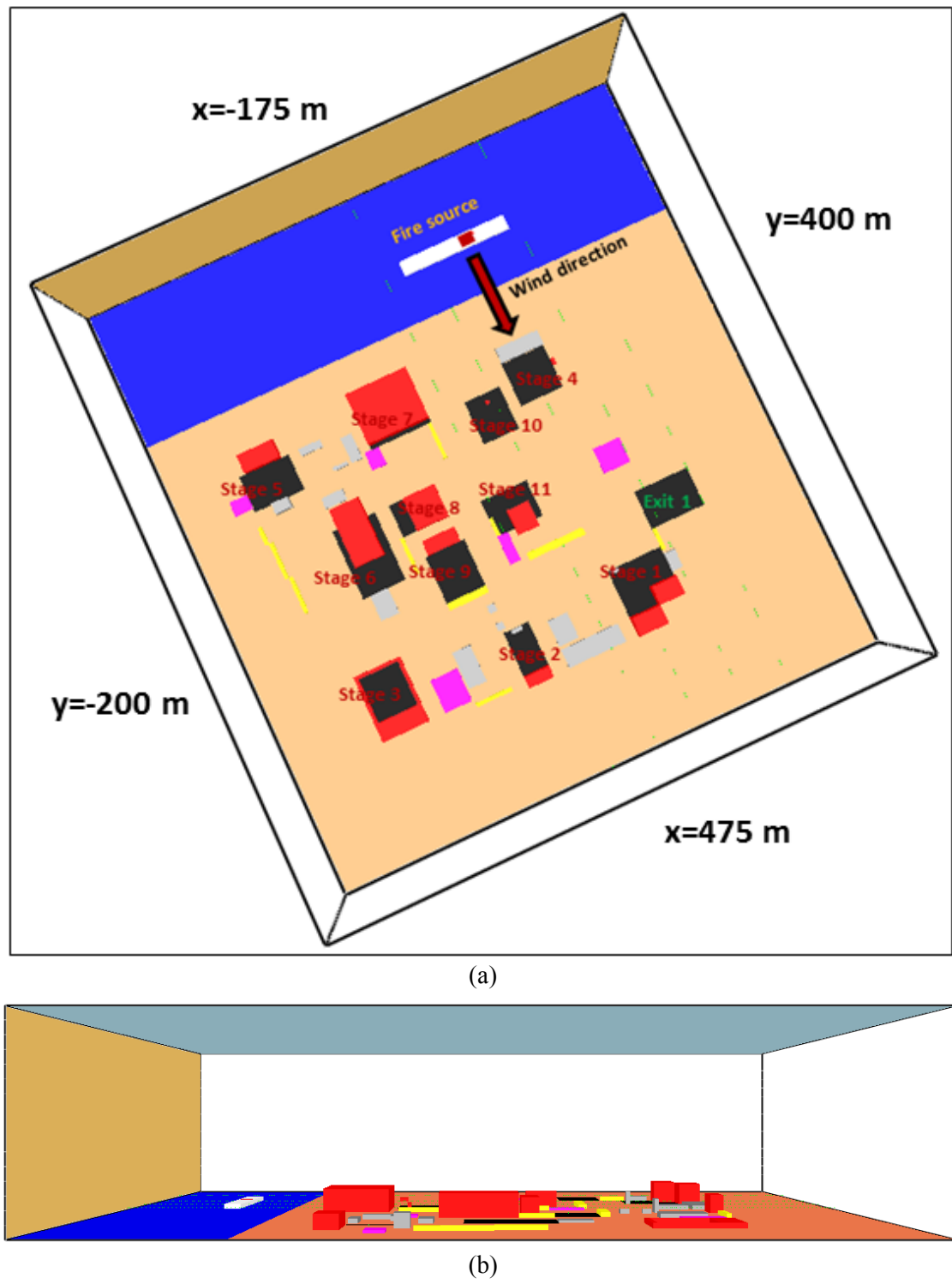


**Figure 5.6 Computational domain used in the numerical simulations from (a) top view and (b) side view.**

An obstacle representing a ship (shown in white colour in Figure 5.6) with dimensions 120 m x 16 m x 4 m was considered in the simulations on which the fire source was considered. An overview of all the buildings considered in the numerical simulations is presented in Table 5.2.

**Table 5.2 Main buildings considered in the numerical simulations.**

Name	Colour	Dimensions: L x W x H (m x m x m)
Stage 1	Red	40 x 60 x 20
Stage 2	Red	12 x 28 x 16
Stage 3	Red	72 x 52 x 4
Stage 4	Red	8 x 4 x 4
Stage 5	Red	20 x 40 x 12
Stage 6	Red	64 x 32 x 20
Stage 7	Red	56 x 68 x 20
Stage 8	Red	36 x 36 x 16
Stage 9	Red	16 x 36 x 16
Stage 10	Red	4 x 4 x 4
Stage 11	Red	28 x 24 x 16
Ship	White	120 x 16 x 4
WC	Purple	Varying
Food kiosks	Yellow	Varying
Various buildings	Grey	Varying

The areas depicted in black colour in Figure 5.6 depict the areas (in this case one in front of each stage of the festival and one in the only exit considered for this scenario) in which the pollutant concentrations were collected every 30 sec of real time. An average concentration over the whole area between heights 1 - 2 m is collected in order to account for the different height of the people occupying the area. These results will not only provide with the average pollutant concentrations and the resulting FED values, important for the study of pollutant dispersion over a polluted area, but will also be used towards a combined CFD and evacuation study of this scenario in the future. The scenario considered in this case involves the pollutant dispersion towards mostly the eastern side of the festival so that mostly Stages 1, 2, 4, 10 and 11 will be affected and only Exit 1 is available for evacuation.

The atmospheric wind profile used in the numerical simulations has the form:

$$u = u_0 \left( \frac{z}{z_0} \right)^p \quad (5.1)$$

where  $u$  is the wind speed,  $u_0$  is the known wind speed at reference height  $z_0$ ,  $z$  is the height and  $p$  is an empirically derived coefficient dependent upon the stability of the atmosphere. For this numerical study the wind data of the month September, the time when the considered music festival usually takes place, in the city of Antwerp have been considered. A wind speed  $u_0=3$  m/s [47] at reference height of  $z_0=10$  m was used with a constant of  $p=0.25$  (corresponding to a D stability class – neutral conditions) [48-50]. In addition, the synthetic eddy method (SEM) model [51] was used, which is a synthetic method of generating turbulence by setting the number of eddies ( $N_{edd}$ ), the characteristic eddy length ( $L_{edd}$ ) and the root mean square (RMS) velocity fluctuations ( $vel_{rms}$ ). The parameters for the SEM model were set to  $N_{edd}=500$ ,  $L_{edd}=10$  m and  $vel_{rms}=0.1$  m/s. A no-slip boundary condition was applied at the bottom of the computational domain while periodic boundaries were used at the sides. In order to correctly capture the atmospheric turbulence associated with environmental flows and to maintain a



consistent level of turbulent fluctuations in the velocity field a special treatment was applied at the top boundary of the computational domain. The tangential velocity was set to 6 m/s, corresponding to the velocity obtained from the atmospheric wind profile at this height, in order to avoid any velocity diffusion towards the top boundary.

The temperature at the source was set to 200 °C, corresponding to the minimum temperature required for self-sustaining decomposition of ammonium nitrate ( $\text{NH}_4\text{NO}_3$ ) [77-78] in which the mass loss rate is relatively small (here taken as 0.5 kg/s [78]). The heat of combustion for  $\text{NH}_4\text{NO}_3$  is 1448 kJ/kg [52] that would give an equivalent HRR of 724 kW. Based on the considered source temperature, the corresponding plume density is then 0.6823 kg/m<sup>3</sup>. This scenario corresponds to the start of a potential accident in which there is a slow increase of the temperature inside the cargo hold where the ammonium nitrate is stored. Similar estimations of the mass loss rate were also reported during the first days of the fire accident aboard the Ostedijk ship carrying 6012 tonnes of NPK fertilizer [42]. It was assumed that the cargo ship's hold doors were opened to avoid further heating of the ammonium nitrate that could lead to a possible explosion. The release of the combustion products was directly modelled to avoid uncertainties related with simulating combustion on relatively coarse meshes that are required for atmospheric flows. A t-squared heat release curve was assumed for estimating the transient growth of the fire in the form:  $\dot{Q} = at^2$  with  $a = 0.0469 \text{ kW} / \text{s}^2$  (fast fire). According to this, the corresponding mass flow rate was then used as input for the fire source. The fire source characteristics considered in the simulations are presented in Table 5.3:

**Table 5.3 Fire source used in the numerical simulations.**

Fire source	Value
Dimensions (m x m)	12 x 12
Fuel	Ammonium nitrate ( $\text{NH}_4\text{NO}_3$ )
Reaction	$6\text{NH}_4\text{NO}_3(\text{s}) \rightarrow \text{N}_2\text{O} + 10\text{H}_2\text{O} + \text{NH}_4\text{NO}_3(\text{aerosol}) + 3\text{N}_2 + 2\text{NO}_2$ [52]
Duration (h)	8
Mass flow rate (kg/s)	0.5

Another parameter considered in the numerical simulations is the temperature lapse rate of the atmosphere. Typically, the temperature of the atmosphere in the first few hundred meters decreases with increasing height. This small temperature change can be important when considering the dispersion of toxic gasses in the open atmosphere since the temperature of the gasses decreases rapidly with increasing height. A lapse rate of -0.01 °C/m was considered in the numerical simulations (the negative sign indicating the decrease of temperature with increasing height).

As originally planned, the dispersion of the toxic gases mostly affects the eastern side of the music festival that includes Stages 1, Stage 4 and Exit 1 but also all the areas surrounding them. The numerical simulation of this scenario will be coupled in the future with an evacuation simulation of the people within the festival due to the danger associated from the dispersion of the toxic gases. This partial evacuation scenario assumes that the only available exit for the people in the festival is Exit 1. Pre-defined areas were set in front of each stage in which one average toxic concentration was obtained for the whole area at heights between 1-2 m. This method of averaging was necessary for the coupling of the gas phase numerical simulation and the evacuation modelling. The numerical simulations were set to run for 3 h while the sampling frequency was set to 30 s.



## 5.4 Results

In this section, results from the numerical simulation of the music festival scenario with FDS are presented. The evolution of NO<sub>2</sub> within the music festival is reported and the concentrations of the toxic gases are presented as a function of time and space. Additionally, the concentrations of the NH<sub>4</sub>NO<sub>3</sub> aerosol and the Fractional Effective Dose (FED) values are also given. Lastly, the turbulence resolution that provides an indication of how well resolved is the kinetic energy within the numerical simulations is reported.

### 5.4.1 NO<sub>2</sub> dispersion

The prediction of NO<sub>2</sub> dispersion into the atmosphere is important due to the severe health risks often associated with it. It has been reported that the exposure to NO<sub>2</sub> is associated with increased all-cause, cardiovascular and respiratory mortality and respiratory morbidity [53-54]. The European air-quality standards for NO<sub>2</sub>, as defined by the Air Quality Directive [55] are set to 200 µg/m<sup>3</sup> (0.1 ppm) for short-term exposure (1-hour) and to 40 µg/m<sup>3</sup> for long-term exposure (annual mean). The Air Quality Directive [55] also defines an 'alert' threshold value of 400 µg/m<sup>3</sup> which if exceeded over three consecutive hours in areas of at least 100 km<sup>2</sup> or an entire air-quality management zone, authorities have to implement short-term action plans. These action plans may include measures related to vehicle traffic, construction works, the use of industrial plants and domestic heating [53]. According to the US Environmental Protection Agency (EPA), the air quality standard for NO<sub>2</sub>, which is designed to protect public health with an adequate margin of safety, is 0.053 ppm (annual average). EPA is required to issue a public alert when NO<sub>2</sub> reaches 0.6 ppm on a one-hour average, a public warning when NO<sub>2</sub> reaches 1.2 ppm, and a declaration of public emergency at the level of 1.6 ppm. The significant harm level, at which serious and widespread health effects occur to the general population, is 2.0 ppm of NO<sub>2</sub> [56].

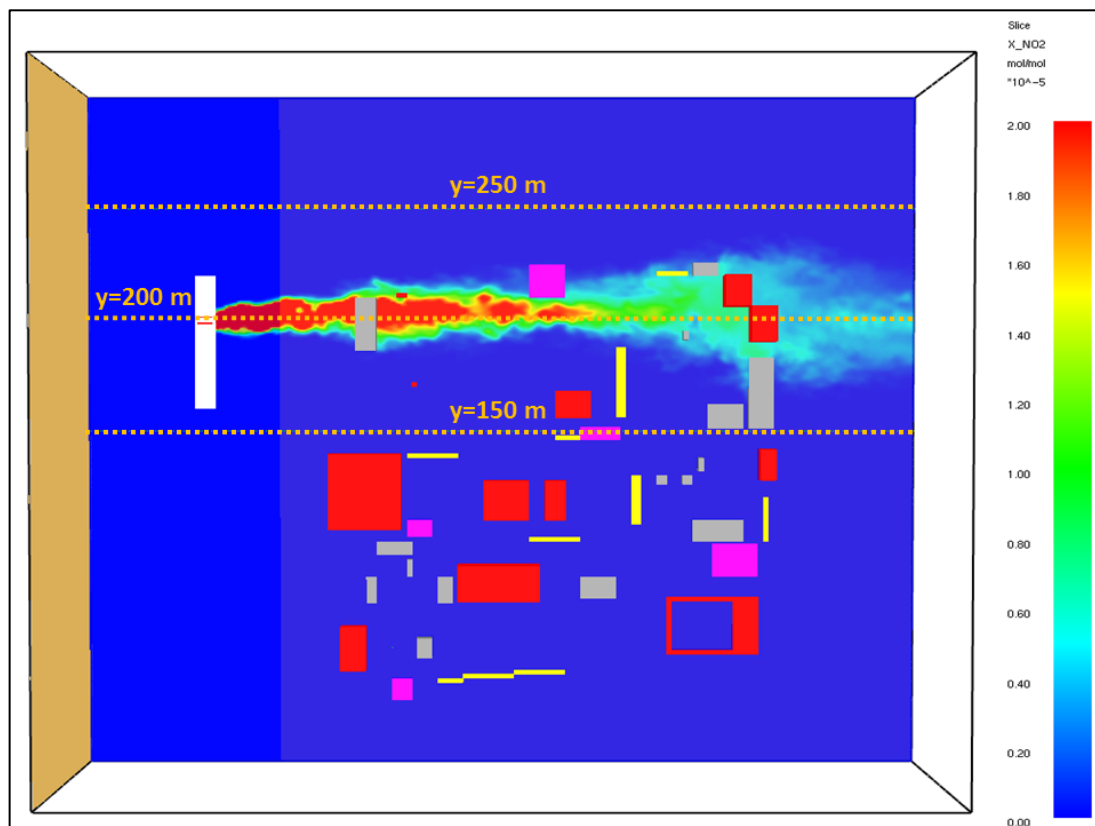


**Figure 5.7 Top view of the NO<sub>2</sub> dispersion (in volume fraction) in the festival area after 30 min.**



A top view of the NO<sub>2</sub> dispersion in the music festival area from the numerical simulation 30 min after the release is presented in Figure 5.7. As originally planned, mostly the eastern side of the festival is affected, which includes Stage 1, Stage 4 and Exit 1 as well as the areas surrounding them. Also shown in the figure, with dotted orange lines, are the three axial lines at different locations  $y$  ( $y=150$  m,  $y=200$  m (axis of the release) and  $y=250$  m) where NO<sub>2</sub> concentrations were measured. The greatest impact from the toxic NO<sub>2</sub> is observed near the Stage 4 area, close to the Entrance of the festival, which is expected since it is the location of the festival that is closest to the release accident. Nitrogen dioxide has a molecular weight of 46.005 g/mol, which makes it heavier than air ( $W_{\text{air}} = 28.8$  g/mol), so that NO<sub>2</sub> remains close to the ground and does not diffuse into the atmosphere. Additionally, the location of the release is approximately 80 m away from the bank of the river Scheldt, positioning the considered source relatively close to the area of the music festival. These two factors, along with the wind conditions considered, contribute so that the toxic plume does not spread a lot (diffuse) radially towards the x direction in the first couple of hundred meters. The spreading of the toxic plume starts after Exit 1 and occurs mostly around the area involving Stage 1. It is, therefore, certain that if the location of the release and the wind conditions considered in the numerical simulation would be different that either a smaller or a much larger area of the festival would be affected by the spreading of the toxic plume.

The NO<sub>2</sub> concentrations (ppm) as a function of time at Stage 1, Stage 4 and Exit 1 are presented in Figures 6.8-6.9. The alarm levels of NO<sub>2</sub> concentrations of 0.1 ppm by EEA and 2.0 ppm by EPA are also presented for comparative reasons. From Figure 5.8 it is observed that the alarm levels of EEA and EPA are exceeded only after 1.5 minutes and 3.5 minutes for Stage 4 and Stage 1, respectively. The toxic concentrations in these two stage areas get alarmingly high very fast and reach average values of 5.94 and 14.2 ppm, respectively, making the conditions of the people in these locations highly dangerous. More in particular, if people in these areas will not be able to evacuate the music festival area fast or if they for some reason cannot leave these areas at all then very quickly the conditions due to the high toxicity can cause a serious problem in their health. The conditions in Exit 1 reported in Figure 5.9 are significantly improved. It takes approximately 12.5 minutes for the instantaneous NO<sub>2</sub> concentration to exceed the limit of 0.1 ppm as set by EEA. Even though the instantaneous NO<sub>2</sub> concentrations reach up to values of 0.25 ppm, the average NO<sub>2</sub> concentration in Exit 1 remains at 0.096 ppm. This value is below but still very close to the alarm limit of 0.1 ppm as set by EEA. Even though the conditions in Exit 1 are significantly better than in Stage 1 and Stage 4, they can potentially still pose a threat for the health of the people that occupy this area if evacuation does not happen fast.

The NO<sub>2</sub> concentration (ppm) as a function of distance  $x$  at different  $y$  locations are presented in Figure 5.10-6.11. As expected at location  $y=200$  m, which is on the axis of the release, the conditions are the worst. Very high levels of NO<sub>2</sub> concentrations are detected close to the fire source (at location  $x=-80$  m) that exceed 400 ppm. The toxic concentrations significantly decrease with increasing distance  $x$  from the source, however, the NO<sub>2</sub> concentrations exceed the alarm levels as set by EEA and EPA at all downstream locations away from the source examined (Figure 5.10). It is worth mentioning that at the locations where the NO<sub>2</sub> drops to 0 buildings are present and no gas phase is present in the numerical simulations. What is observed from Figure 5.11 is that the NO<sub>2</sub> concentrations also start to become alarmingly high at  $y=150$  m and  $y=250$  m at downstream distances of  $x>175$  m. These locations effectively start at a location which is just before Exit 1 and reach until its outlet of the computational domain. The levels of NO<sub>2</sub> concentrations obtained at Exit 1 (located at  $272 \text{ m} > x > 230 \text{ m}$  and  $300 \text{ m} > y > 240 \text{ m}$ ), previously seen in Figure 5.9, are also confirmed here. It is expected that if the relative location of Exit 1 with respect to the source of the release were different, the amount of measured NO<sub>2</sub> concentrations would also be substantially different.



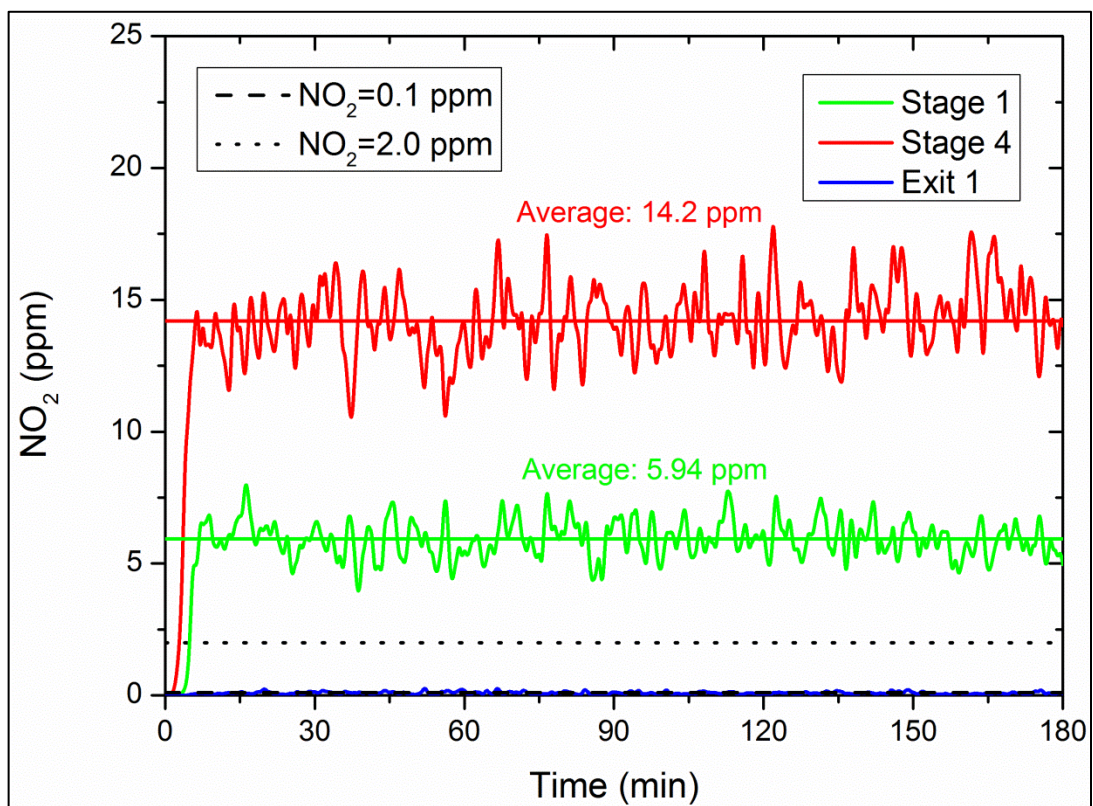


**Figure 5.8**  $\text{NO}_2$  concentration (ppm) as a function of time at Stage 1, Stage 4 and Exit 1.

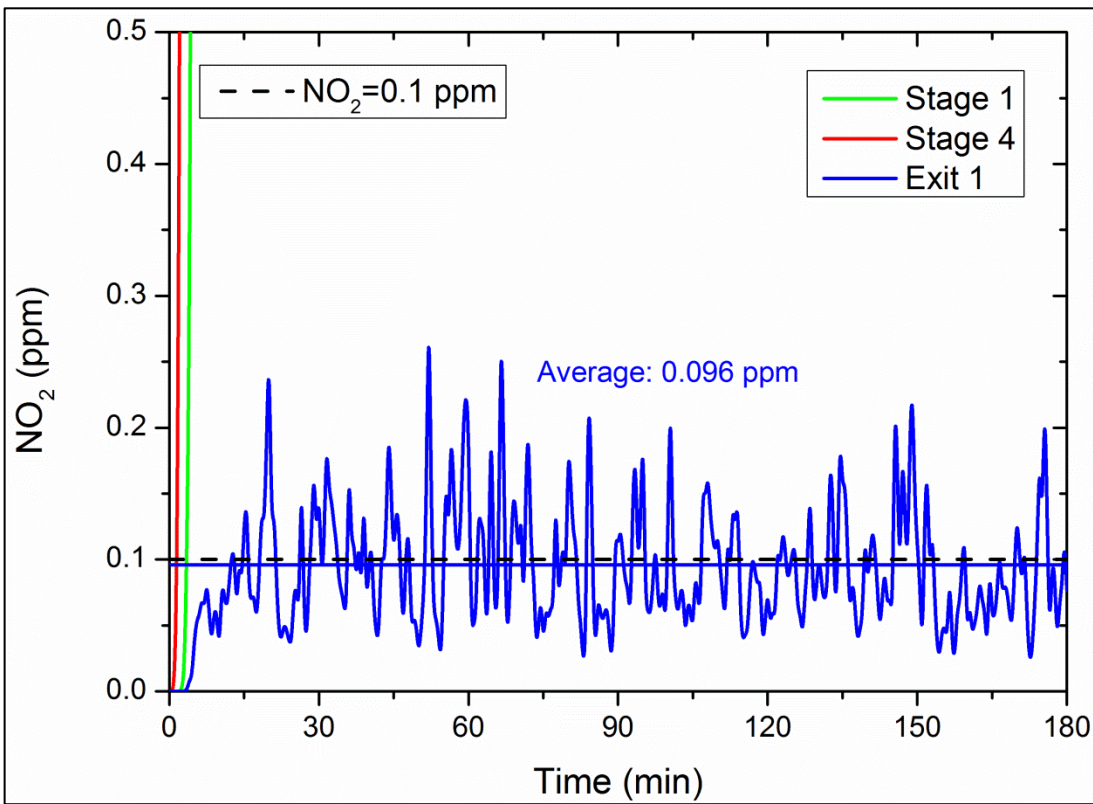


**Figure 5.9**  $\text{NO}_2$  concentration (ppm) as a function of time at Stage 1, Stage 4 and Exit 1 (zoom).



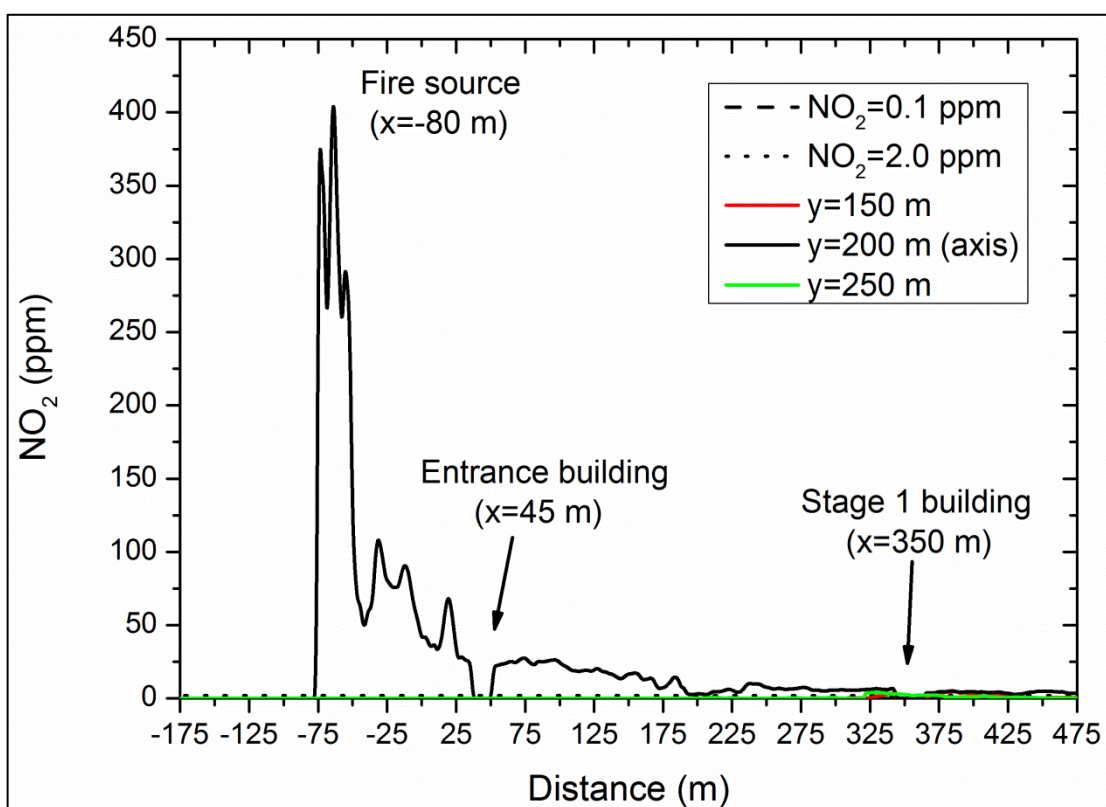


Figure 5.10 NO<sub>2</sub> concentration (ppm) as a function of distance at different positions y.

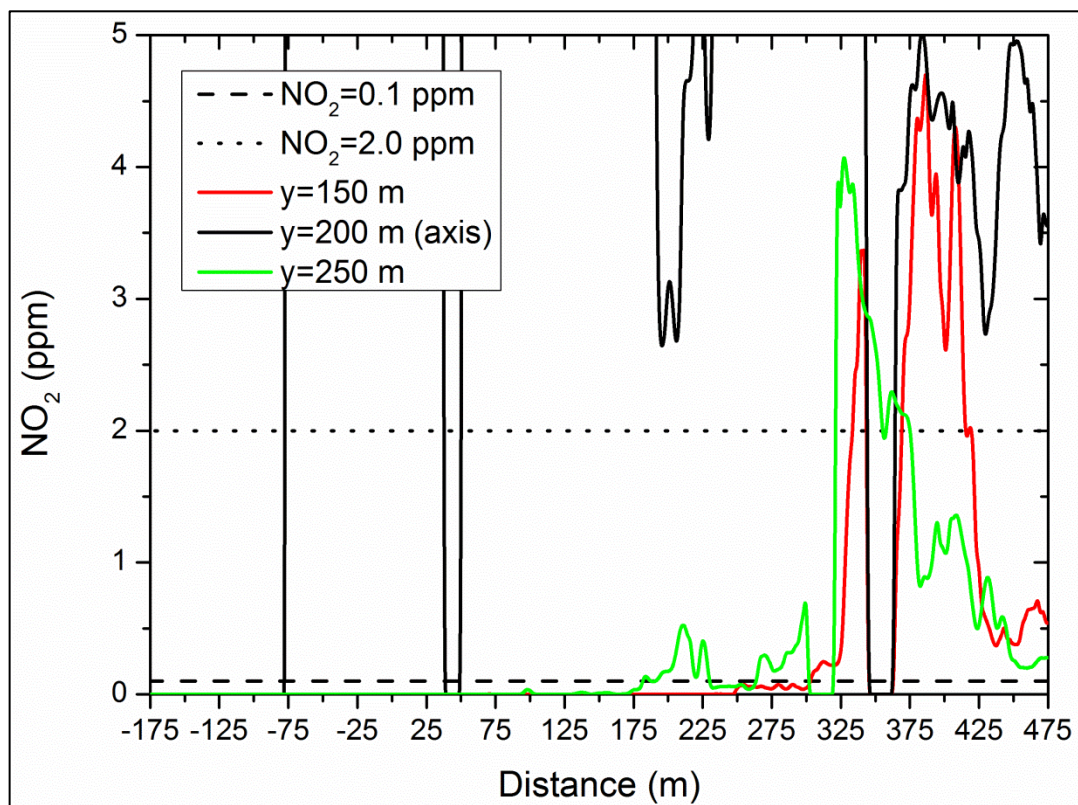


Figure 5.11 NO<sub>2</sub> concentration (ppm) as a function of distance at different positions y (zoom).



### 5.4.2 NH<sub>4</sub>NO<sub>3</sub> aerosol

Keeping track of the ammonium nitrate (NH<sub>4</sub>NO<sub>3</sub>) concentration in the numerical simulations is also important due to the potential health risks associated with it. Even though no clear evidence that direct exposure to NH<sub>4</sub>NO<sub>3</sub> can e.g. lead to untoward respiratory response has been reported in the past, the possibility of ammonium nitrate interacting with other pollutants to produce appreciable respiratory effects is still present [57]. Ammonium nitrate is a major component of atmospheric aerosols, and secondary NH<sub>4</sub>NO<sub>3</sub> particles from the reaction of gaseous ammonia (NH<sub>3</sub>) and nitric acid (HNO<sub>3</sub>) have been reported [58-59]:



Both the ammonia and nitric acid are very hazardous gases that can potentially cause serious health problems to people exposed to them. It has been suggested that the ‘worst case’ exposure concentration of NH<sub>4</sub>NO<sub>3</sub> for a 2-h period is approximately 200µg/m<sup>3</sup> (0.1 ppm) [60].

The NH<sub>4</sub>NO<sub>3</sub> concentration as a function of time at Stage 1, Stage 4 and Exit 1 are presented in Figures 6.12-6.13. Similarly to the NO<sub>2</sub> concentration presented before in Figures 6.8-6.9, the concentrations of the NH<sub>4</sub>NO<sub>3</sub> aerosol follow the same trends. The ‘worst case’ exposure concentration of 0.1 ppm is rapidly exceeded within 2 min and 4 min for Stage 4 and Stage 1, respectively. The concentrations of ammonium nitrate aerosol in these areas then remain relatively high and reach average values of 6.99 ppm and 2.96 ppm for Stage 4 and Stage 1, respectively (Figure 5.12). However, the conditions in Exit 1, shown in zoom in Figure 5.13, are significantly better. The instantaneous values of the NH<sub>4</sub>NO<sub>3</sub> aerosol concentration barely exceed the alarm level of 0.1 ppm and maintain an average value of 0.048 ppm. These conditions imply that people in Exit 1 will not be strongly affected by the NH<sub>4</sub>NO<sub>3</sub> aerosol.

The evolution of the NH<sub>4</sub>NO<sub>3</sub> aerosol concentrations with distance x at different location y are shown in Figures 6.14-6.15. Large values of ammonium nitrate near the source are evident (200 ppm) with decreasing trend as the downstream distance increases at y=150 m. This is natural since this location is on the axis of the toxic release where the highest concentrations are expected (Figure 5.14). These values exceed the ‘worst case’ exposure concentration of 0.1 ppm by far and render the area surrounding the source highly dangerous. The risk of deposition of NH<sub>4</sub>NO<sub>3</sub> in the Scheldt river is very high, increasing the risk of water contamination in the nearby area of Antwerp.

The NH<sub>4</sub>NO<sub>3</sub> concentrations at locations y=150m and y=250 m only start to be significant at downstream distances of x>175 m and reach high values towards the outlet of the computational domain (Figure 5.15). This behavior is of course related to the wind conditions present and the distance of the source from the festival area, and as explained before for NO<sub>2</sub>, it also reflects on the spreading of the toxic plume as well. What is observed is that the areas surrounding Stage 1 and Stage 4 receive high amounts of NH<sub>4</sub>NO<sub>3</sub> and are particularly danger for the people present in them. The relatively low levels of NH<sub>4</sub>NO<sub>3</sub> reported in Exit 1 (located at 272 m>x>230 m and 300 m>y>240 m) are also reflected in the results presented in Figure 5.15



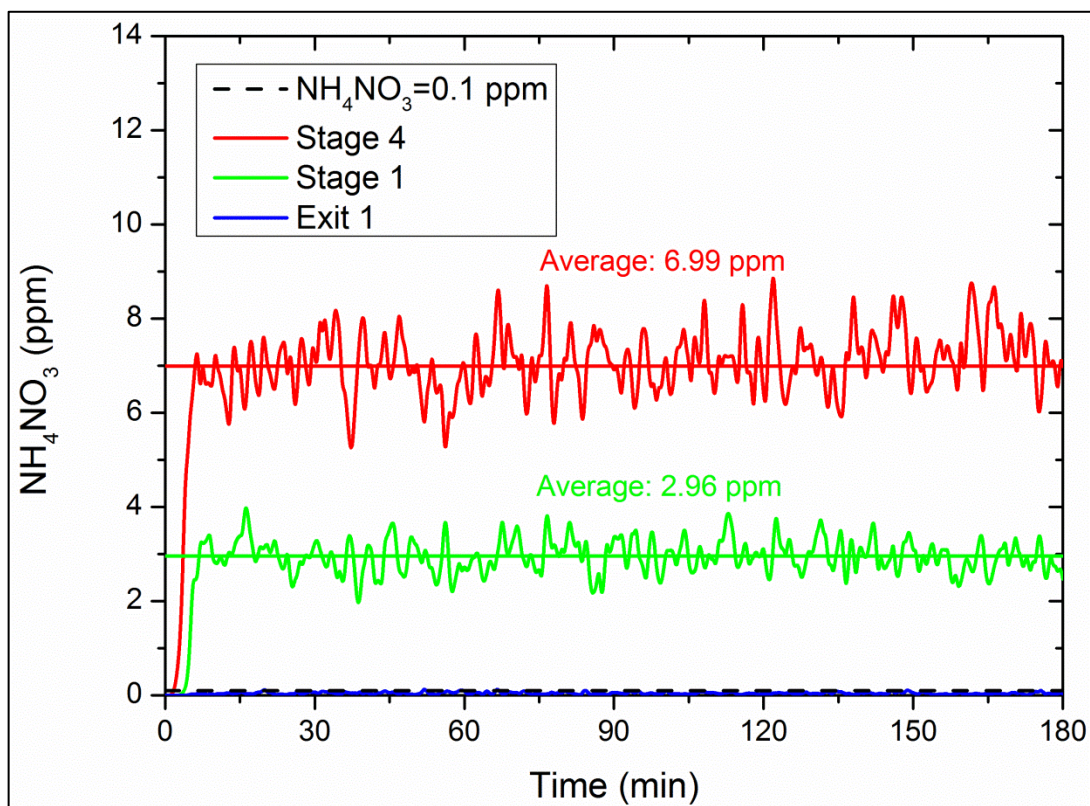


**Figure 5.12**  $\text{NH}_4\text{NO}_3$  concentration (ppm) as a function of time at Stage 1, Stage 4 and Exit 1.

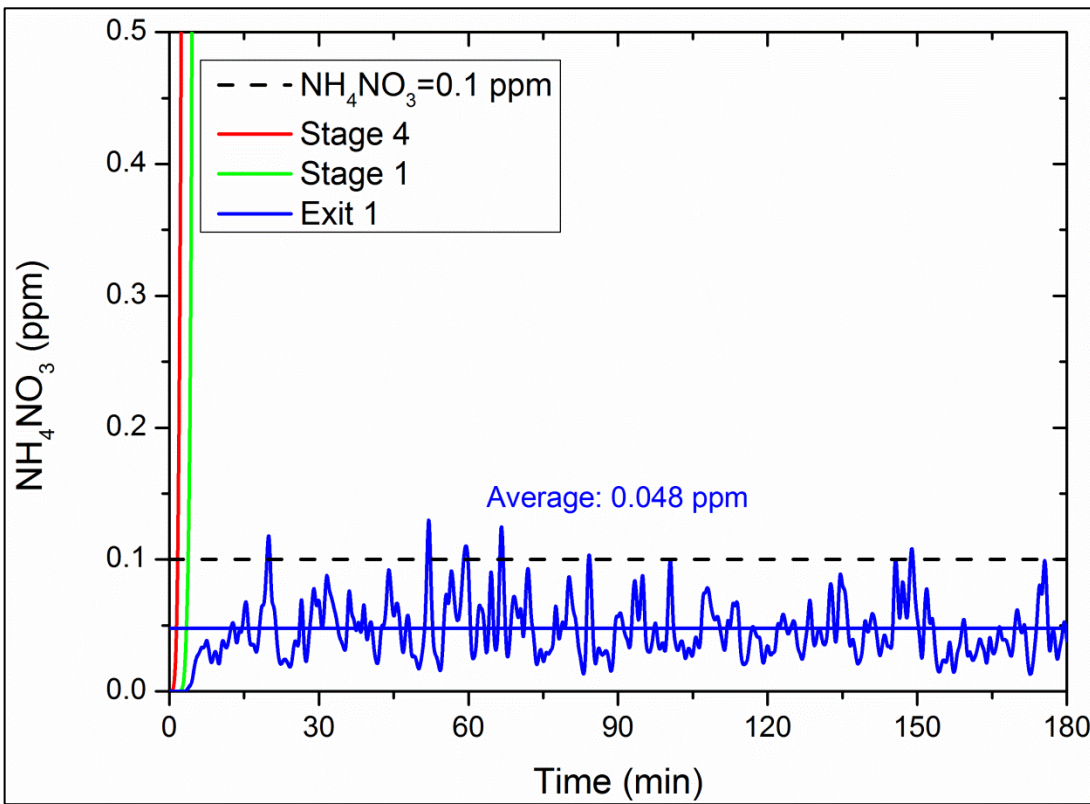


**Figure 5.13**  $\text{NH}_4\text{NO}_3$  concentration (ppm) as a function of time at Stage 1, Stage 4 and Exit 1 (zoom).



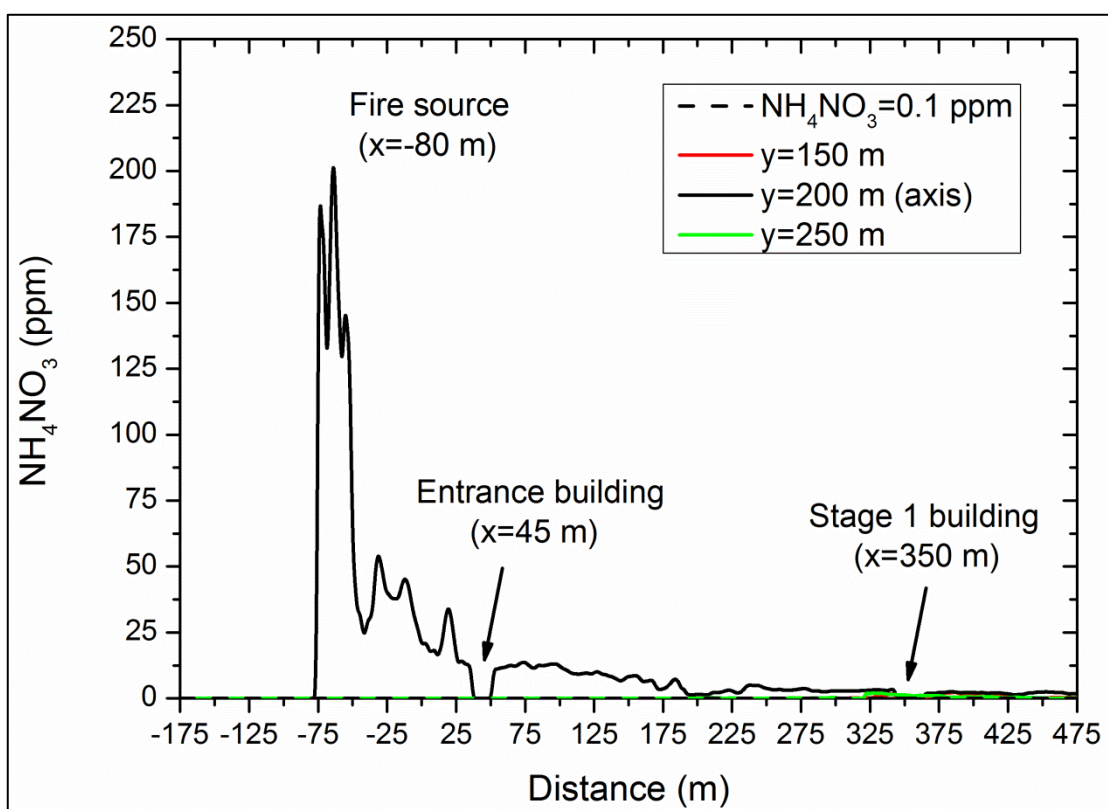


Figure 5.14  $\text{NH}_4\text{NO}_3$  concentration (ppm) as a function of distance at different positions  $y$ .

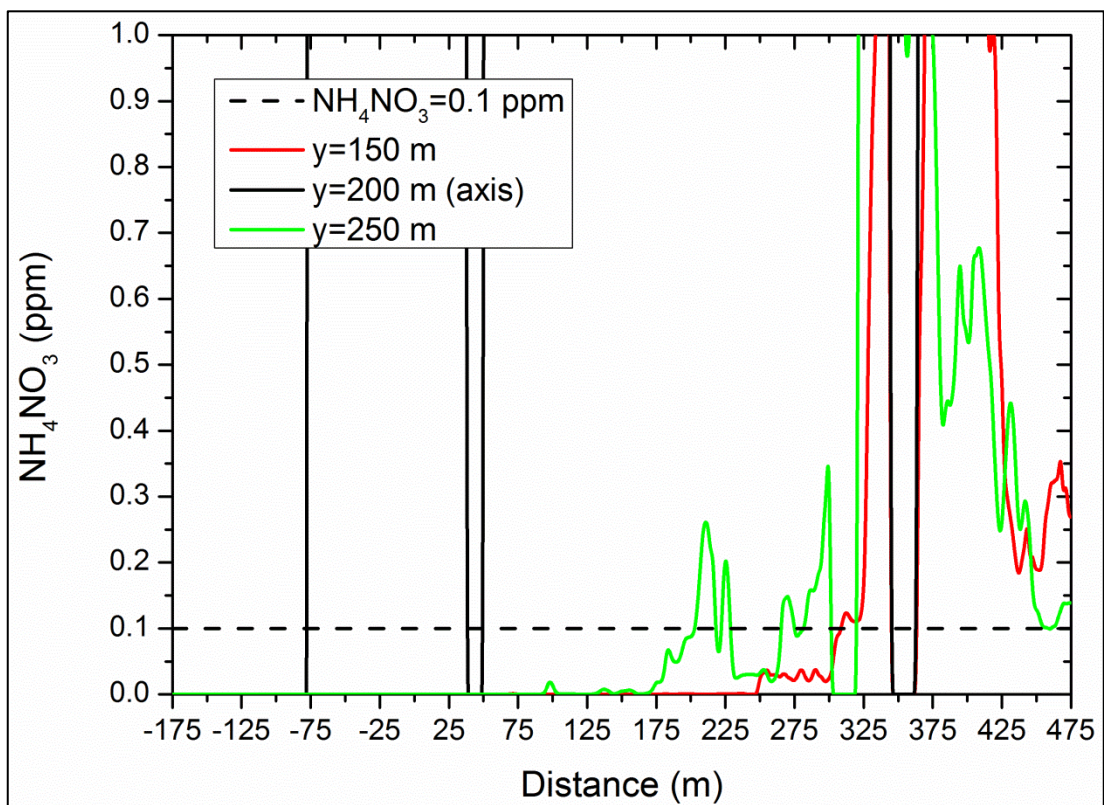


Figure 5.15  $\text{NH}_4\text{NO}_3$  concentration (ppm) as a function of distance at different positions  $y$  (zoom).



### 5.4.3 Fractional Effective Dose (FED)

The Fractional Effective Dose index (FED) is a commonly used measure of human incapacitation due to the combustion gases [28]. Generally values of FED that are less than 1 are considered safe for human people. This criterion is adopted in this study in order to determine whether the conditions in the music festival area are safe for the people to evacuate.

The Fractional Effective Dose (FED) is calculated as [29]:

$$FED_{total} = (FED_{NO_x} + FLD_{irr}) \times HV_{CO_2} + FED_{O_2} \quad (5.3)$$

The fraction of an incapacitating dose of  $NO_x$  is calculated as:

$$FED_{NO_x} = \int_0^t \frac{C_{NO_x}(t)}{1500} dt \quad (5.4)$$

where  $t$  is time (min) and  $C_{NO_x}$  is the sum of  $NO$  and  $NO_2$  concentrations (ppm).

The Fractional Lethal Dose (FLD) of irritants is calculated as:

$$FLD_{irr} = \int_0^t \frac{C_{NO_2}(t)}{F_{FLD,NO_2}} dt \quad (5.5)$$

where  $t$  is time (min), the nominator is instantaneous concentration (ppm) of  $NO_2$  and the denominator is the exposure dose of  $NO_2$  predicted to be lethal to half the population ( $F_{FLD,NO_2} = 1900 \text{ ppm} \times \text{min}$  ).

The hyperventilation factor caused by carbon dioxide,  $HV_{CO_2}$ , and the fraction of an incapacitating dose of  $O_2$  hypoxia,  $FED_{O_2}$ , are calculated the same way as previously described in Section 5.3 for the Mont Blanc tunnel festival scenario.

As expected, an increasing trend in the FED values is observed with time. Significant FED values above the limit of 1 are observed at Stage 1 and Stage 4 while they remain insignificant at Exit 1 (Figure 5.16). The criterion of  $FED > 1$  is exceed after 45 min in Stage 4 while after 137 min in Stage 1, making the conditions in these areas hazardous for the people present. These values are expected to become larger with increasing time above the 3 h of real time that is presented here. Nevertheless, the time at which the limit of 1 is exceeded is more important than the limiting value that will be reached in these areas, as it depicts the time after which hazardous conditions are present. These times also give an indication on how the conditions are in these areas and how safe people will be during the evacuation procedures employed. Similar observations are made by examining Figures 6.17-6.18, presenting the FED values as a function of distance  $x$  at different locations  $y$ . Large FED values are reported on the axis of the source ( $y=200 \text{ m}$ ) that reach up to 50, near the source, and decrease with increasing downstream distance  $x$ . At this location, FED values above or close to 1 are observed at all downstream distances from the source examined, revealing that it is not safe for people to be present in these locations for a very long amount of time, as they will be exposed to hazardous substances. At different locations  $y$  examined ( $y=150\text{m}$  and  $y=250\text{ m}$ ) the FED values only start increasing after  $x>250 \text{ m}$  but remain below the acceptable limit ( $FED < 1$ ) for all downstream distances.



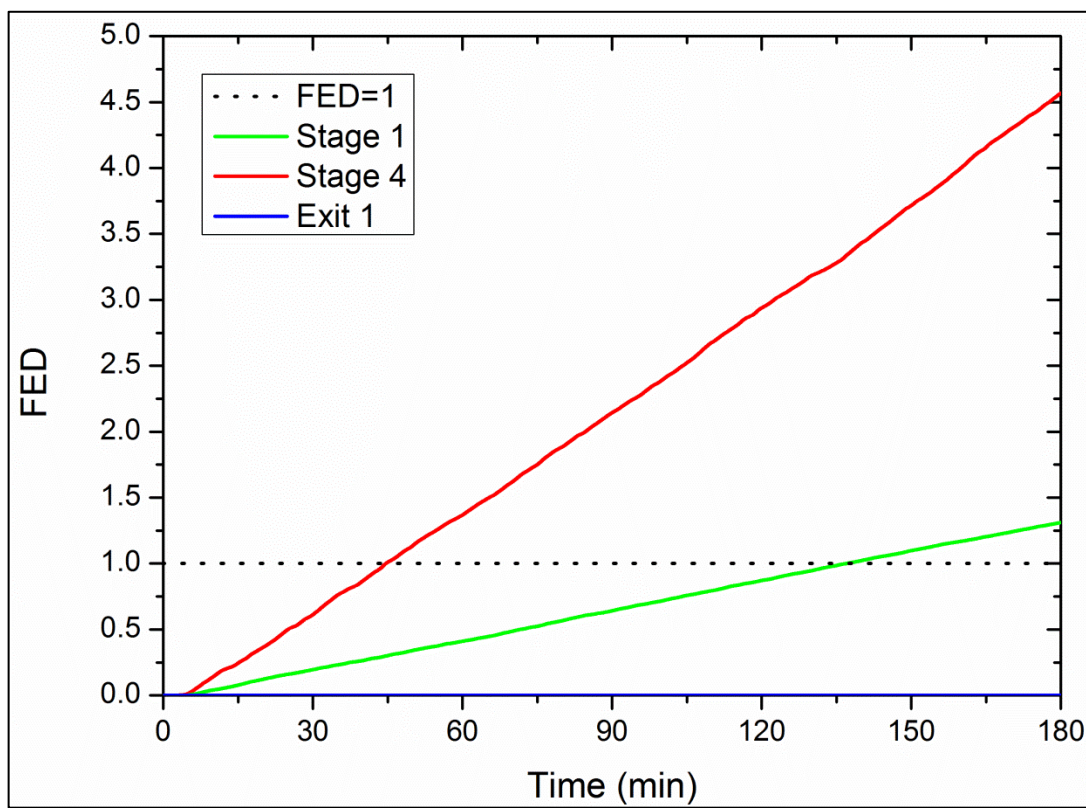


Figure 5.16 FED values as a function of time at Stage 1, Stage 4 and Exit 1.

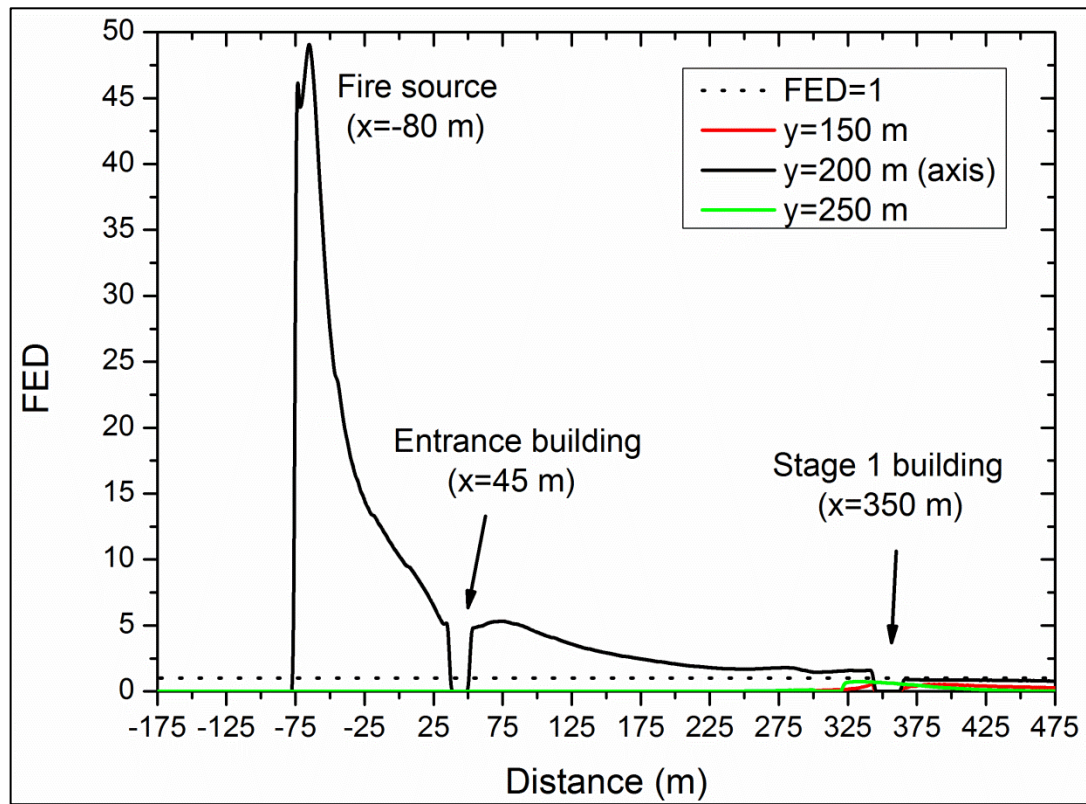
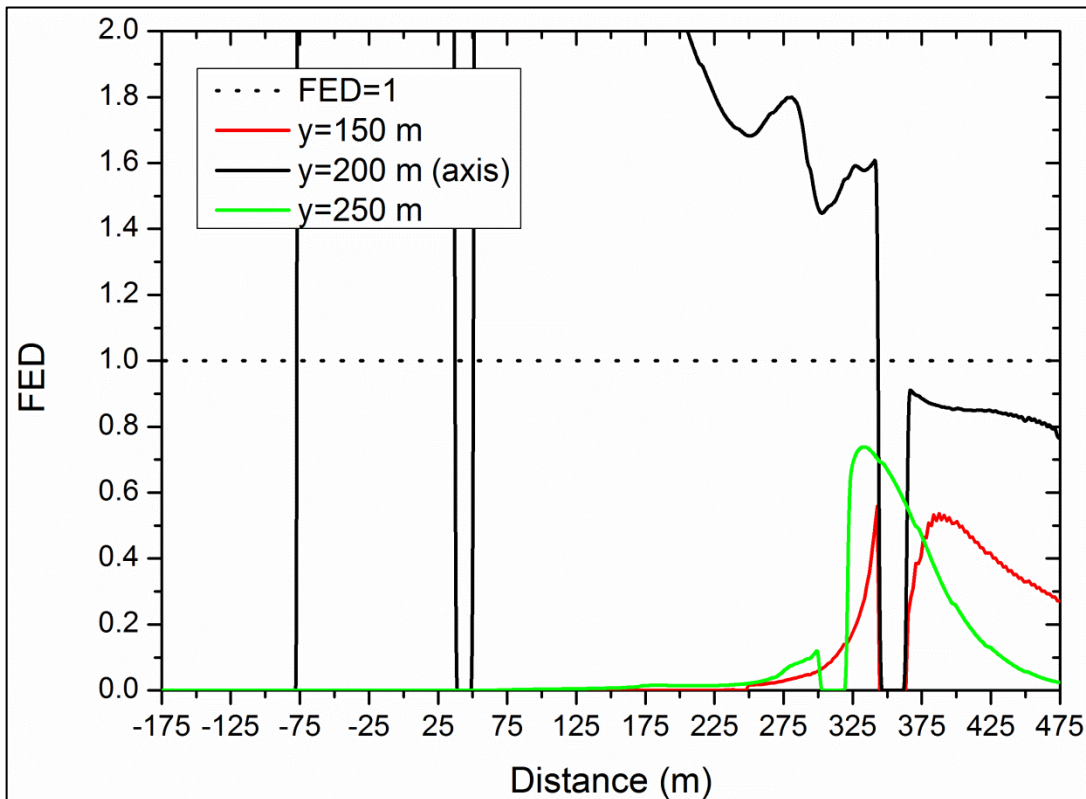


Figure 5.17 FED values as a function of distance at different positions y.





**Figure 5.18 FED values as a function of distance at different positions y (zoom).**

#### 5.4.4 Cascading effects

An overview of the initiating event, the different systems affected and their interdependency for the music festival scenario considered is presented below. Additionally, a qualitative presentation of the possibility of having cascading effects and the magnitude of the impact of the different scenarios considered in the numerical simulations is given in Table 5.4.

**Initiating event:** Accidental (fire in a tunnel).

**Originating system:** A ship.

**Dependent/Impacted system:** Human people (deaths, evacuation), festival and city infrastructure (possible damage due to detonation of  $\text{NH}_4\text{NO}_3$ ), traffic control (blocked traffic on the Scheldt river and in the city of Antwerp).

**Interdependencies:** Physical (ship), geographical (proximity of the human people and the infrastructure) and logical (traffic congestion in the Scheldt river and the city of Antwerp).

**Table 5.4 Possibility of cascading effects and magnitude of impact of the music festival scenario considered in the numerical simulations. Critical response time is  $\approx 40$  min.**

Possibility of cascading effects		Magnitude of impact	
$t < t_{\text{crit}}$	$t > t_{\text{crit}}$	$t < t_{\text{crit}}$	$t > t_{\text{crit}}$
Minimum	High	Average	High

Possibility of cascading events - Magnitude of impact: Minimum, Average, High.



From the numerical simulation of the music festival scenario, it was concluded that it is crucial for the festival organizers, fire services and local authorities to have a fast response to the accident. It is important to immediately organize a plan for the evacuation of people in the music festival and to deal with the fire in the ship at its early stages before it reaches the stage where a possible detonation of  $\text{NH}_4\text{NO}_3$  can occur. Based on the numerical simulation results, the critical time of response (for evacuation), based on the  $\text{FED} < 1$  criterion, is found to be approximately 40 min. If response occurs before this critical time limit then the possibility of having cascading effects is minimum, however, if the response occurs after this time limit then the possibility of having cascading effects is high.



## 6 Scenario: Wildfire – Skatås forest fire

### 6.1 Introduction

The Skatås forest is located around lakes Stora Delsjön and Lilla Delsjön east of the city of Gothenburg on the west coast of Sweden, Figure 6.1. The initial event was a forest fire, which was started by children who were playing with fire. The incident started in the forest area just north of the transition between the two lakes, Stora Delsjön and Lilla Delsjön. The red “x” in Figure 6.2 denotes the starting location of the incident. The initial impact was a forest fire which spread throughout the forested area.

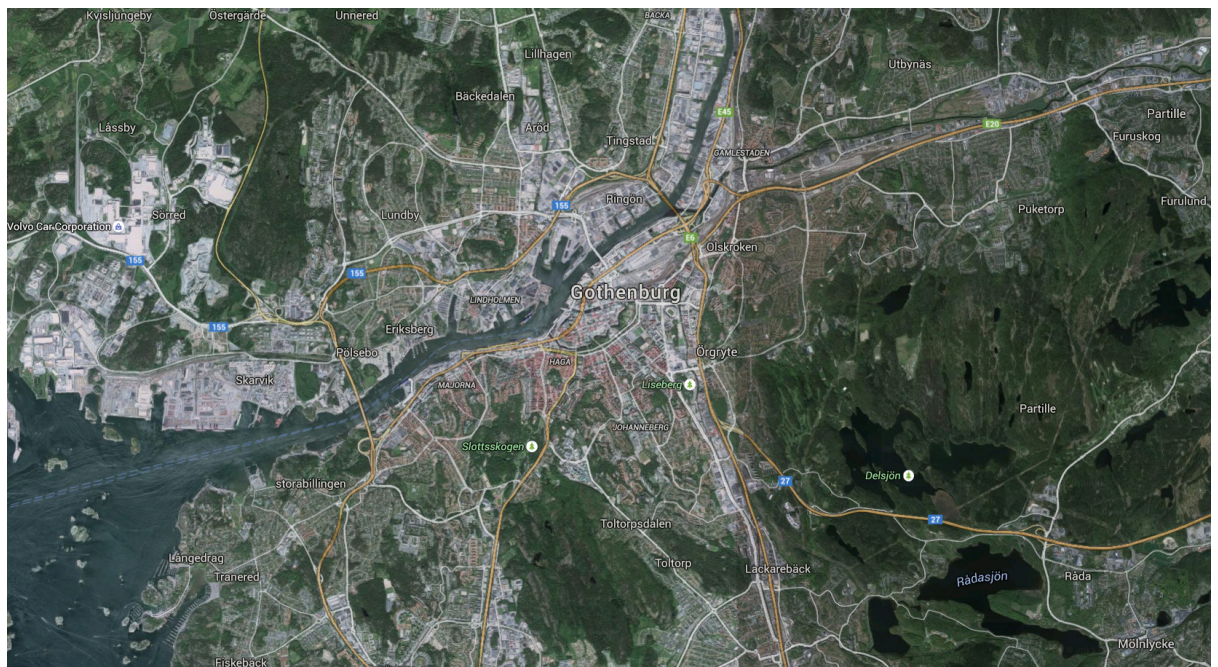


**Figure 6.1. The Skatås forest to the east of the city of Gothenburg and around the lakes Stora and Lilla Delsjön**



**Figure 6.2. The Skatås forest to the east of Gothenburg around the lakes Stora and Lilla Delsjön**

## 6.2 Description of the initial system including more details on the initial event

The two bodies of water are connected by a narrow channel. The two lakes and the surrounding forest are a popular destination for locals and tourists for water sports such as fishing, canoeing and kayaking, as well as hiking, running, mountain biking, picnicking and sunbathing.

The lakes are a part of the potable water supply for the city of Gothenburg and act as a reservoir for the city. Water is pumped to the lakes from the Göta älv, the river which flows into the estuary south of which Gothenburg is built.

South of the two lakes is the Riksväg 27 highway, which runs from the city out to the airport and then east towards the city of Borås. The Riksväg 27 is an important commuter and transportation highway for the region. South of the highway from Delsjön is a water treatment plant which treats the water in Stora Delsjön prior to distribution around the city. There is one other water treatment plant in the north of the city closer to the Göta älv.

There are dirt roads throughout the forest. These are mainly used for running, hiking and for mountain biking.

There is a telecommunications mast near to the location of the fires ignition. This includes a small office amongst other buildings as well as a mast which is 300 m high. The mast is anchored to the ground with steel cables, which also have hydraulic dampers. Although the area around the telecommunications mast is secure the vegetation does continue throughout the compound (see Figure 6.3).



**Figure 6.3. The telecommunications mast is located in a secure compound however vegetation does continue through the compound and the cables for the mast extend towards the perimeter**

There are also buried power lines within the forest. Although these were not affected by the fire there is a risk that they could have been damaged during either the fire or as a result of fire fighting operations.

The wind speed on the day of the incident was 15 m/s and the wind direction was SSE. The weather on the day of the incident was sunny and 15 °C. Before the event there had been a generally dry climate for a few weeks contributing to the low moisture content of the fuel and rapid fire spread. The total area directly affected by the fire was 2.88 km<sup>2</sup>. The wind direction and the approximate area directly affected by the fire are shown in Figure 6.2.

The first call to the emergency services was made at 11:24 local time on the 29<sup>th</sup> of April in 2008. The incident occurred after several weeks of dry weather. The point of ignition was at the transition between the two lakes of Stora Delsjön and Lilla Delsjön. The point of ignition is about 2.8 km from the city of Gothenburg.

### **6.3 Description of cascading effects, types of dependencies, systems involved after the spread from the initial system**

In this section we list interdependencies as they exist. Some of these did not contribute to the chain of events or the impact of the incident because of the initial conditions, however they are listed here for completeness.

The following geographical interdependencies exist in the possible chain of events and impact of the system:

- Between the forest and the telecommunications mast
- Between the forest and the public who may have been using the area for recreation
- Between the forest and the hospital
- Between the forest and the city of Gothenburg
- Between the forest and the electrical cables buried underground
- Between the forest and the lakes Stora Delsjön and Lilla Delsjön
- Between the forest and the Riksväg 27 highway (or other roads)

The following physical interdependencies exist in the possible chain of events and impact of the system:

- Between the lakes Stora Delsjön, Lilla Delsjön and the city of Gothenburg
- Between the electrical cables buried underground in the forest and the city of Gothenburg



- Between the Riksväg 27 highway and Landvetter airport
- Between the Riksväg 27 highway and commuter towns and cities
- Between other roads and the community in the city of Gothenburg

The following logical interdependencies exist in the possible chain of events and impact of the system:

- Between the power lines buried underground and infrastructure in the city of Gothenburg
- Between the telecommunications mast and infrastructure in the city of Gothenburg

## 6.4 Real consequences and possible consequences

The real consequences of the incident were limited.  $2.88 \text{ km}^2$  of the forested area was affected by the fire, and one fire fighter was injured. There was no interruption to service in the hospital or the telecommunications mast, however workers at the telecommunications mast were evacuated and the hospital did close external ventilation and make plans for evacuation.

Possible consequences include:

- injuries to members of the public
- contamination of the drinking water supply
- ecological damage
- interruption to usability of the Riksväg 27 highway
- damage to the Riksväg 27 highway
- damage to the telecommunications mast and interruption to or reduced telecommunications service
- evacuation of the hospital as a result of smoke spread over the urban area, interruption to provision of medical care as a result of reduced number of hospital beds and surgical theatres
- damage to power lines and interruption to power supply to some neighborhoods
- social consequences including reduced access, delays in collecting children from day care or returning home from school or work
- evacuation of residential areas
- spread of the fire to the wildland urban interface and subsequent damage to property

All of these possible consequences were prevented by either the actions of the fire and rescue service or the conditions (wind conditions) on the day.

## 6.5 Modelling of wildfires

Empirical, semi-empirical and physics based models of forest fires have been under development since 1940 [61]. Empirical models or conceptual models from experience and intuition from past fires can partly be used to anticipate fires in the future and can thus provide with valuable information regarding fighting woodland fires. Most semi-empirical fire spread equations have been developed for Australasian fuel complexes that can be used for quick estimation of fundamental parameters of interest such as fire spread rate, flame length, and fire intensity of surface fires. A number of key assumptions are built in to these semi-empirical models such as, assuming a representative location, wind and terrain slope.

More complex models where the two-dimensionality of fire spread is taken into account have been developed, such as FARSITE [62] and Prometheus [63], for Canadian conditions. Here semi-empirical relationships regarding ground-to-crown transitions to calculate fire spread and



other parameters along the surface are considered however the model relies on the Huygens principle of wave propagation to shape the fire growth.

The most complete models combine CFD models with a wildfire components while allowing the fire to have a feedback loop with the atmosphere. These models include NCAR's Coupled Atmosphere-Wildland Fire-Environment (CAWFE) model [64], WRF-Fire at NCAR and University of Colorado Denver [65] which combines the Weather Research and Forecasting model with a spread model using the level set method, University of Utah's Coupled Atmosphere-Wildland Fire Large Eddy Simulation [66], Los Alamos National Laboratory's FIRETEC [67] and the WUI (Wildland Urban Interface) Fire Dynamics Simulator (WFDS) [68]. All these complex modelling tools have different emphases and have been applied to better understand the fundamental aspects of fire behaviour. In Ref. [67] the fuel in homogeneities on fire behaviour was investigated and in [69-70] the feedback between the fire and the atmospheric environment as the basis for the universal fire shape. Presently complex modelling is applied to the wildland – urban interface where fire spread on a community scale is achievable.

In this particular work the wildfire modelling has been performed using the extended WFDS (Wildland Urban Interface FDS) built on the regular FDS model described earlier in this report [68, 71]. WFDS was originally created for simulating stationary outdoor fires however, starting with the 5th official release of FDS, WFDS was expanded to contain routines which are aimed at predicting wildland fire scenarios [72]. The effect of the solid fuel such as wood, grass, pine needles i.e. vegetation is represented by a series of correlations [71-72]. This includes representing phenomena such as heat sources and sinks from the solid as well as the mass flow of pyrolysis gases from the solid. The physics for the gas phase is solved by the regular FDS. The model will hereafter be referred to as WFDS. The Skatås wildfire occurred over an extended area which means that some simplifications are needed in order to have a tractable model. The present approach is a coarse graining process, starting with a single tree burning including pyrolysis and detailed thermal modelling on a rather small grid, and then making simplifications to be able to consider a large area with randomly distributed trees on a coarse grid. In this process we will consider a meso-scale model with approximately 100 identical trees randomly distributed over approximately 1200 m<sup>2</sup> while keeping a simplified combustion model. Furthermore, in order to model a large area of the size of the scenario containing thousands of trees, bulk obstructions with tree properties are created that are larger than regular trees however they contain the same amount of fuel and also representing a similar impedance to the flow of hot gases created by the wind and the fire. In WFDS, two approaches for modelling vegetation have been developed which are called the fuel element and the boundary fuel models. The fuel element method can be used to represent surface or raised vegetation. The boundary fuel method is used to represent surface fuels only and was designed to operate at coarser grid resolutions than the fuel element model. The current version of WFDS uses fuel elements to represent vegetation. The boundary fuel element was used in earlier versions of WFDS and is being added to the current version.

## 6.6 WFDS model and input

One particular difficulty in wildfire CFD modelling is treating the interaction between vegetation and the turbulent flow of the gas phase components. In WFDS, the effect of the vegetation on the solution of the momentum equation is represented in the form of a body force (Fd), called the drag force [73, 74], which approximates the drag created by vegetation. The second particularity with WFDS is the use of the fuel model. In the fuel model the following parameters have to be set:



- VEG BULK DENSITY: Bulk density of vegetation in kg/m<sup>3</sup>. Default is 0.3 kg/m<sup>3</sup>. This can be determined from field measurements of the fuel loading (kg/m<sup>2</sup>) divided by the height of the vegetation (m). It is the mass of dry vegetation divided by the bulk volume containing that vegetation.
- VEG BURNING RATE MAX: Maximum value allowed for the rate that fuel gases can be created per unit volume in a grid cell, kg/(m<sup>3</sup>s). Default is 0.4 kg/(m<sup>3</sup>s), based on Douglas fir tree burning experiments. For some problems this bound is needed to avoid too rapid of a burning rate. Whenever possible it should be based on experimental measurements.
- VEG CHAR FRACTION: Fraction of virgin dry virgin vegetation that becomes char. Default value is 0.25.
- VEG DEHYDRATION RATE MAX: Maximum value allowed for the loss of moisture during the thermal degradation of the vegetation in kg/(m<sup>3</sup>s). Default is 0.5 kg/(m<sup>3</sup>s).
- VEG DENSITY: Density of vegetative fuel in kg/m<sup>3</sup>. Default is 540 kg/m<sup>3</sup>.
- VEG DRAG COEFFICIENT: Non-dimensional multiplicative factor used in the drag model. Default value is 1.
- VEG INITIAL TEMPERATURE: Initial temperature of vegetation in °C. Default value is 20 °C or TMPA which is set in the MISC namelist (see FDS user guide about TMPA).
- VEG MOISTURE: Fraction of moisture on a dry mass basis (mass of moisture in vegetation / dry mass of vegetation). Default value is 10.
- VEG REMOVE CHARRED: Either .TRUE. or .FALSE., default is .TRUE.. Specifies if, once the thermal degradation has reduced the vegetation to pure char, the fuel element should be removed
- (.TRUE.) or kept. If the vegetation is kept then it participates in the computation as a source of drag and head sink (or source) through radiative and convective heat transfer. Currently the thermal degradation model does not include char oxidation (smoldering combustion).
- VEG SV: Surface-to-volume ration of the vegetation element in 1/m. Default value is 4000 1/m.

In general detailed measurements have been performed for the particular trees in the region of interest however there are a few studies already present such as the NIST Douglas fir tree experiments [73] that will be used in the current model.

## 6.7 Single burning tree model

The single burning tree model uses the fuel element model in WFDS where an ignitor fire starts a fire on the ground a few meters from the tree. The HRRPUA of the fire is 260 kW/m<sup>2</sup> on 0.2 m x 2.0 m area. This case is built on the example files available for the WFDS [73, 75] however it is customised to northern European condition in terms of moisture content etc. the vegetation data of the tree crown is based on results in Ref. [73].

The WFDS input variables for our model are summarized here for ground element such as grass:

- VEG\_SV=4000,
- VEG\_MOISTURE=0.17,
- VEG\_CHAR\_FRACTION=0.20,
- VEG\_DRAG\_COEFFICIENT=0.375,
- VEG\_DENSITY=514,
- VEG\_BULK\_DENSITY=0.626,



- VEG\_BURNING\_RATE\_MAX=0.45,
- VEG\_DEHYDRATION\_RATE\_MAX=0.45.

However, the tree will be considered pine trees with properties according to Ref. [73].

In Figure 6.4 and 6.5 snapshots of the model are shown. The tree with an ignitor fire to the left is displayed. Utilizing this model while varying the grid size from 10 cm x 10 cm x 10 cm to 5 cm x 5 cm x 5 cm yield a slight differences however as is displayed in Figure 6.6 the moisture content of the ground material (grass) is rather important for the fire spread rate. This effect will be important in modelling a larger scenario where the fire will consume the ground material as it progresses yielding a fire spread time constant that differs with moisture content. Note ground vegetation with large surface to volume fraction as used for Australian grass (VEG\_SV) may burn too fast to allow for ignition of trees, c.f. the green line in Figure 6.6.

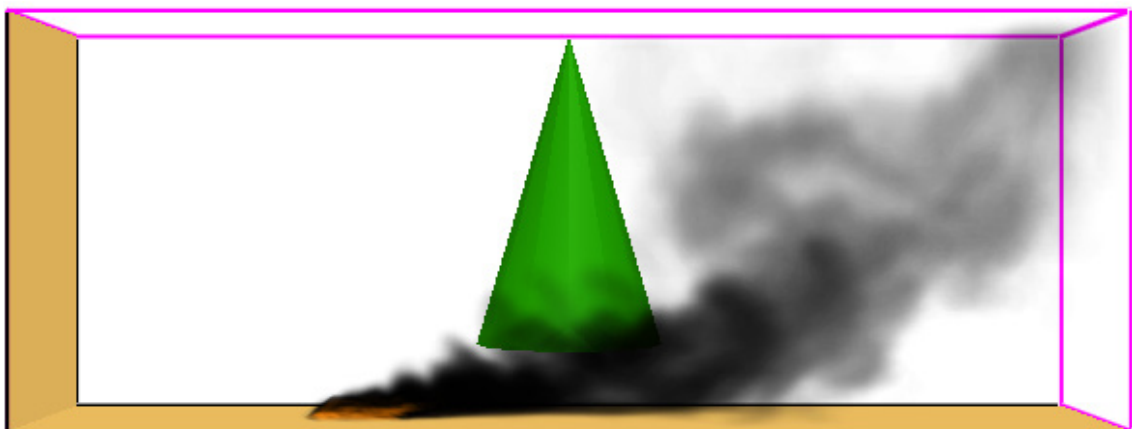


**Figure 6.4 The geometry of the tree with an ignitor fire on the left with grass material on the ground.**

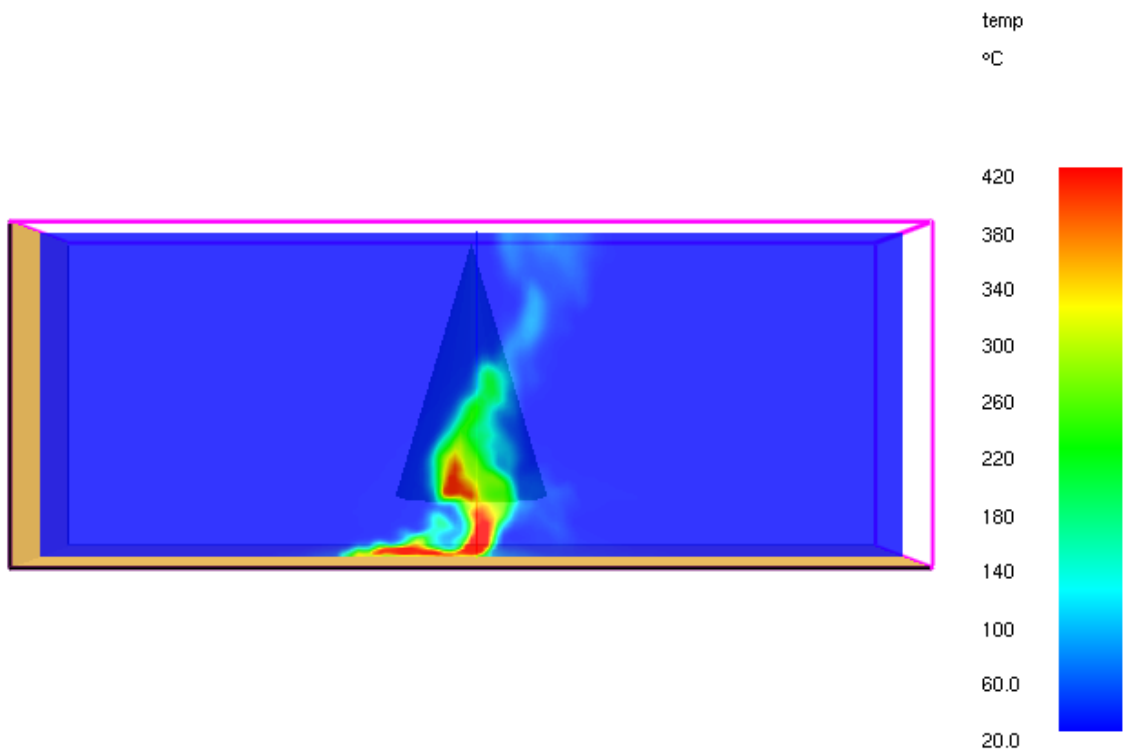


**Figure 6.5** A snapshot of the temperature distribution after 31s where the fire has started consuming the tree.

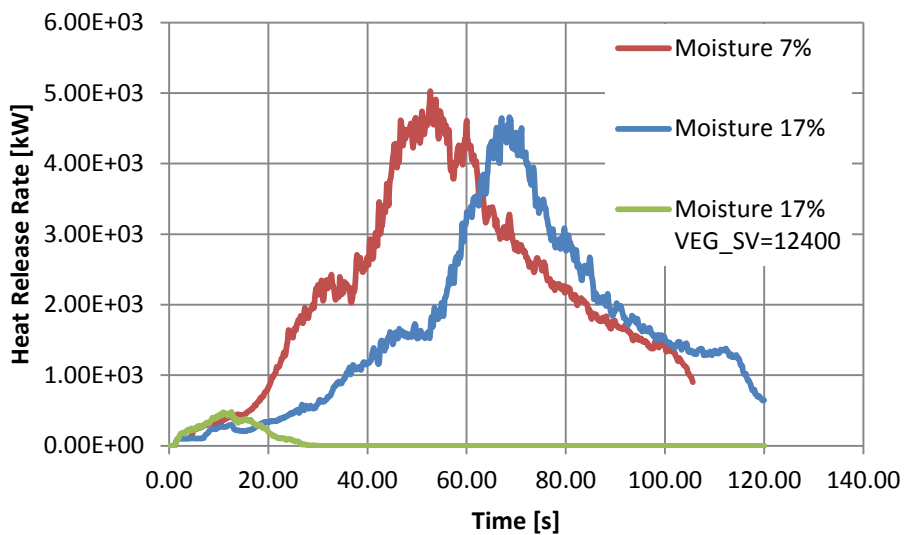


**Figure 6.6** The heat release rate as a function of time for varying degree of moisture content.

## 6.8 A field of several burning trees

The field is populated with 93 randomly placed identical trees in a domain that is 40 m x 32 m x 20 m. All trees are 6m high and the base of the crown is 3m wide with grass covered ground. The physical properties are similar to those used in the single tree model of 7.7. A wind with velocity 2 m/s in the positive x direction is applied on the surface at minimum x.



Every single tree is modelled using the same properties as follows:

- VEG\_INITIAL\_TEMPERATURE=20.,
- VEG\_SV=4000., VEG\_MOISTURE=1.0,
- VEG\_CHAR\_FRACTION=0.25,
- VEG\_DRAG\_COEFFICIENT=0.375,
- VEG\_DENSITY=520.,
- VEG\_BULK\_DENSITY=2.2,
- VEG\_BURNING\_RATE\_MAX=0.4,
- VEG\_DEHYDRATION\_RATE\_MAX=0.4,
- VEG\_REMOVE\_CHARRED=.TRUE..

Where the stem is modelled separately as

- VEG\_SV=3., VEG\_MOISTURE=1.0,
- VEG\_DRAG\_COEFFICIENT=0.375,
- VEG\_DENSITY=520.,
- VEG\_BULK\_DENSITY=520.

In Figure 6.7 the geometry of the forest is displayed including trees and ground vegetation. In Figure 6.8 a snapshot of the temperature distribution in the small part of the forest after 36 s is displayed. Here it is observed that an increased moisture level prolongs the fire spread using a 0.5 m x 0.5 m x 0.5 m grid however larger grids may have a much smaller heat release rate compared to the current simulation since the average temperature of the larger cells will be smaller meaning that the trees will not catch fire and only the ground vegetation will be completely burnt out. Decreasing the grid only has a limited effect on the results. This may be very important for the large wildfire scenario since only a coarse grid will be practical to use.

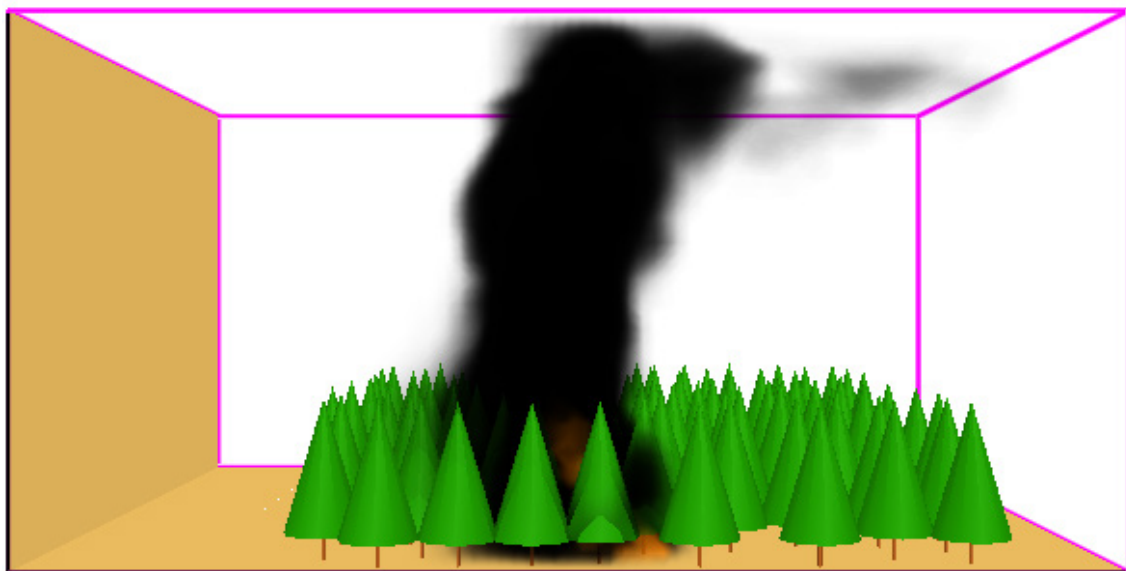


**Figure 6.7 The geometry of the field with randomly distributed trees.**

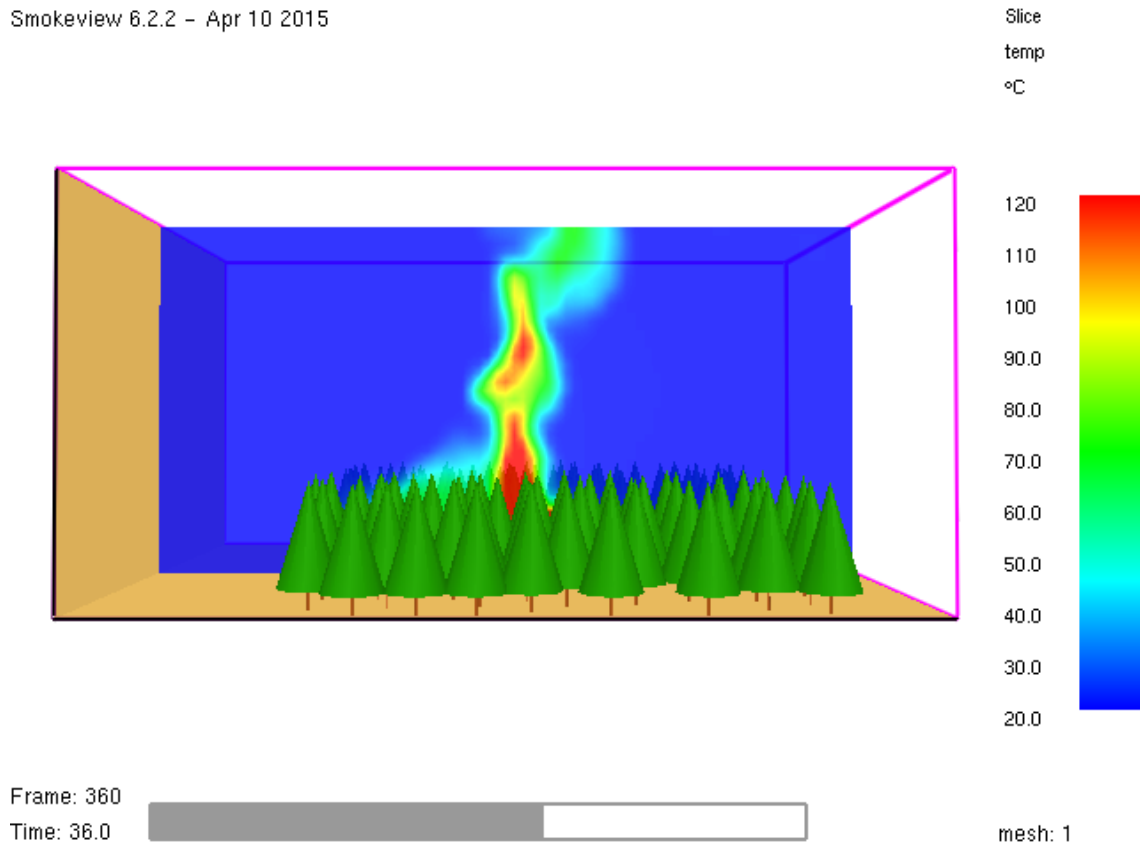


**Figure 6.8** A snapshot of the temperature slice file.

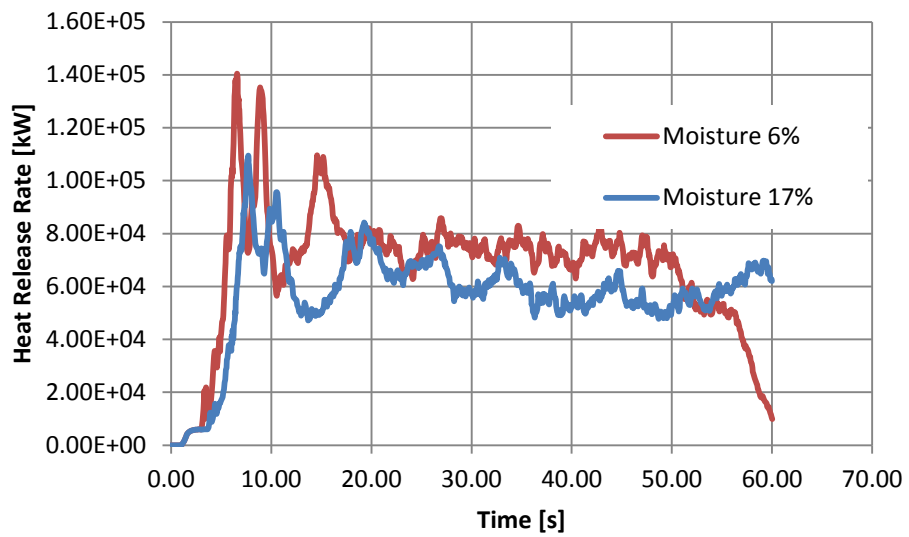


**Figure 6.9** The heat release rate as a function of time for two different values of the moisture content.

## 6.9 The wildfire scenario

The wildfire scenario is modelled using a similar approach as in section 6.7 and 6.8 however the natural amount of trees is impractical to implement as well as requiring very small grid sizes in



comparison to the size of the model. In the scenario a slope upwards to the telecom tower is presently modelled through different levels in the models where ground vegetation is present on all surfaces even the vertical surfaces. Using a 2m x 2m x 2m grid results in no fire spread at all since the grid is too coarse whereas halving the grid seems to support fire spread. One other important factor is the tree density; the tree density will affect the flows and wind close to the ground and may obstruct the fire spread. To illustrate this we have set-up a model including 5000 trees on a 100 m x 200 m piece of land covered by grass c.f. Figure 6.10, 6.11 and 6.12. Although a fire starts using an ignitor fire for 27s and spread with the wind for a while it later stops due to flow interference caused by the density of the trees, see the time evolution of the heat release rate in Figure 6.13. A comparison is done for lowered moisture content as well increased VEG\_SV as used for Australian grass. Note that there is plenty of combustible material left to burn in the high moisture content case whereas in the low moisture content case most of the trees take part in the fire.

Smokeview 6.2.2 - Apr 10 2015

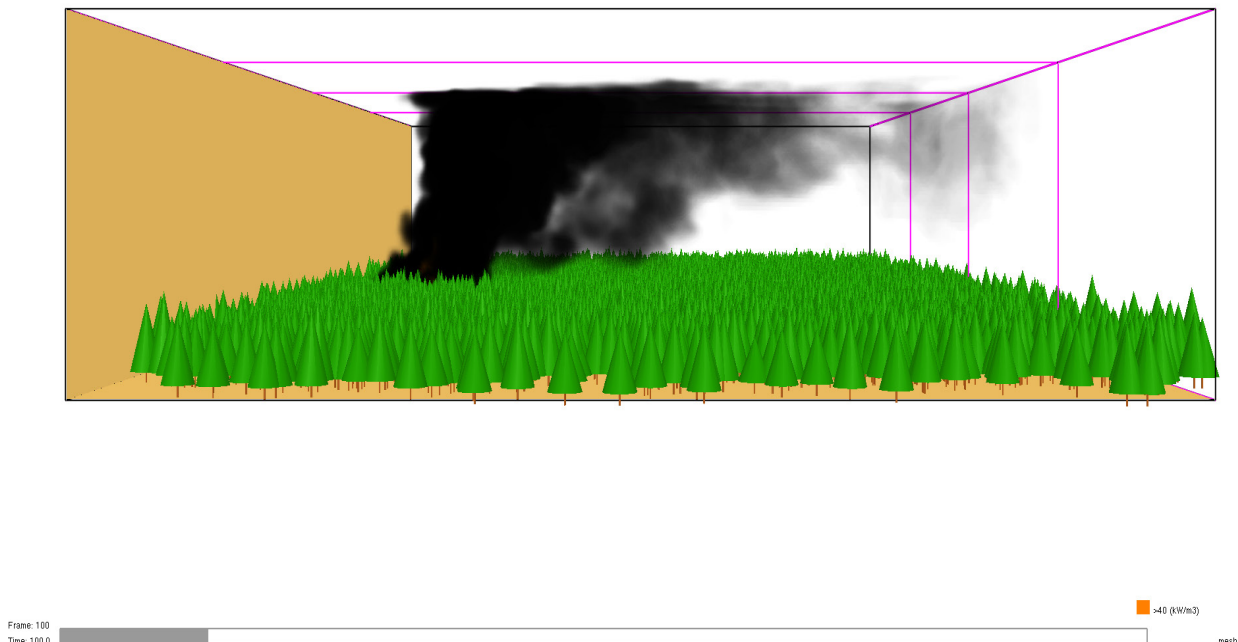


**Figure 6.10 A medium sized model 100mx200mx30m with 5000 randomly distributed trees.**

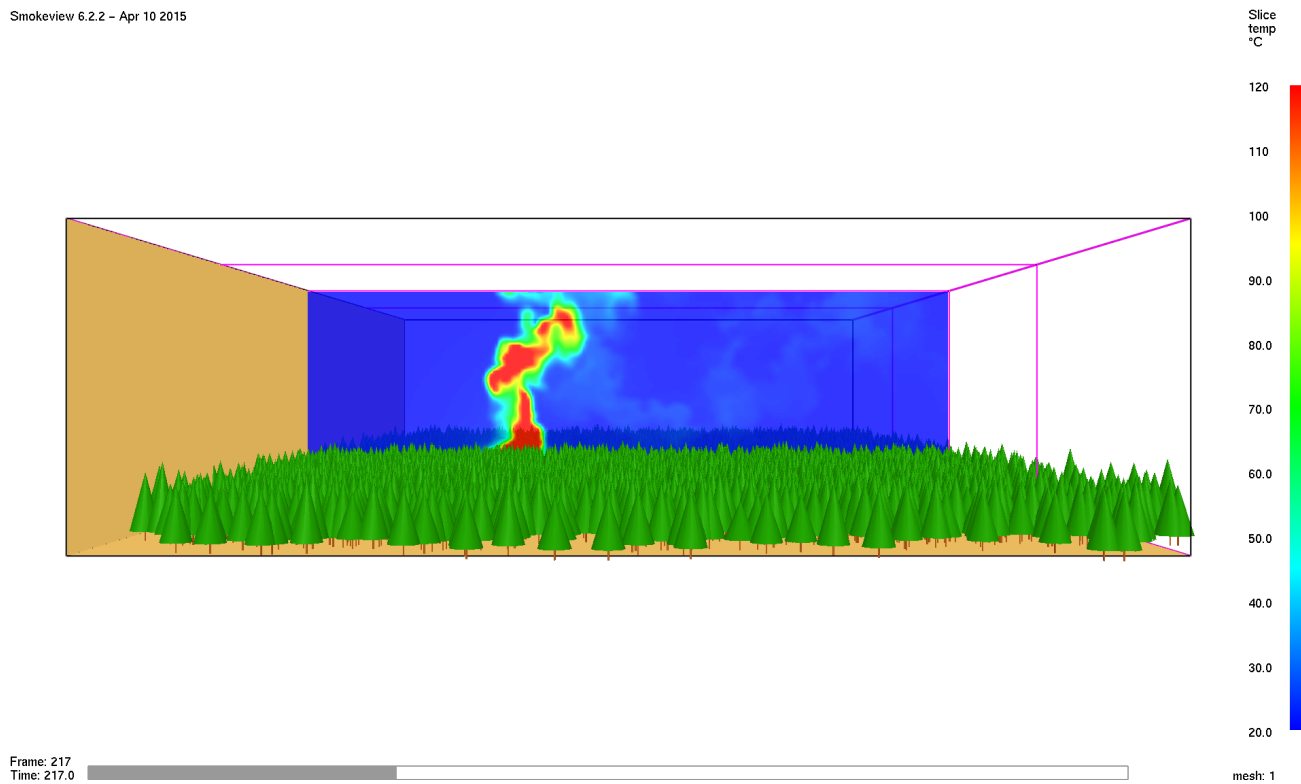


**Figure 6.11** A snapshot of the temperature after 217s with moisture content 17%.

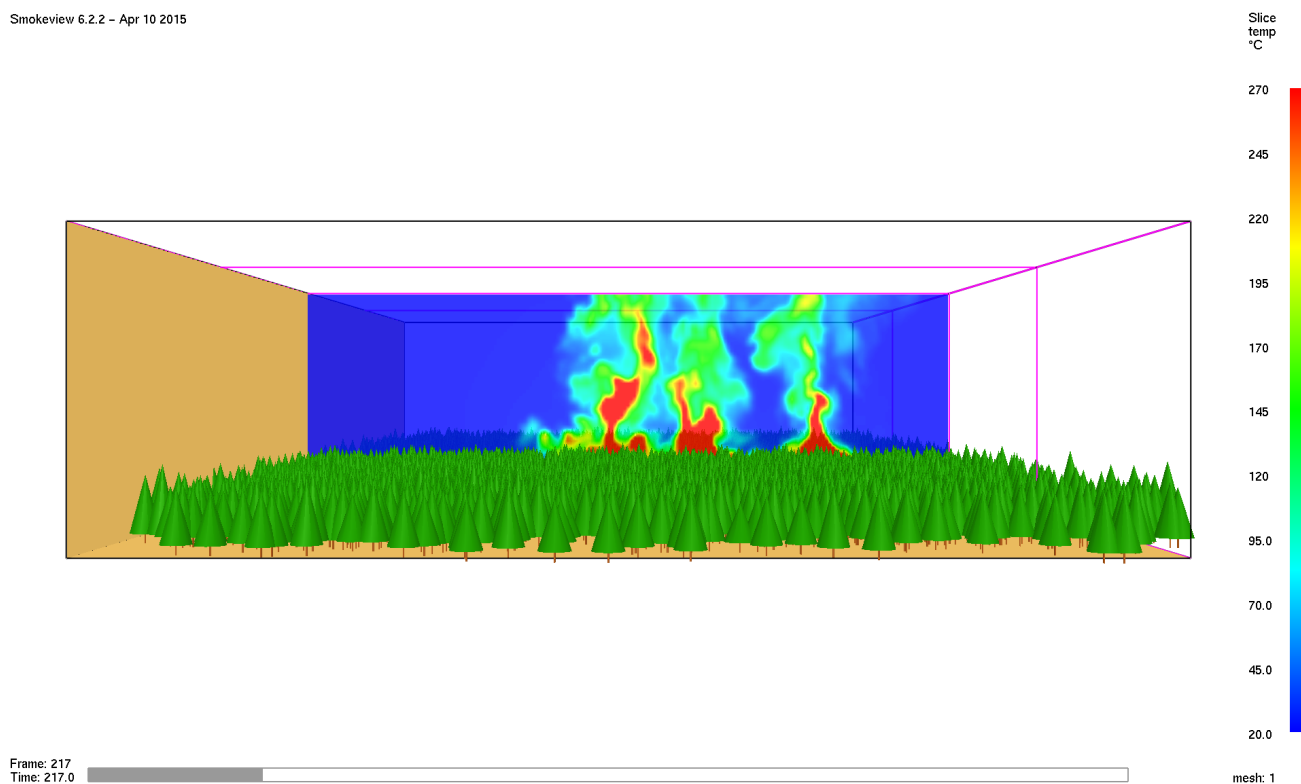


**Figure 6.12** A snapshot of the temperature after 217s with moisture content 6% and VEG\_SV = 12240 which is relevant for Australian grass ground material.



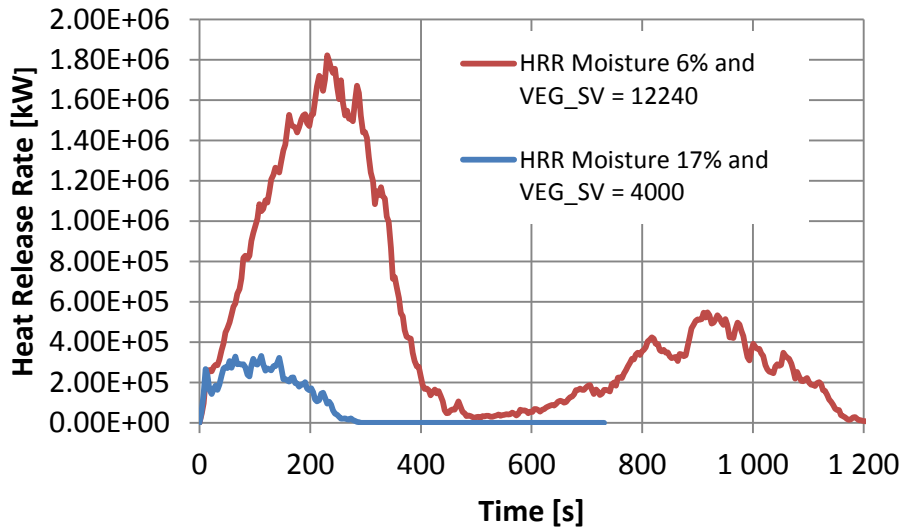


**Figure 6.13** A comparison of the heat release rate as a function of time.

The next step is to model the proximity to the telecom mast in order to investigate the possible adverse effects of the forest fire on the mast itself but also on the cables with hydraulic dampers to the tower that may be affected earlier in the development. The telecom mast is visible in Figure 6.14 in the model as a thin tower that measures 2 m x 2 m x 30 m.

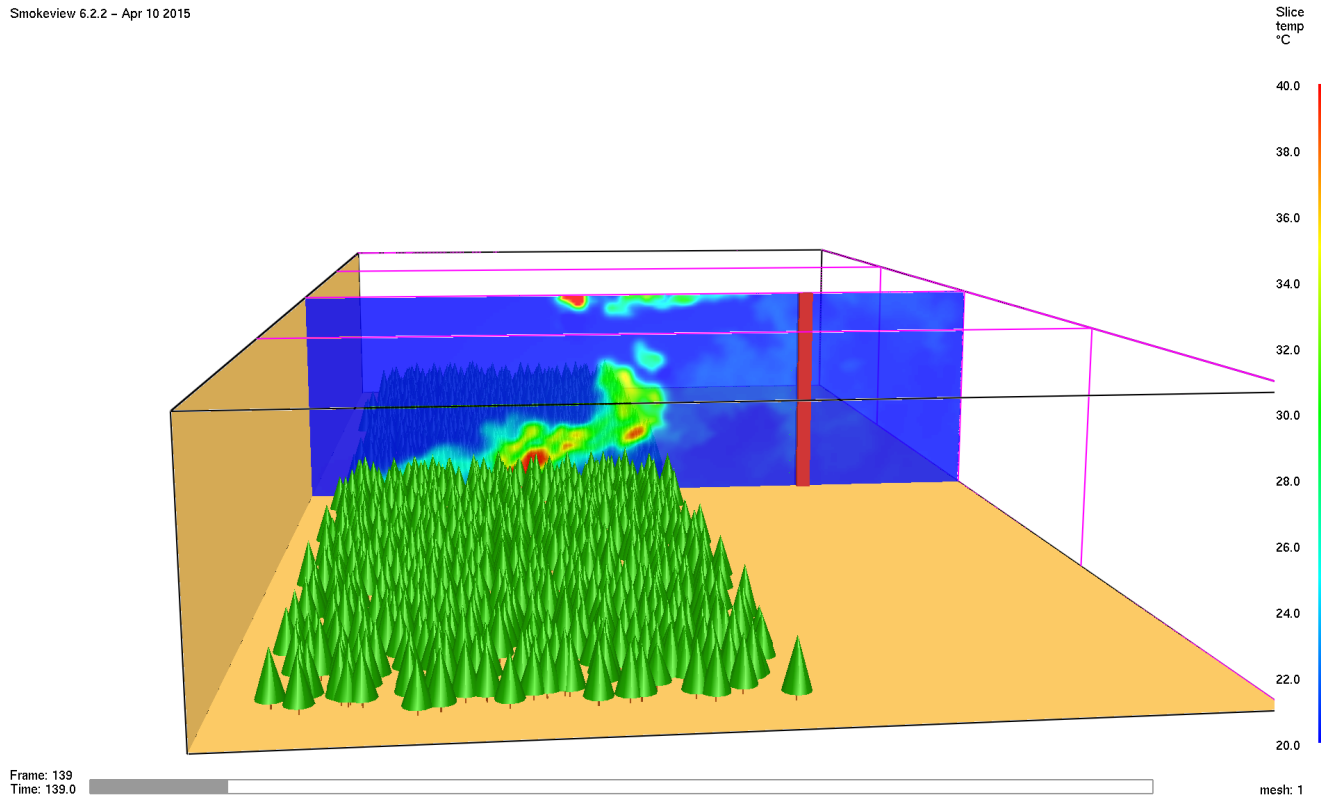


**Figure 6.14.** The model of the neighbourhood of the telecom mast.



The model is similar in size as the previous medium scale forest fire however the area around the tower is cleared trees. It should be noted that the tree density is around half of the density of the previous model. Due to stability problems with the model the wind speed is only 2 m/s however in the actual scenario it was around 15 m/s this may cause hot gases to pass close by to the tower. In this model the cleared safety distance from the forest was large enough to keep down the temperatures in the vicinity of the tower.

One large model was created that spanned approximately 1000 m x 200 m x 120 m where the height is increased along the slope up to the telecom mast. The telecom mast is visible in Figure 6.15 in the model as a thin tower that measures 2 m x 2 m x 30 m.

One further simplification is to utilize larger but fewer trees however this may have an impact on the fire spread and in future studies this simplification has to be more closely evaluated.

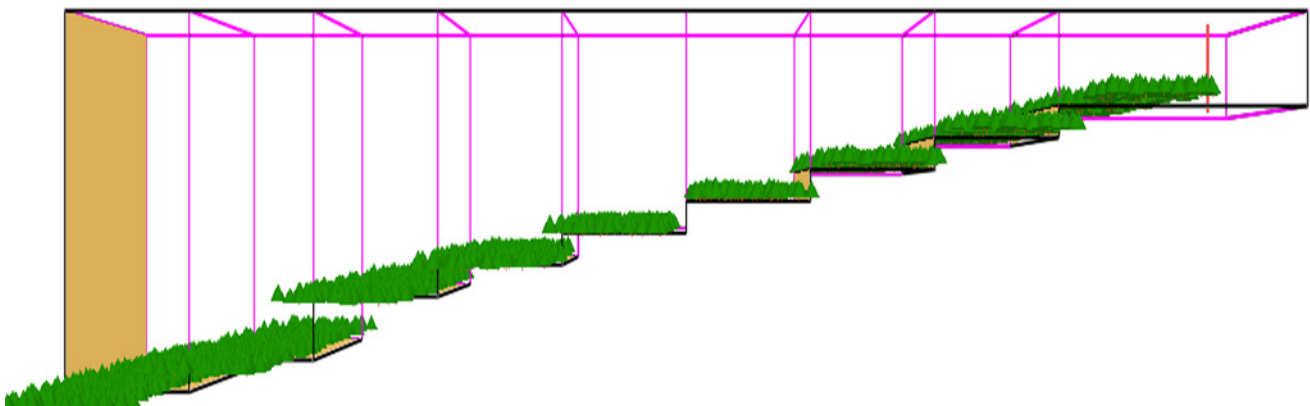


**Figure 6.15 The outline of the wildfire scenario.**

In Figure 6.16, a snapshot of the temperature distribution after 140s is displayed.

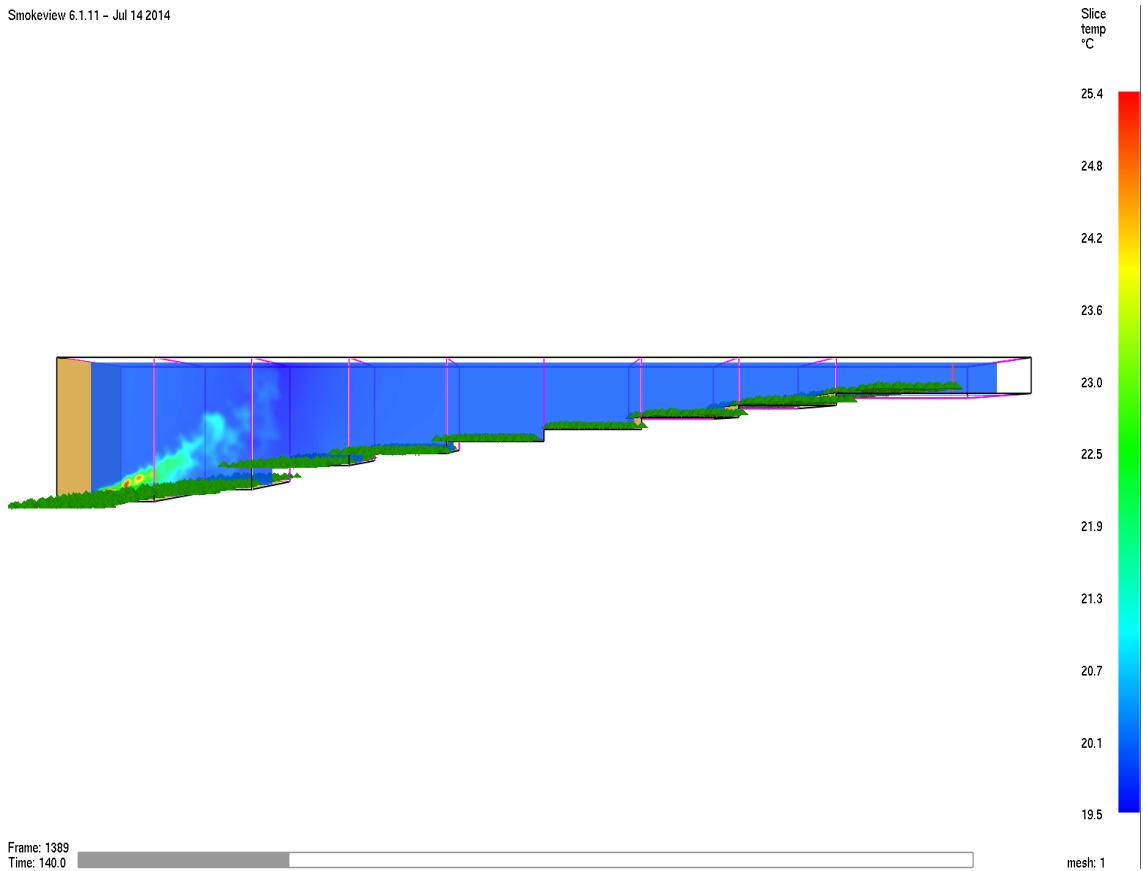


**Figure 6.16 The outline of the wildfire scenario.**

Modeling forest fires on these rather large areas is very demanding computationally and generates an enormous amount of data. For the fire spread model to at least function a comparably small grid size is needed otherwise the spread stops or is not well represented which means that these models will become huge. Unfortunately, the current case stopped due to limited disc memory.

## 6.10 Discussion

In this work the WFDS model is evaluated as a tool for fire spread estimation in rural/woodland areas. It is found that comparing to Ref. [73] that the fire spread from the ground vegetation to a crown fire the overall trends are reproduced.

It has been noted that the performance of WFDS is better for dry fuels whereas the performance elsewhere is mixed. It is found that reasonable fire spread in small forests can be obtained although the results are quite dependent on grid resolution as well as moisture content. In most realistic scenarios the computational volume is rather large yielding massive amounts of data. In this work a part of a real wildland fire has been modelled in order to investigate if WFDS can provide qualitative agreement with incident reports and in the future evaluate the likelihood of possible other severe outcomes with small variations in the data. The recorded weather data only provides wind direction and speed at the start of the fire however the wildfire continued for several hours.

There are several likely sources of errors such as the particular drag and heat transfer models used in WFDS, the simulated wind field, thermal degradation of the materials, spatial and size



distributions of the vegetation. Furthermore, the model is simplified to only accommodate for one type (pine) and shape of tree.

In using WFDS a rather small grid size is needed to appropriately model the fire spread this will be a severely limiting factor in creating large models

In comparison with the actual incident, and addressing the question of whether or not WFDS is a suitable tool for modelling such a large incident, the following comments are made:

- Given the wind speed measured on the day the WFDS software would require a significantly smaller cell size to have modelled the incident as it occurred. The practicalities of this are rather difficult because of the size of the model. The cell size of the models presented was of the order of 0.5 m to 1.0 m cubed. For the larger models this results in a total number of cells of between 24 and 100 million. These were run on 9 cores. The authors did try to run smaller celled models on as many as 43 cores but ran into memory issues as a result of the cluster which was being used. As a result of this the wind speed in the models is generally much lower than it was on the day.
- The impact of cell size on flame spread rate as discussed above is also significant, leading to reduced burning rates.

Given these computational limitations it is not practical to model the wildfire scenario in its current state. The computational effort required for the wind speed and which would result in a satisfactory fire spread rate is simply too high.

## 6.11 Cascading effects

An overview of the initiating event, the different systems impacted and their interdependencies for the wildfire scenario is presented below. In this instance, however, because of the limitations in the capabilities of modelling the scenario as presented, it is not possible to estimate the impact of the scenario as described based on the numerical simulations alone.

**Initiating event:** Children playing

**Originating system:** The Skatås forest around Stora and Lilla Delsjön

**Dependent / Impacted systems:** The forest, telecommunications mast, public, recreational areas, hospital, city of Gothenburg, buried electrical cables, the lakes Stora and Lilla Delsjön, Riksväg 27 and other roads

**Interdependencies:** Logical and physical



## 7 Conclusions

With the work performed within deliverable D2.5 it was illustrated how computer modelling can be used as an input to the incident evolution tool and how valuable computer modelling is as a tool towards accurately predicting and capturing the physics in cascading effects. Focus was mainly given on modelling the physics of technological accidents, involving fire-related and dispersion scenarios, additionally we presented the results of simulations of forest fires which present their own challenges. Two main approaches of modelling the physics were presented; the use of simplified models / correlations and the use of Computational Fluid Dynamics (CFD). An overview of some of the most well-known experimental correlations related to fire, dispersion and explosions scenarios were reported while an overview of the Fire Dynamics Simulator (FDS), and a development of it intended for modelling wild fires (WFDS), a widely used CFD code applicable to fire-related and pollutant dispersion scenarios, was given. The limitations, as well as the advantages and disadvantages, of each approach were analysed and guidelines regarding their use in modelling the physics in cascading effects were reported.

Task 2.5 aimed at modelling the necessary processes in order to completely perform and understand the simulated exercises in WP5 based on the physical effects identified in Task 2.3. Examples of such test cases included: plume spread (originating from a chemical hazard or a large fire), fire development and spread, toxicity. More specifically, in total three different scenarios were simulated within the task. Two scenarios involved fire; (the Mont Blanc tunnel fire scenario and a wildland fire scenario, dealing with fire development and spread) and one scenario involved pollutant dispersion; (the music festival scenario in which the dispersion of toxic substances towards the area of a music festival was considered). Based on the numerical modelling of the physics of the different scenarios, the goal was also to support understanding of cascading effects in crisis situations by identification of initiators, dependencies and key decision points within the different accidents.

Based on the work performed within the task, it was concluded that the physical modelling approach of the different kinds of scenarios would strongly depend upon the level of accuracy the user wants to achieve in the given timeline available. No universal approach exists which can be followed for every scenario at hand. If the scope of the study is a full investigation with great detail and accuracy of all possible cascading effects then the use CFD modelling is necessary. In this case, it will be possible to have distinct links between systems, accurate modelling of different originators but also to model the dependencies between different systems. However, this will be limited by the computational capacity of the users and the size and complexity of the model which is being attempted, as evidenced by the wildfire scenario modelling reported hereing. If the scope of the study is to have a rough estimate or outputted quantities in short time then the use of correlations or simplified models is more appropriate and still acceptable.

The use of physical modelling (either simplified or CFD modelling) can inherently provide a lot of valuable information to be used towards decision making during crisis situations and the study of cascading events. Generally, the use of physical modelling can be used in all three phases of a possible accident with cascading effects: beforehand, as a form of training exercise for prevention of future accidents; during, in order to provide valuable information about future events that might occur and help during the decision making process; and afterwards, with providing information about the consequences of the accident but also revisit the conditions and the evolution of the accident in order to learn lessons from it. During all three stages of an accident, physical modelling can play an important and valuable role during the planning, decision-making process and action phases. The level of accuracy of the information required from the physical modelling will determine the modelling approach chosen. All the different



physical modelling approaches can be useful and provide valuable information for the study of cascading effects. Depending on the conditions present, the type of accident and the actions that need to be performed the use of one approach or the other (or combination of both) can be appropriate.



## 8 References

- [1] CascEff - Modelling of dependencies and cascading effects for emergency management in crisis situations, Deliverable 2.1: Method to study cascading effects, 2015.
- [2] A. Alvares, B.J. Meacham, N.A. Dembsey, J.R. Thomas, Twenty years of performance-based fire protection design: challenges faced and a look ahead, Journal of Fire Protection Engineering, 23:249-276 (2013).
- [3] V. Babrauskas, Performance-based building codes: what will happen to the levels of safety, Fire Science and Technology Inc., USA.
- [4] Industrial Safety Series, Volume 8: Evaluation of the Effects and Consequences of Major Accidents in Industrial Plants, Edited by Joaquim Casal, Pages 1-363 (2008).
- [5] R.A.P.M. Weterings, The revised Yellow Book - educational concept, TNO Centre for Technology and Policy Studies (STB), Apeldoorn, October 1993.
- [6] F. Kadri, E. Chatelet, Domino Effect Analysis and Assessment of Industrial Sites: A Review of Methodologies and Software Tools, International Journal of Computers and Distributed Systems, 2:1-10 (2013).
- [7] K. McGrattan, S. Hostikka, R. McDermott, J. Floyd, C. Weinschenk, K. Overholt, Fire Dynamics Simulator Technical Reference Guide Volume 1: Mathematical model, NIST Special Publication 1018, Sixth Edition (2014).
- [8] J. Smagorinsky, General circulation experiments with the primitive equations: I. The basic experiment, Mon Weather Rev. 91:99-164 (1963).
- [9] J.W. Deardorff, Numerical Investigation of Neutral and Unstable Planetary Boundary Layers, Journal of Atmospheric Sciences, 29:91-115 (1972).
- [10] B.F. Magnussen, B.H. Hjertager, On Mathematical Modeling of Turbulent Combustion with Special Emphasis on Soot Formation and Combustion, Proc. Comb. Inst., 16:719-729 (1976).
- [11] W.L. Grosshandler, RADCAL: A Narrow-Band Model for Radiation Calculations in a Combustion Environment, NIST technical note 1402 (1993).
- [12] Task Force for Technical Investigation of the 24 March 1999 Fire in the Mont Blanc Vehicular Tunnel - Report of 30 June 1999, Minister of the Interior, and Ministry of Equipment, Transportation and Housing (France), English translation, 1999.
- [13] A.V. Cete, A. Dix, A comparative analysis of the Mont Blanc, Tauern and Gotthard tunnel fires, PIARC Ref. RR324-018, 2004.
- [14] <http://www.landroverclub.net/Club/HTML/MontBlanc.htm>
- [15] H.K. Kim, A. Lönnérmark and H. Ingason, Effective Firefighting Operations in Road Tunnels, SP Technical Research Institute of Sweden, 2010.
- [16] F. Peter, The causes, effects & control of real tunnel fires.
- [17] D.A. Purser, Application of human behaviour and toxic hazard analysis to the validation of CFD modelling for the Mont Blanc Tunnel fire incident. Proceedings of the Advanced Research Workshop on Fire Protection and Life Safety in Buildings and Transportation Systems 2009, Santander, Spain, 23–57, 2009.
- [18] H.K. Kim, A. Lönnérmark, H. Ingasson, Effective firefighting operations in road tunnels, SP Technical research institute of Sweden, SP Report 2010:10, 2010.
- [19] H. Ingason, Fire development in catastrophic tunnel fires (CTF), International symposium on catastrophic tunnel fires (CTF), 31-47, Borås, Sweden, 20-21 November 2003.
- [20] <http://www.mace.manchester.ac.uk/project/research/structures/strucfire/CaseStudy/HistoricFires/InfrastructuralFires/mont.htm>
- [21] European Commission, Overview of natural and man-made disaster risks in the EU, 2014.
- [22] C. Oboni and F. Oboni, Quantifying Social Perception of an Industrial Accident Risk, Oboni Riskope Associates, 2013.
- [23] A. Dix, The fatal Burnley tunnel crashes, 2011.



- [24] Promat, Tunnel fire protection, 2008.
- [25] <http://tunnels.piarc.org/en/safety/experience.htm>
- [26] PIARC Committee on Road Tunnels, Chapter 3 "Lessons learned from recent fires" of report 05.16.B, 2006.
- [27] UPTUN, Development and Mitigation Measures: Target Criteria, Work package 2 D22IFire, 2008.
- [28] D.A. Purser, SFPE Handbook of Fire Protection Engineering, chapter Toxicity Assessment of Combustion Products. National Fire Protection Association, Quincy, Massachusetts, 3rd edition, 204-205, 2002.
- [29] K. McGrattan, S. Hostikka, R. McDermott, J. Floyd, C. Weinschenk, K. Overholt, Fire Dynamics Simulator User's Guide, NIST Special Publication 1019, Sixth Edition, 2013.
- [30] G.W. Mulholland. SFPE Handbook of Fire Protection Engineering, chapter Smoke Production and Properties. National Fire Protection Association, Quincy, Massachusetts, 3rd edition, 2002.
- [31] A. Lönnermark, On the characteristics of fires in tunnels, PhD thesis, Lund University, 2005.
- [32] H. Ingason, A. Lönnermark, Recent achievements regarding measuring of time-heat and time-temperature developments in tunnels, Safe & Reliable Tunnels. Innovative European Achievements, First International Symposium, Prague, 2004.
- [33] S.B. Pope, Turbulent Flows, Cambridge University Press, 2000.
- [34] <http://www.internationaltransportforum.org/IntOrg/road/pdf/weights.pdf>
- [35] B. Babrauskas, Glass breakage in fires, Fire Science & Technology, 1997.
- [36] Ineos Olefins & Polymers USA, Typical Engineering properties of Polypropylene (online), 2010.
- [37] K. McGrattan, R. McDermott, S. Hostikka, J. Floyd, Fire Dynamics Simulator, Technical reference guide, National Institute of Standards and Technology, version 5.5, USA, 2010.
- [38] Matbase, Material Database, thermal properties of natural rubber (online), 2012.
- [39] AIS Glass Solutions Ltd., Thermal properties of laminated glass (online), 2005.
- [40] SFPE, National fire Protection Engineering association, The SFPE Handbook of Fire protection engineering, Third Edition, 2002.
- [41] Society of Fire Safety, Practice note for design fires, Engineers Australia, version 1.1, 2012.
- [42] R.M. Hadden, G. Rein, Small-scale experiments of self-sustaining decomposition of NPK fertilizer and application to events aboard the Ostedijk in 2007, Journal of Hazardous Materials, 186:731-737, 2011.
- [43] R.M. Hadden, G. Rein, Investigation of the Fertilizer Fire aboard the Ostedijk, Fire Safety Science, 9:1091-1101, 2009.
- [44] G. Maragkos, P. Rauwoens, Y. Wang, B. Merci, Large eddy simulations of the flow in the near-field region of a turbulent buoyant helium plume, Flow Turb. Combust., 90:511-543 (2013).
- [45] Y. Mouilleau, A. Champassith, CFD simulations of atmospheric gas dispersion using the Fire Dynamics Simulator, Journal of Loss Prevention in the Process Industries, 22:316-323 (2009).
- [46] J-M. Lacome, G. Leroy, B. Truchot, L. Joubert, X. Wei, E. Duport, E. Gilbert, B. Carissimo, Large-eddy simulation of wind flows and comparisons with very-near field campaign data, 16<sup>th</sup> International Conference on Harmonisation within Atmospheric Modelling for Regulatory Purposes, Varna, Bulgaria, 8-11 September 2014.
- [47] <https://weatherspark.com/averages/28600/Antwerp-Deurne-Flemish-Region-Belgium>
- [48] <http://es.ucsc.edu/~jnoble/wind/extrap/>
- [49] <http://wind-data.ch/tools/profile.php?lng=en>
- [50] R. Barratt, Atmospheric Dispersion Modelling: An Introduction to Practical Applications, 2001



- [51] N. Jarrin. Synthetic Inflow Boundary Conditions for the Numerical Simulation of Turbulence. PhD thesis, The University of Manchester, Manchester M60 1QD, United Kingdom, 90-91 (2008).
- [52] S. Chaturvedi, P.N. Dave, Review on Thermal Decomposition of Ammonium Nitrate, Journal of Energetic Materials, 31:1-26 (2013).
- [53] European Environmental Agency, Air quality in Europe - 2014 report, EEA Report No 5/2014.
- [54] T.W. Hesterberg, W.B. Bunn, R.O. McClellan, A.K. Hamade, C.M. Long, P.A. Valberg, Critical review of the human data on short-term nitrogen dioxide ( $\text{NO}_2$ ) exposures: evidence for  $\text{NO}_2$  no-effect levels, Crit. Rev. Toxicol., 39:743-81 (2009).
- [55] EU, 2008c, Directive 2008/50/EC of the European Parliament and of the Council of 21 May 2008 on ambient air quality and cleaner air for Europe (OJ L 152, 11.6.2008, pp. 1–44).
- [56] Office of Air Quality Planning and Standards, Measuring Air Quality: The Pollutant Standards Index, US EPA, EPA 451/K-94-001, February 1994.
- [57] M.T. Kleinman, W.S. Linn, R.M. Bailey, M.P. Jones, J.D. Hackney, Effect of Ammonium Nitrate Aerosol on Human Respiratory Function and Symptoms, Environmental Research, 21:317-326 (1980).
- [58] Air Pollution Modeling and Its Application III, Editor: C. De Wispelaere, Springer, 2012.
- [59] H. Kobara, K. Takeuchi, T. Ibusuki, Effect of Relative Humidity on Aerosol Generation through Experiments at Low Concentrations of Gaseous Nitric Acid and Ammonia, Aerosol and Air Quality Research, 7:193-204 (2007).
- [60] B.R. Appel, E.L. Kothney, E.M. Hoffer, G.M. Hidy, J.J. Wesolowski, Sulfate and nitrate data from the California aerosol characterization experiment (ACHEX), Environ. Sci. Tech., 12:418-425 (1978).
- [61] E. Pastor, L. Zarate, E. Planas and J. Arnaldos. Mathematical models and calculation systems for the study of wildland fire behaviour. Progress in Energy and Combustion Science, 29:139–153 (2003).
- [62] Mark A. Finney. FARSITE: Fire area simulator-model development and evaluation. Res. Pap. RMRS-RP-4, Ogden, UT: U.S. Department of Agriculture, Forest Service, Rocky Mountain Research Station. 47 p., <http://www.farsite.org> (1998).
- [63] C. Tymstra, R. W. Bryce, B. M. Wotton, O. B. Armitage, Development and structure of Prometheus: the Canadian wildland fire growth simulation Model. Inf. Rep. NOR-X-417. Nat. Resour. Can., Can. For. Serv., North. For. Cent., Edmonton, AB.. PROMETHEUS (2009)
- [64] J. L. Coen. Simulation of the Big Elk Fire using coupled atmosphere-fire modeling. International Journal of Wildland Fire, 14(1):49–59 (2005).
- [65] Jan Mandel, Jonathan D. Beezley, Janice L. Coen, Minjeong Kim, Data Assimilation for Wildland Fires: Ensemble Kalman filters in coupled atmosphere-surface models, IEEE Control Systems Magazine 29, Issue 3, June 2009, 47-65.
- [66] R. Sun, S. K Krueger, M. A. Jenkins, M. A. Zulauf, and J. J. Charney. The importance of fire-atmosphere coupling and boundary-layer turbulence to wildfire spread. Int. J. of Wildland Fire, 18(1) 50–60 (2009).
- [67] R. Linn, J. Reisner, J. J. Colman, and J. Winterkamp. Studying wildfire behavior using FIRETEC. Int. J. of Wildland Fire, 11:233—246 (2002).
- [68] W. Mell, M. A. Jenkins, J. Gould, and P. Cheney. A physics-based approach to modelling grassland fires. Intl. J. Wildland Fire, 16:1--22 (2007).
- [69] J. L. Coen, T. L. Clark, and D. Latham. Coupled atmosphere-fire model simulations in various fuel types in complex terrain. In 4th. Symp. Fire and Forest Meteor. Amer. Meteor. Soc., Reno, Nov. 13-15, pages 39—42 (2001).
- [70] Terry L. Clark, Janice Coen, and Don Latham. Description of a coupled atmosphere-fire model. International Journal of Wildland Fire, 13:49--64 (2004).
- [71] W. Mell, User Guide to WFDS



- [72] E. W. Mueller, LES Modelling of Flow through Vegetation with Applications to Wildland Fires, MSc thesis, Worcester Polytechnic Institute
- [73] W. Mell, A. Maranghides, R. McDermott, S. L. Manzello, Numerical simulation and experiments of burning douglas fir trees. Combustion and Flame. 156, pp. 2023-2041 (2009).
- [74] A. M. Grishin, Mathematical modeling of forest fires and new methods of fighting them, Publishing House of the Tomsk State University, Tomsk, Russia, 1997.
- [75] <http://www.fs.fed.us/pnw/fera/wfds/index.shtml>



# Appendix 1: Types of accidents

This appendix discusses various types of accidents for the modelling of which CFD may be a suitable tool. These include Fire, Explosion and Release type incidents. The information presented refers specifically to work which is carried out in the process industries, however the models which are used to determine the impact of these accidents and the magnitude of these accidents themselves are general applicable.

## A1.1 Introduction

The potential sources of danger leading to cascading effects vary in nature and can be triggered by different initiating events [1]. Typically, they can be categorized by the origin of the initiating event in: natural (e.g. geological, weather, extra-terrestrial), technological (e.g. fire, explosion, toxic chemical release) and human (e.g. organizational, malice). An overview of some different initiating events is presented in Table A1.1.

**Table A1.1 Example classification of some initiating events.**

Type of event	Event breakdown
Natural	<p><i>Geological:</i> Landslides, earthquakes, tsunamis, volcanic eruptions</p> <p><i>Weather:</i> Forest fires, floods, avalanches, hurricanes and tornados, storms, effects of climate change.</p> <p><i>Extra-terrestrial (rare):</i> Meteorites</p> <p><i>etc.</i></p>
Human	<p><i>Organizational:</i> Human error, defects in design, procedures and/or organization.</p> <p><i>Malice:</i> Theft, sabotage and/or revenge.</p> <p><i>etc.</i></p>
Technological	<p><i>Fire:</i> Pool fire, flash fire, tank fire, jet fire and fireball.</p> <p><i>Explosion:</i> Vapour cloud explosion, dust explosion, vessel explosion, Boiling Liquid Expanding Vapour Explosion (BLEVE).</p> <p><i>Toxic chemical release:</i> From storage sites, transport accidents.</p> <p><i>etc.</i></p>

A recent study [2] on past cascading effects resulting from, e.g., disruption in the process industries revealed that the most frequent causes of cascading effects were explosions (57 %) and fires (43 %). In addition, from an analysis of 261 past events involving cascading events [3] it was concluded that, in addition to cases of mechanical failure and external events, the cases of cascading effects due to a human event were in the order of 21 %. In the remaining of the report, focus will be given on modelling the physics in cascading effects caused by initiating events of a technological nature in the case of the mont blanc tunnel and the festival scenario, and of a natural nature in the case of the wildfire scenario. These scenarios not only represent the type of events with the highest frequency of occurrence but furthermore the initiating event and the resulting cascading effects can more accurately be predicted, quantified and studied with physical models.

In the case of technological events we can define the term “major accident” as [4]: “an occurrence such as a major emission, fire, or explosion resulting from uncontrolled developments in the course of the operation of any establishment ... and leading to serious danger to human and/or the environment, immediate or delayed, inside or outside the establishment, and involving one or more dangerous substances”.



Major accidents are typically associated with dangerous physical phenomena and with the exclusion of natural phenomena can be classified as:

- *Thermal*: incorporating thermal effects
- *Mechanical*: explosion and ejection of fragments
- *Chemical*: release of toxic materials.

Such accidents can have an effect on humans, material property and the environment. Human consequences can be either physical or psychological and can affect both the employees of the establishment in which the accident takes place and the external population. Material property typically involves the destruction of equipment and buildings. Environmental consequences can be immediate or delayed and include the release of toxic materials into the atmosphere, the ground or the water. Major accidents also include indirect losses such as e.g. the loss of profit of the establishment involved in an accident.

## A1.2 Accidents

Continuing the discussion on accidents, focussing on the process industry as an example, these can involve three different physical phenomena [5]: fires (e.g. pool fire, tank fire, jet fire, flash fire and fireball), explosions (e.g. vapour cloud explosion, dust explosion, vessel explosion and Boiling Liquid Expanding Vapour Explosion (BLEVE)) and release of hazardous substances. An accident can involve more than one of such phenomena, e.g. a fire can cause an explosion, a fire can follow an explosion or an explosion can cause the dispersion of a toxic substance into the atmosphere. A definition of each type of physical phenomenon involved in these accidents is presented below:

### A1.2.1 Fire accidents

- *Pool fires*: Flammable pool of liquid fuel with a given size and shape most likely in the open air. Often combustion is poor and is accompanied by large amounts of black smoke.
- *Jet fires*: Turbulent diffusion flames with large length/diameter ratio, caused by the ignition of a turbulent jet of flammable gas or vapour.
- *Tank fires*: Similar to pool fires, typically with a circular shape determined by the diameter of the tank, where flames are located at a certain height from the ground. These can contain a large amount of fuel.
- *Flash fires*: Sudden, intense fires capable of propagating through a flammable gas/air mixture within flammability limits of the material in question.
- *Fireballs*: Caused by the ignition of a liquid/vapour mixture and are typically associated with the explosion of the vessel containing the flammable liquid. Large but short in duration, fireballs can occur in tank fires in the case of a boilover.



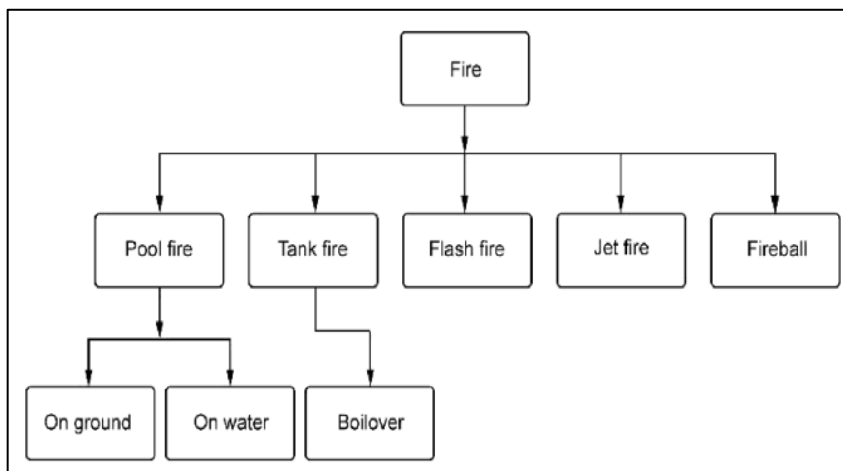


**Figure A1.1 Types of fire accidents.**

### A1.2.2 Explosion accidents

- *Vapour cloud explosions*: Chemical explosions involving a significant amount of flammable gas or vapour mixed with air. A flash fire always accompanies them.
- *Vessels explosions and BLEVEs*: Physical explosions triggered by a sudden failure of a vessel containing a pressurized gas or superheated liquid in equilibrium with its vapour. Under certain conditions this type of explosion may be referred to as a BLEVE (Boiling Liquid Expanding Vapour Explosion).
- *Dust explosion*: Explosion caused by the fast combustion of fine oxidizable particulate solids (e.g. coal, flour, sugar, aluminium) with air, often occurring in confined spaces.

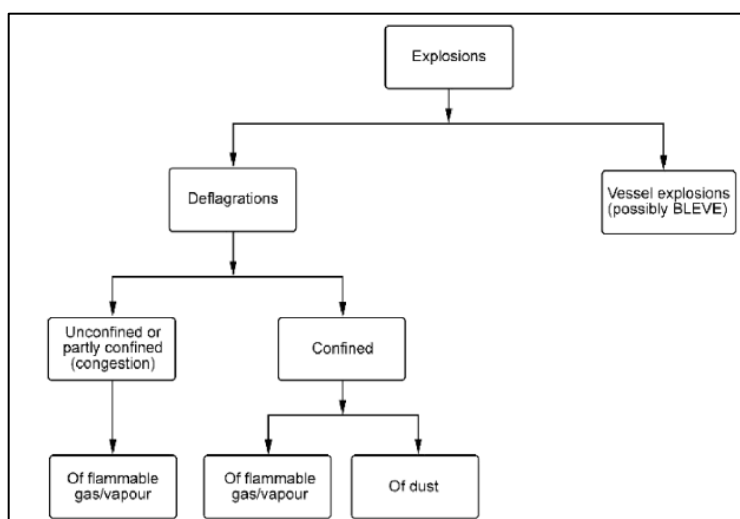


**Figure A1.2 Types of explosion accidents.**

### A1.2.3 Release accidents

Release accidents typically involve the discharge of a substance into the atmosphere due to e.g. an accident or loss of container. The release of a toxic substance into the atmosphere can produce a toxic cloud. Depending on the density of the toxic cloud (if the cloud is heavier or lighter than air) and the meteorological conditions, the cloud can either be dispersed into the atmosphere or evolve close to the ground and move with wind speed. There are numerous



different accidents that can occur following a release of a toxic material into the atmosphere, examples of which are presented in Figure A1.3.

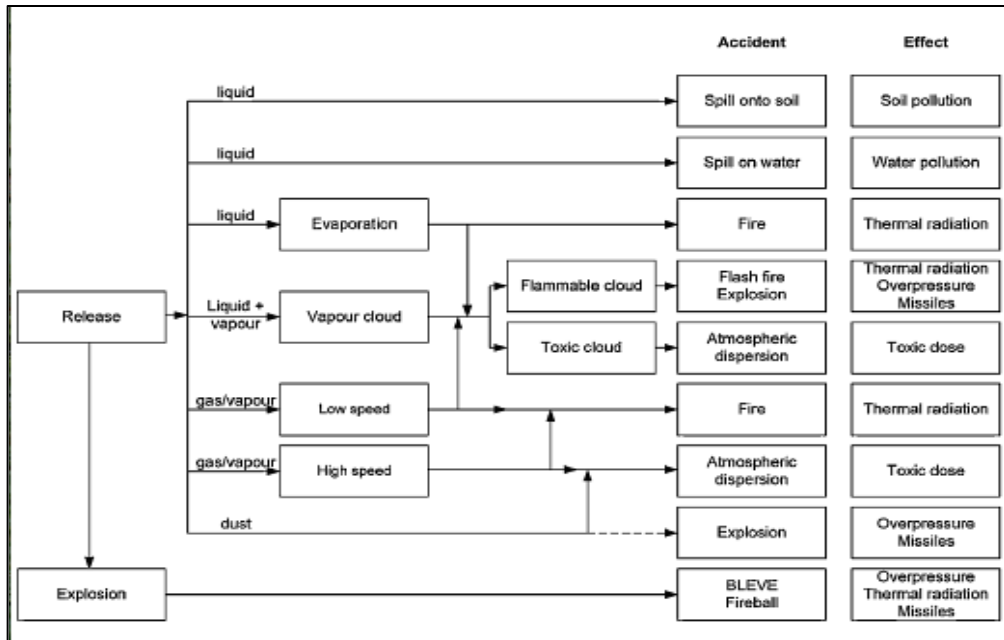


**Figure A1.3 Schematic representation of the possible accidents following a release event.**  
The relative occurrence of the different types of accidents in process plants and in the transportation of hazardous material is presented in Table A1.2.

**Table A1.2 Distribution of major accidents in process plants and in the transportation of hazardous materials [5].**

Type of accident	%
Fire	47
Explosion	40
Gas cloud	13

From the different types of accidents that can potentially occur, fire accidents are the ones whose effects have a significant effect over the shortest distances (exception being the wildland fires); explosions and toxic gas clouds typically affect much larger areas. Nevertheless, the effects from fire accidents can be potentially be very severe as they can lead to cascading effects and give rise to secondary events such as e.g. power outage or explosions of toxic gas releases increasing the severity of the accident.

## A 1.2 Cascading effects in accidents

According to the technical definition given within the context of the CascEff project [6], cascading effects are the impacts of an initiating event where:

1. System dependencies lead to impacts propagating from one system to another, and;
2. The combined impacts of the propagated event are of greater consequences than the root impacts, and;
3. Multiple stakeholders and/or responders are involved.

A more specific definition of cascading effect (commonly referred to as “domino effects” in literature) in the case of a technological event has been previously defined as [7]: “a cascade of events in which the consequences of a previous accident are increased both spatially and



temporally by following ones, thus leading to a major accident. A cascading effect involves a primary event that affects a primary installation, which induces one or more secondary accidents that affect other installations. The spread of damage can be either spatial (areas not involved in the primary accident are damaged) or temporal (the same area is involved but the secondary events are delayed), or both. Installations involved in a cascading effect may or may not belong to the same establishment." A graphic representation of such a cascading effect in an industrial facility is presented in Figure A1.4. This representation, while specific to the process industries not fitting the definition within the CascEff project since only one system is affected in the illustration, helps to understand the concept of cascading effects.

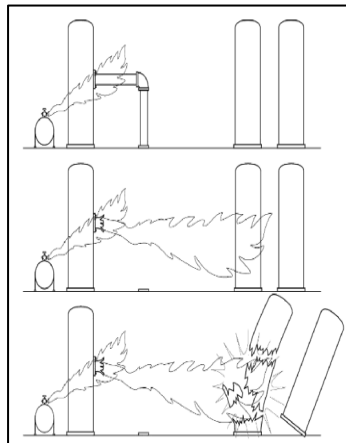


**Figure A1.4 Example of cascading effects in an industrial facility. Figure reproduced from [5].**

Based on historic data, cascading effects can be classified based on two criteria: the type of the primary and secondary systems involved in the accident, and on the nature of the primary and secondary physical effects produced from an accident. The types of installations commonly affected by cascading effects include pressure storage tanks, atmospheric or cryogenic storage tanks, process equipment, pipe networks and small conditioners. The relative occurrence of the different types of installations is given in Table A1.3.

**Table A1.3 Contribution of the different types of installation to primary or secondary accidents [6].**

Type of installation	Primary (%)	Secondary (%)
Pressurized storage tanks	30	33
Atmospheric or cryogenic storage tanks	28	46
Process equipment	30	12
Pipe networks	12	-
Small conditioners	-	9

The primary effects can be either thermal or mechanical. The secondary effects can be thermal, mechanical or toxic. The different physical effects in primary and secondary accidents and their relative occurrence are presented in Table A1.4.

**Table A1.4 Effects of major accidents related with cascading effect [5].**

Effects in primary accidents	Effects in secondary accidents
Mechanical (35 %)	Mechanical (37 %)
Thermal (77 %)	Thermal (93 %)
	Toxic (10 %)

From a literature study of past accidents [3] it was reported that the most common sequence of events in case of an accident involving cascading effects was explosion-fire (21 %), followed by release-fire-explosion (15 %) and fire-explosion (14 %).

More in particular, the study of fire plumes has received a lot of attention in the past due to the great environmental impact and dangers often associated with them. More specific, large-scale fire plumes, often encountered after natural fires and industrial accidents, can lead not only to severe air pollution due to the release of unburned hydrocarbons and soot into the atmosphere but can also trigger more severe cascading effects involving explosions, causing huge losses of human lives and material properties.

### **References:**

- [1] F. Kadri, B. Birregah, E. Chatelet, The Impact of Natural Disasters on Critical Infrastructures: A Domino Effect-based Study, *Homeland Security & Emergency Management*, 11:217-241 (2014).
- [2] B. Abdolhamidzadeh, T. Abbasi, D. Rashtchian, S.A. Abbasi, Domino Effect in Process-Industry Accidents – An inventory of Past Events and Identification of Some Patterns, *Journal of Loss Prevention in the Process Industries*, 24:575-593 (2011).
- [3] F. Clinì, R.M. Darbra, J. Casal, Historical Analysis of Accidents Involving Domino Effect, *Chemical Engineering*, 19:335-340 (2010).
- [4] Council Directive 96/82/EC of 9 December 1996 on the control of major-accident hazards involving dangerous substances. OJ No. 10, 14 January 1997.
- [5] Industrial Safety Series, Volume 8: Evaluation of the Effects and Consequences of Major Accidents in Industrial Plants, Edited by Joaquim Casal, Pages 1-363 (2008).
- [6] CascEff - Modelling of dependencies and cascading effects for emergency management in crisis situations, Deliverable 2.1: Method to study cascading effects, 2015.
- [7] C. Delvosalle, Domino Effects Phenomena: Definition, Overview and Classification, First European Seminar on Domino Effects, Leuven, 1996.



## Appendix 2: Correlations / simplified models

### A2.1 Introduction

In the remaining part of this section, experimentally derived, empirical correlations related to the scenarios studied in this report, but also relevant for a wide range of possible scenarios involving cascading effects, are reported and possible limitations of their used are analysed. However, it is important to note that a complete list of all available, experimentally derived, correlations for every possible scenario is not feasible due to the wide range of available formulas available in literature. The reader is directed to e.g. [1 - 2] for a more complete list of the available correlations in literature.

### A2.2 Fire-related correlations

#### A2.2.1 Introduction

In this section well-known fire-related correlations reported in literature are presented [3]. These correlations have been established based on experiments and can be used as a first estimation of important quantities in case of scenarios involving fire. It is worth noting, however, that the report of every existent fire-related correlation and formula is not feasible due to the wide range of available correlations in literature. Nevertheless, some of the most widely known and frequently used experimental correlations are reported in this section.

#### A2.2.2 Flame height

An estimate of the flame height,  $L$ , can be important in determining exposure hazards associated with a burning fuel. A priori knowledge of the flame height for a burning fuel can be important in many cases involving, e.g., flame spread. Heskstad's correlation [4] can be used to evaluate the flame heights for pool fires or horizontal burning fuels:

$$\frac{L}{D} = -1.02 + 15.6N^{1/5} \quad (\text{A2. 1})$$

where

$L$  = mean flame height (m)

$D$  = diameter of fire source (m)

$N$  = non-dimensional number

and  $N$  is calculated as:

$$N = \left[ \frac{c_p T_\infty}{g \rho_\infty^2 \left( \frac{\Delta h_c}{r_s} \right)^3} \right] \frac{\dot{Q}^2}{D^5} \quad (\text{A2. 2})$$

where

$c_p$  = specific heat of air at constant pressure [(kJ/kg)K]

$T_\infty$  = ambient temperature (K)

$g$  = acceleration of gravity (9.81 m/s<sup>2</sup>)

$\rho_\infty$  = ambient air density (kg/m<sup>3</sup>)

$\Delta h_c$  = heat of combustion (kJ/kg)



$r_s$  = stoichiometric air/fuel mass ratio

$\dot{Q}$  = total heat release rate (kW)

For non-circular fuel packages, an effective diameter,  $D$ , can be calculated as:

$$D = 2 \left( \frac{A_f}{\pi} \right)^{1/2} \quad (\text{A2.3})$$

where

$D$  = effective diameter (m)

$A_f$  = area of fire ( $\text{m}^2$ )

### A2.2.3 Plume centerline temperature

The plume centerline temperature at heights above the mean flame height is estimated as [5]:

$$T = T_\infty + 9.1 \left( \frac{T_\infty}{gc_p^2 \rho_\infty^2} \right)^{1/3} \dot{Q}_c^{2/3} (z - z_0)^{-5/3} \quad (\text{A2.4})$$

where

$T$  = plume temperature (K)

$T_\infty$  = ambient temperature (K)

$g$  = acceleration of gravity ( $9.81 \text{ m/s}^2$ )

$c_p$  = specific heat of air at constant pressure [ $(\text{kJ/kg})\text{K}$ ]

$\rho_\infty$  = ambient air density ( $\text{kg/m}^3$ )

$\dot{Q}_c$  = convective heat release rate (kW)

$z$  = elevation above burning fuel fire source (m)

$z_0$  = location of virtual fire source (m)

An estimation of the virtual origin,  $z_0$ , (Figure A2.1) for pool fires and horizontal burning is estimated as [4]:

$$z_0 = -1.02D + 0.083\dot{Q}^{2/5} \quad (\text{A2.5})$$

where

$D$  = diameter of burning fuel surface (m)

$\dot{Q}$  = total heat release rate (kW)

$z_0$  = location of virtual fire source (m)

Typically the virtual origin is neglected in calculations where the distance above the fire is many times the diameter of the fire.



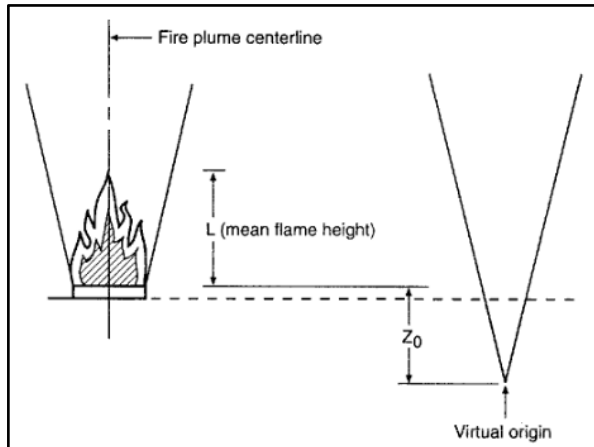


**Figure A2.1 Flame and fire plume characteristics.** Figure reproduced from [3].

#### A2.2.4 Radiant heat flux to a target

An estimation of the heat flux from a burning fuel array to a target fuel at a given distance from the fire can be calculated as:

$$\dot{q}_r'' = \frac{P}{4\pi R_o^2} = \frac{\chi_r \dot{Q}}{4\pi R_o^2} \quad (\text{A2.6})$$

where

$\dot{q}_r''$  = incident radiation on the target ( $\text{kW/m}^2$ )

$R_o$  = distance to target fuel (m)

$P$  = total radiative power of the flame (kW)

$\chi_r$  = radiative fraction

$\dot{Q}$  = total heat release rate (kW)

Experimental measurements have indicated that the above expression has good accuracy for  $(R_o / R) > 4$ , where  $R$  (in m) is the radius of the base of the fire (Figure A2.2). Estimates of the radiative fraction,  $\chi_r$ , for a variety of fuels and fire dimensions has been given experimentally and can be easily obtained from literature. Examples of experimentally obtained radiative fractions are presented in Figure A2.3 and Table A2.1 [6].

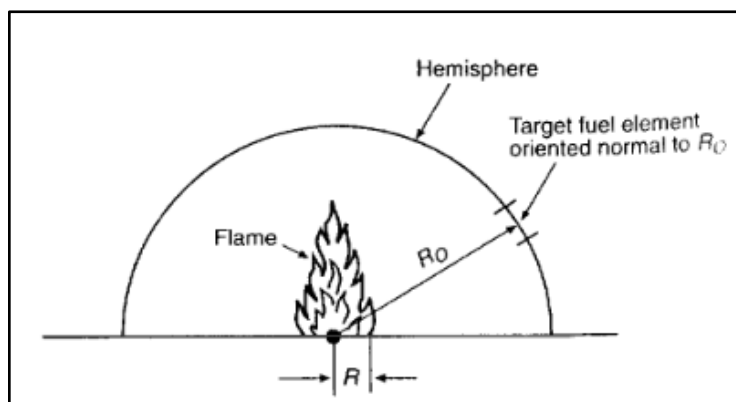


**Figure A2.2 Schematic of radiant heat transfer to a target.** Figure reproduced from [3].

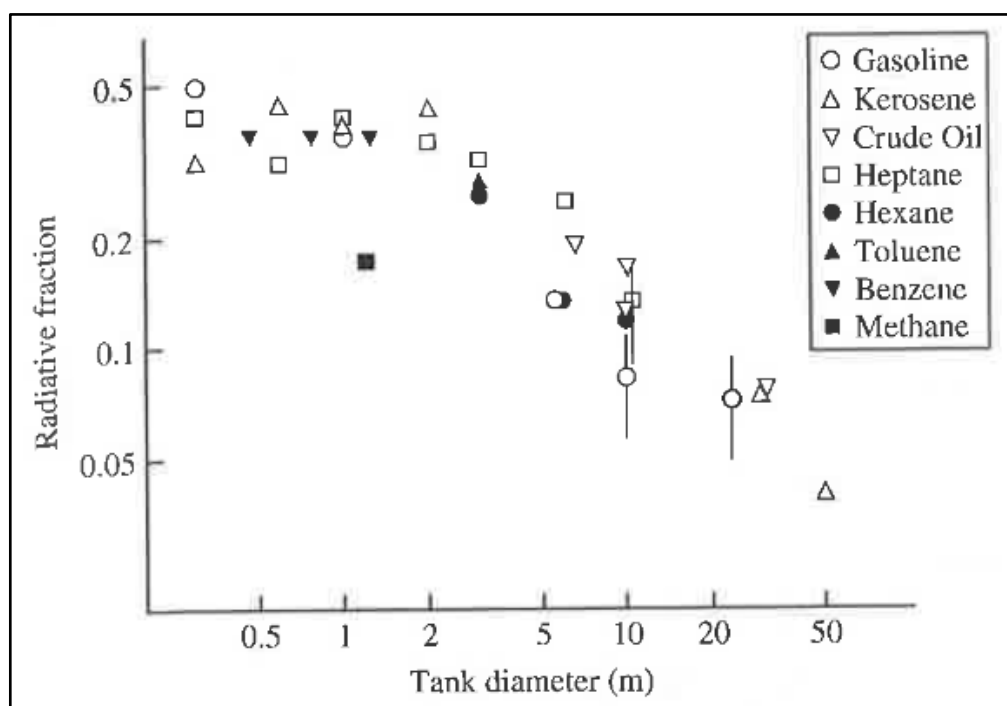


**Figure A2.3 Radiative fractions ( $\chi_r$ ) measured for pool fires of diameters from 0.3 to 50 m.**  
**Figure reproduced from [6].**

**Table A2.1 Fraction of heat of combustion released during burning [6].**

Fuel	$\dot{Q}_E''$ (kW/m <sup>2</sup> )	$\chi$	$\chi_{conv}$	$\chi_r$
Methanol (l)	0	0.993	0.853	0.141
Heptane (l)	0	0.690	0.374	0.316
Cellulose	52.4	0.716	0.351	0.365
Polyoxymethylene	0	0.755	0.607	0.148
Polymethylmethacrylate	0 39.7 52.4	0.867 0.710 0.710	0.622 0.340 0.410	0.245 0.360 0.300
Polypropylene	0 39.7 52.4	0.752 0.593 0.679	0.548 0.233 0.267	0.204 0.360 0.413
Styrene (l)	0	0.550	0.180	0.370
Polystyrene	0 32.5 39.7	0.607 0.392 0.464	0.385 0.090 0.130	0.222 0.302 0.334
Polyvinylchloride	52.4	0.357	0.148	0.209

The intensity of the heat flux from a fire can have various effects on humans and material property, e.g., a heat flux in the order of 37 kW/m<sup>2</sup> can cause severe damage to process equipment of other installations operating under atmospheric conditions. A list of the various effects caused by the intensity of heat fluxes is presented in Table A2.2.

**Table A2.2 Various effects for different heat flux intensities (Source: AIChE/CCPS, Guideline for chemical process quantitative risk analysis).**

Intensity of heat radiation (kW/m <sup>2</sup> )	Various effects
1.6	Insufficient to cause no discomfort for long exposure
2.2	Threshold pain. No reddening or blister.
4.0	Glass cracks
4.2	First degree burn
8.3	Second degree burn
10.8	Third degree burn
12.0	Plastic melts
15.0	Piloted ignition of wood
19.0	Cable insulation degrades
25.0	Spontaneous ignition of wood
37.5	Damage to process equipment
100.0	Steel structure fail

### A2.2.5 Time to failure

A simplified model for the estimation of the time to failure (ttf) of industrial equipment subjected to a fire, based on the probit approach, has also been proposed [7 - 9] and is presented in Table A2.3, in which  $Y$  is the probit function,  $ttf$ (s) is the time to failure,  $V$ (m<sup>3</sup>) is the vessel volume, and  $\dot{q}_r$  (kW/m<sup>2</sup>) is the amount of heat radiation received by the target vessel.

**Table A2.3 Probability models and threshold values for thermal heat radiation.**

Equipment category	Threshold	Correlation
Atmospheric vessels	15 kW/m <sup>2</sup> t ≥ 10 min	$Y = 12.54 - 1.847 \times \ln(ttf)$ $\ln(ttf) = -1.128 \times \ln(\dot{q}_r) - 2.667 \times 10^{-5}V + 9.887$
Pressurized vessels	50 kW/m <sup>2</sup> t ≥ 10 min	$Y = 12.54 - 1.847 \times \ln(ttf)$ $\ln(ttf) = -0.947 \times \ln(\dot{q}_r) + 8.835V^{0.032}$

### A2.2.6 Ignition time of solid materials

An estimation of the time to ignition for flame spread of solid fuels exposed to a constant external heat flux can be given for thermally thin and thermally thick materials, respectively [5]. These are described in separate sections below.

The equations are approximate and have been derived based on the following assumptions:

- The solid is inert and homogeneous
- The thermal properties are constant
- The material surface emissivity and absorptivity are both unity
- The incident heat flux is much greater than the surface heat losses

If the incident heat flux,  $\dot{q}_r$ , on a material surface is above the critical heat flux for ignition,  $\dot{q}_{r,crit}$ , of the material then ignition and flaming combustion will occur. Depending on whether the material is thermally thick or thermally thin the time to ignition can be estimated from the above-mentioned equations. A list of the critical heat fluxes for ignition of some commonly used solid materials is presented in Table A2.4.



**Table A2.4 Flame spread properties of common materials (Source: <http://www.nrc.gov>)**

Material	Ignition Temperature $T_{ign}$ (K)	Thermal inertia $kpc_p$ (kW/m <sup>2</sup> K <sup>2</sup> )	Critical heat flux for ignition $\dot{q}_{r,crit}''$ (kW/m <sup>2</sup> )
PMMA Polycast (1.59 mm)	278	0.73	9
Hardboard (6.35 mm)	298	1.87	10
Carpet (Arcylic)	300	0.42	10
Fiber Insulation Board	355	0.46	14
Hardboard (3.175 mm)	365	0.88	14
PMMA Type G (1.27 cm)	378	1.02	15
Asphalt Shingle	378	0.7	15
Douglas Fire Particle Board (1.27 cm)	382	0.94	16
Plywood Plain (1.27 cm)	390	0.54	16
Plywood Plain (0.635 cm)	390	0.46	16
Foam Flexible (2.54 cm)	390	0.32	16
GRP (2.24 mm)	390	0.32	16
Hardboard (Gloss Paint) (3.4 mm)	400	1.22	17
Hardboard Nitrocellulose Paint)	400	0.79	17
GRP (1.14 mm)	400	0.72	17
Particle Board (1.27 cm Stock)	412	0.93	18
Carpet (Nylon/Wool Blend)	412	0.68	18
Gypsum Board, Wallboard (S142M)	412	0.57	18
Carpet # 2 (Wool Untreated)	435	0.25	20
Foam Rigid (2.54 cm)	435	0.03	20
Fiberglass Shingle	445	0.5	21
Polyisoyanurate (5.08 cm)	445	0.02	21
Carpet # 2 (Wool Treated)	455	0.24	22
Carpet # 1 (Wool, Stock)	465	0.11	23
Aircraft Panel Epoxy Fiberite	505	0.24	28
Gypsum Board FR (1.27 cm)	510	0.4	28
Polycarbonate (1.52 mm)	528	1.16	30
Gypsum Board (Common) (1.27 mm)	565	0.45	35
Plywood FR (1.27 cm)	620	0.76	44
Polystyrene (5.08 cm)	630	0.38	46



Thermally thick materials (e.g. brick walls)

$$t_{ign} = \frac{\pi}{4} k \rho c_p \frac{(T_{ign} - T_0)^2}{\dot{q}_r''} \quad (\text{A2.7})$$

where

$t_{ign}$  = material ignition time (s)  
 $k\rho c_p$  = material thermal inertia ( $\text{kW}/(\text{m}^2\text{K}^2)$ )  
 $T_{ign}$  = material ignition temperature (K)  
 $T_0$  = ambient air temperature (K)  
 $\dot{q}_r''$  = external radiative heat flux ( $\text{kW}/\text{m}^2$ )

Thermally thin materials (e.g. steel plates)

$$t_{ign} = \rho c_p \tau \frac{(T_{ign} - T_0)}{\dot{q}_r''} \quad (\text{A2.8})$$

where

$t_{ign}$  = material ignition time (s)  
 $\rho$  = material density ( $\text{kg}/\text{m}^3$ )  
 $c_p$  = material specific heat capacity at constant pressure [ $(\text{kJ}/\text{kg})/\text{K}$ ]  
 $\tau$  = material thickness (m)  
 $T_{ign}$  = material ignition temperature (K)  
 $T_0$  = ambient air temperature (K)  
 $\dot{q}_r''$  = external radiative heat flux ( $\text{kW}/\text{m}^2$ )

### A2.2.7 Pre-flashover temperature in an enclosure

An estimation of the temperature rise in developing fires for naturally ventilated fires in an enclosure can be estimated as [10]:

$$\frac{\Delta T}{T_\infty} = 1.63 \left( \frac{\dot{Q}}{c_p \rho_\infty T_\infty A_v \sqrt{gh_v}} \right)^{2/3} \left( \frac{h_k A_s}{c_p \rho_\infty A_v \sqrt{gh_v}} \right)^{-1/3} \quad (\text{A2.9})$$

where

$\Delta T$  = temperature rise of the upper gas ( $T_g - T_\infty$ ) (K)  
 $T_g$  = gas temperature (K)  
 $T_\infty$  = ambient air temperature (K)  
 $\dot{Q}$  = total heat release rate (kW)  
 $g$  = acceleration of gravity ( $9.81 \text{ m/s}^2$ )  
 $c_p$  = specific heat of air at constant pressure [ $(\text{kJ}/\text{kg})\text{K}$ ]  
 $\rho_\infty$  = ambient air density ( $\text{kg}/\text{m}^3$ )  
 $A_s$  = total surface area of enclosure interior excluding vent area ( $\text{m}^2$ )  
 $A_v$  = vent area ( $\text{m}^2$ )  
 $h_v$  = vent height (m)  
 $h_k$  = effective enclosure conductance [ $(\text{kW}/\text{m})/\text{K}$ ]

The terms  $h_k A_s$  and  $A_v \sqrt{h_v}$  are summed for multiple materials and openings, respectively.



In case of completely forced ventilation conditions the temperature rise within the compartment can be estimated as [11]:

$$\frac{\Delta T}{T_\infty} = 0.63 \left( \frac{\dot{Q}}{\dot{m}_v c_p T_\infty} \right)^{0.72} \left( \frac{h_k A_s}{\dot{m}_v c_p} \right)^{-0.36} \quad (\text{A2.10})$$

where

$\dot{m}_v$  = compartment forced mass ventilation rate (kg/s)

### A2.2.8 Prediction of flashover

A critical point in fire growth inside rooms, often called “flashover”, is associated with a rapid transition in the fire behavior from localized fuel burning to instantaneous ignition of all the combustible materials inside the enclosure. Based on experimental observation, a flashover can typically occur when the upper room temperatures are between 400-600 °C. An estimation of the necessary heat release rate to achieve flashover in naturally ventilated enclosures is given by [6]:

$$\dot{Q}_{fo} = 610 \left( h_k A_s A_v \sqrt{h_v} \right)^{1/2} \quad (\text{A2.11})$$

where

$\dot{Q}_{fo}$  = total heat release rate at flashover (kW)

$h_k$  = effective enclosure conductance [(kW/m)/K]

$A_s$  = total surface area of enclosure interior excluding vent area ( $m^2$ )

$A_v$  = vent area ( $m^2$ )

$h_v$  = vent height (m)

### A2.2.9 Post- flashover temperature

The peak enclosure temperatures under both natural and forced ventilation can also be estimated based on post-flashover enclosure fire data. The following equations do not consider variation in the thermophysical properties of the room linings and have been mainly developed based on tests involving room lined with gypsum boards or concrete blocks. Caution should be taken when applying such correlations to scenarios involving rooms lined with highly insulated materials, such as fiberglass or foamed materials, or rooms in which the linings are thermally thin such as steel or glass.

Under natural ventilation conditions [6]:

$$\Delta T_{max} = 6000 \left[ \frac{(1 - e^{-0.036\eta})}{\eta^{1/2}} \right] (1 - e^{-0.05\psi}) \quad (\text{A2.12})$$

where

$\Delta T_{max}$  = peak temperature rise (K)

$\eta = [A_s / A_v(h)]^{1/2}$

$\psi = L_f / (A_v A_s)^{1/2}$

$A_s$  = total surface area of enclosure interior excluding vent area ( $m^2$ )

$A_v$  = vent area ( $m^2$ )



$h$  = height of compartment (m)

$L_f$  = total enclosure fire load (equivalent weight of wood) (kg)

Under forced ventilation conditions [6]:

$$\Delta T_{\max} = 1200 \left(1 - e^{-0.04\psi}\right) \quad (\text{A2.13})$$

### A2.2.10 Equivalent fire duration

The equivalent fire duration or fire severity is an estimate of the potential destructive impact from the consumption of all of the available fuel present in an enclosure with at least one opening. The correlation assumes that all of the potential energy of the fuel is released in the involved enclosure [6].

$$t = 60 \left( \frac{L_f}{\sqrt{A_s A_v}} \right) \quad (\text{A2.14})$$

where

$t$  = fire severity (s)

$A_s$  = total surface area of enclosure interior excluding vent area ( $\text{m}^2$ )

$A_v$  = vent area ( $\text{m}^2$ )

$L_f$  = total enclosure fire load (equivalent weight of wood) (kg)

### A2.2.11 Smoke production rate

The rate at which smoke is produced during a fire is nearly equal to the rate air is entrained into the rising fire plume, so that the mass production rate of smoke can be estimated as equal to the mass flow rate of gas in the fire plume according to [6]:

$$\dot{m}_s = 0.18 \dot{Q}^{1/3} \rho_\infty^{2/3} c_p^{-1/3} T_\infty^{-1/3} g^{1/3} Y^{5/3} \quad (\text{A2.15})$$

where

$\dot{m}_s$  = rate of smoke production ( $\text{kg/s}$ )

$\dot{Q}$  = total heat release rate ( $\text{kW}$ )

$\rho_\infty$  = density of air ( $\text{kg/m}^3$ )

$c_p$  = specific heat capacity of air at constant pressure [ $(\text{kJ/kg})/\text{K}$ ]

$T_\infty$  = ambient gas temperature (K)

$g$  = acceleration of gravity ( $\text{m/s}^2$ )

$Y$  = distance from the virtual point source for the fire to bottom of smoke layer (m)

### A2.2.12 Enclosure smoke filling

The rate at which smoke produced from a fire will fill an enclosure depends on the smoke production rate and the size and locations of vents. For an enclosure vented in the lower layer, the upper layer descends with a velocity estimated as [6]:

$$U_l = \frac{\dot{m}_s}{\rho_l A_p} \quad (\text{A2.16})$$

where

$U_l$  = rate of layer descent ( $\text{m/s}$ )



$\dot{m}_s$  = mass rate of smoke production (kg/s)

$\rho_l$  = density of smoke layer (kg/m<sup>3</sup>)

$A_p$  = enclosure floor area (m<sup>2</sup>)

### A2.2.13 Flame spread in forests

Flame spread in forests can be affected by many parameters such as the fuel type and configuration, terrain, wind conditions and humidity. The rate of flame spread in forests will depend on only the radiative heat transfer but also on the convective heating induced by the wind or the slope of the terrain. Wind currents can transport large embers from the initial location of the fire at great distances, enhancing this way the flame spread. A comparison of fire spread rate for urban and wildland fires as a function of wind speed is presented in Figure A2.4. An approximate formula applicable to wildland fires is given by Thomas [12]:

$$V \rho_b = k(1 + V_\infty) \quad (\text{A2.17})$$

where

$\rho_b$  = bulk density of the fuel (kg/m<sup>3</sup>)

$V$  = wind speed (m/s)

$k = 0.07$  for wildland fires (kg/m<sup>3</sup>)

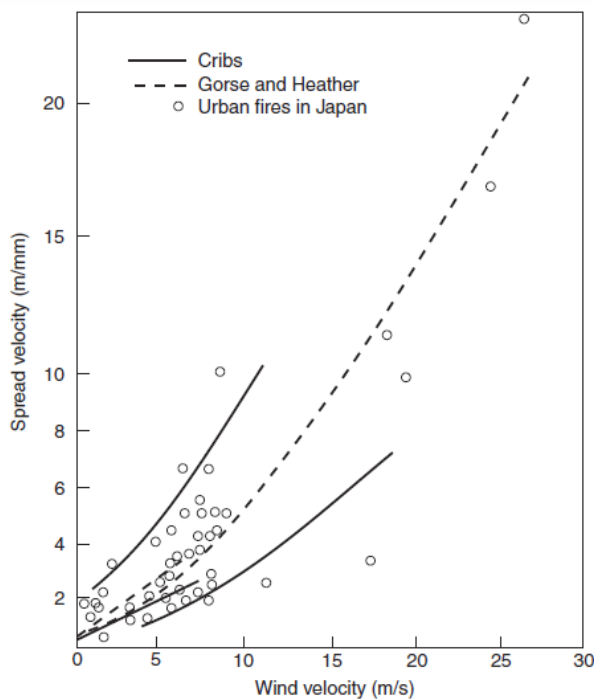


**Figure A2.4** Comparison of rates of fire spread for urban and wildland fires as a function of wind speed [12].

### A2.3 Pollutant dispersion modelling

#### A2.3.1 Introduction

Many models already exist in literature focusing on modelling the process of air pollution dispersion such as, e.g., box model, Gaussian model, lagrangian model, Eulerian model, dense gas model, etc. A great amount of CFD codes exist with which atmospheric pollutant dispersion can be studied and simulated for a wide variety of scenarios. A detailed presentation of each

method and model is not feasible in the present report; however, an overview of the main atmospheric dispersion models can be found in [13].

### A2.3.2 Simple approach

Regarding toxicity dispersion, a dose-response relationship is a simple approach to relate the lethality to the dose received at a point. The dose is simply calculated as the product of concentration by time, assuming that the concentration remains constant over time, and is expressed as:

$$A = C^n t \quad (\text{A2. 18})$$

where  $A$  is the relevant dose,  $C$  is the concentration,  $n$  is an exponent and  $t$  is the time. Two values of  $A$  are used [14]:

- SLOT (Specified Level of Toxicity): the dose that results in highly susceptible people being killed and in a great amount of people exposed to require medical attention.
- SLOD (Significant Likelihood of Death): the dose that typically results in 50 % fatality of an exposed population.

Typical values of the SLOT and SLOD for different substances are given in Table A2.5.

**Table A2.5 SLOT and SLOD values (in ppm) for different substances.**

Concentration	SLOT	SLOD	n
Ammonia	$3.78 \times 10^8$	$1.09 \times 10^9$	2
Carbon monoxide	40125	57000	1
Chlorine	$1.08 \times 10^5$	$4.84 \times 10^5$	2
Hydrogen sulphide	$2.0 \times 10^{12}$	$1.5 \times 10^{13}$	4
Sulphur dioxide	$4.66 \times 10^6$	$7.45 \times 10^7$	2
Hydrogen fluoride	12000	41000	1
Oxides of nitrogen	96000	$6.24 \times 10^5$	2

### A2.3.3 Gaussian dispersion model

One of the most commonly used approaches in modelling the pollutant dispersion in the atmosphere, the Gaussian dispersion model [15 - 17], is presented in this section. The model assumes that the air pollution has a Gaussian distribution, meaning that the pollutant distribution has a normal probability distribution. A graphic representation of the Gaussian air pollutant dispersion plume is presented in Figure A2.5 while the equations that estimate the plume contamination concentrations for different cases are given in Table A2.6.



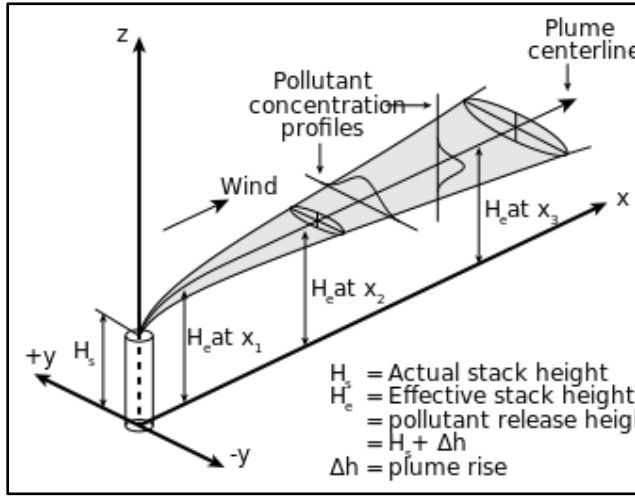


**Figure A2.5 Visualization of the Gaussian air pollutant dispersion plume.**

**Table A2.6 Gaussian plume dispersion model**

Concentration	Applicability
$C(x, y, z) = \frac{Q}{2\pi u \sigma_y \sigma_z} e^{-\frac{y^2}{2\sigma_y^2}} \left( e^{-\frac{(z+H)^2}{2\sigma_z^2}} + e^{-\frac{(z-H)^2}{2\sigma_z^2}} \right)$	Plume contamination concentration at a point in space
$C(x, y, 0) = \frac{Q}{\pi u \sigma_y \sigma_z} e^{-\frac{y^2}{2\sigma_y^2}} e^{-\frac{H^2}{2\sigma_z^2}}$	Plume contaminant concentration at ground level
$C(x, y, 0) = \frac{Q}{\pi u \sigma_y \sigma_z} e^{-\frac{H^2}{2\sigma_z^2}}$	Contaminant concentration at ground level along the plume centerline
$C(x, y, 0) = \frac{Q}{\pi u \sigma_y \sigma_z}$	Contaminant concentration at ground level along the plume centerline when the emission source is at ground level

where

$C$  = Downwind concentration ( $\text{g}/\text{m}^3$ )

$Q$  = Pollution source emission rate ( $\text{g}/\text{s}$ )

$u$  = Average wind speed (m)

$\sigma_y$  = y direction (horizontal) plume standard deviation (m)

$\sigma_z$  = z direction (vertical) plume standard deviation (m)

$x$  = Position in the x direction or downwind direction (m)

$y$  = Position in the y direction (m)

$z$  = Position in the z direction (m)

$H$  = Effective stack height (m)

However, the derivation of the Gaussian dispersion model is based on several assumptions that should be considered before it is applied to study a specific scenario and are presented below.

#### Assumptions of the Gaussian dispersion model:

1. The emission rate is constant.
2. Dispersion (diffusion) is negligible in the downwind (x) direction.
3. Horizontal meteorological conditions are homogeneous over the space being modelled.  
For each hour modelled:



- An average wind speed is used
  - Wind direction is constant
  - Temperature is constant
  - Atmosphere stability class is constant
  - Mixing height is constant
4. No wind shear in the horizontal or vertical direction.
  5. Plume is infinite with no plume history (each hour being modelled is independent of the previous hour)
  6. The pollutants are non-reactive gases or aerosols that remain suspended in the air following the turbulent movement of the atmosphere.
  7. The plume is reflected at the surface with no deposition or reaction with the surface.
  8. The dispersion in the crosswind (y direction) and vertical (z direction) take the form of Gaussian distributions about the plume centreline.

The horizontal ( $\sigma_y$ ) and vertical ( $\sigma_z$ ) standard deviations, commonly called diffusion coefficients, vary depending on the height above the surface, the surface roughness, sampling time, wind speed and distance downwind from the source. The values of the diffusion coefficients are typically determined based on the stability of the atmosphere that has been divided into six distinct classes presented in Table A2.7.

**Table A2.7 Atmosphere stability classes**

Stability description	Stability class
Extremely unstable	A
Moderately unstable	B
Slightly unstable	C
Neutral conditions	D
Slightly stable	E
Moderately stable	F

Simple methods have been developed to determine the atmospheric stability class based on the given wind speed and insolation in the day or cloud cover at night. An overview of the determination of the stability class based on such information is presented in Table A2.8 and Table A2.9.

**Table A2.8 Atmosphere stability classes**

Sky cover	Solar elevation Angle>60 degrees	Solar elevation Angle>35 degrees ≤60 degrees	Solar elevation Angle>15 degrees ≤35 degrees
	strong	moderate	slight
4/8 or less or High thin clouds			
5/8 to 7/8 middle clouds *	moderate	slight	slight
5/8 to 7/8 low clouds **	slight	slight	slight

\* middle clouds – base at 2000 to 5000 m, \*\* low clouds – base less than 2000 m



**Table A2.9 Atmosphere stability classes**

Surface wind speed (m/s)	Daytime insolation			Nighttime	
	strong	moderate	slight	Thin overcast or >4/8 low cloud cover	<3/8 cloud cover
<2	A	A-B	B	-	-
2-3	A-B	B	C	E	F
3-5	B	B-C	C	D	E
5-6	C	C-D	D	D	D
>6	C	D	D	D	D

Neutral class (D) is assumed for all overcast conditions during day or night.

The diffusion coefficients,  $\sigma_y$  and  $\sigma_z$ , are based on the atmospheric stability classes and can be obtained from Figure A2.6 and Figure A2.7, respectively.

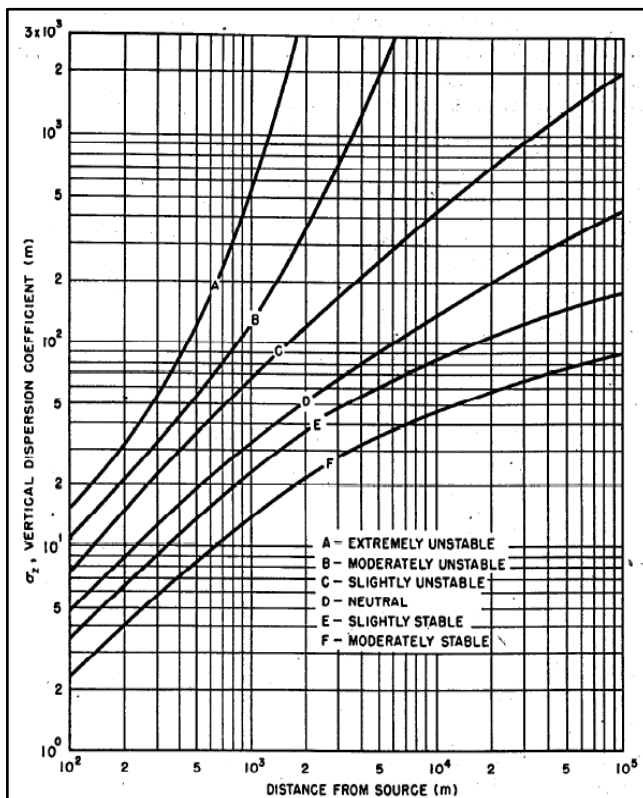


**Figure A2.6** Vertical diffusion  $\sigma_z$  coefficient vs downwind distance from the source. Figure reproduced from [16].

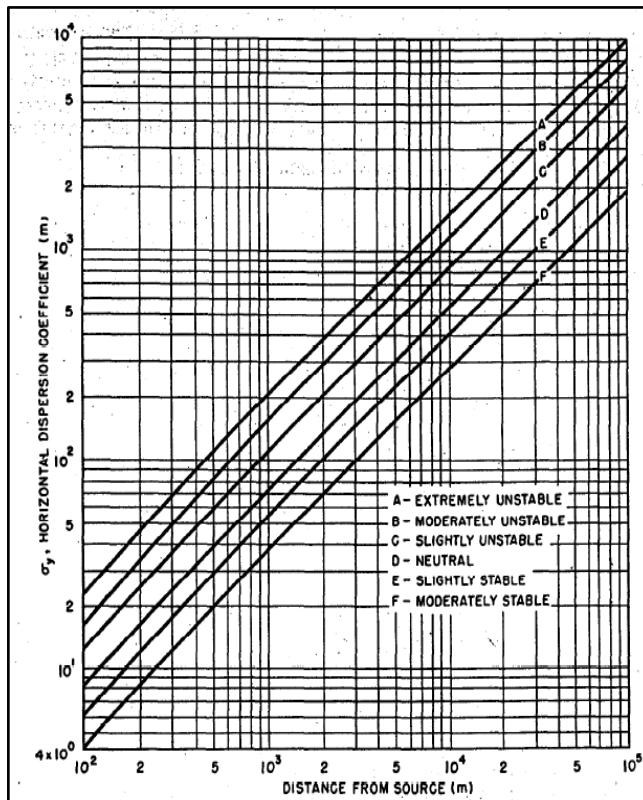


**Figure A2.7**Lateral diffusion  $\sigma_y$  coefficient vs downwind distance from the source. Figure reproduced from [16].

In order to evaluate the contaminant concentration with the Gaussian dispersion model the height of the plume rise is also needed. The most comprehensive and widely used approach is that developed by Briggs, based on theoretical relationships and empirical data derived from measurements of plume rise, presented in Table A2.10.

**Table A2.10 Plume rise estimation**

	Stable atmosphere	Neutral/Unstable atmosphere
Buoyancy dominated	$\Delta h(x) = 1.6F^{1/3}x^{2/3}u^{-1}$ or $\Delta h_{\max} = 2.6(F/u s)^{1/3}$ where $s = 0.02g/T_A \text{ for E stability}$ $s = 0.035g/T_A \text{ for F stability}$	$\Delta h(x) = 1.6F^{1/3}x^{2/3}u^{-1}$ for $x < 3.5x^*$ or $\Delta h_{\max} = 1.6F^{1/3}(3.5x^*)^{2/3}u^{-1}$ for $x > 3.5x^*$ where $x^* = 14F^{5/8} \text{ if } F < 55$ $x^* = 34F^{2/5} \text{ if } F > 55$
Momentum dominated	$\Delta h_{\max} = 1.6(vR)^{2/3}u^{-1/3}s^{-1/6}$ where s is defined as above	$\Delta h(x) = 3.78 \left( \frac{v^2}{u(v+3u)} \right)^{2/3} \left( \frac{xR^2}{2} \right)^{1/3}$ or $\Delta h_{\max} = 3 \frac{vD}{u}$

where



$$F = gvR^2 \frac{(T - T_A)}{T}$$

$T$  = source temperature (K)

$T_A$  = source temperature (K)

$v$  = stack exit velocity (m/s)

$R$  = stack radius (m)

$D$  = stack diameter (m)

$X$  = downwind distance (m)

$u$  = wind speed at physical source height (m/s)

$g$  = acceleration due to gravity (9.8 m/s<sup>2</sup>)

$\Delta h$  = plume rise (m)

$\Delta h_{max}$  = final plume rise (m)

## A2.4 Explosion modelling

### A2.4.1 Introduction

For modelling gas explosions there are typically three types of models of varying complexity that can be applied:

- *Empirical models*: Derived based on correlations obtained from experimental data. Examples of such models are the TNT equivalency method, the TNO method, the multi-energy concept, the Baker-Strehlow method, the Congestion Assessment Method (CAM) and the Sedwick loss assessment method.
- *Phenomenological models*: Simplified physical models that only represent the essential physics of explosions. With these models the actual scenario geometry is not modelled. Rather, it is represented by an idealized system. Examples of such models are the Shell Code for Over-pressure Prediction in gas Explosions (SCOPE) and the Confined LInked CHamber Explosion (CLICHE) code.
- *CFD models*: Models that solve partial differential equations governing the explosion processes. Examples of such codes include the EXSIM, FLACS, AutoReaGas, CFX, COBRA, NEWT, REACFLOW.

Each of the above mentioned approaches have different levels of accuracy of the output results that they provide and a varying complexity in their use. They also have their strengths and weaknesses and they should be applied in studies of gas explosions with caution always considering their limitations but also their degree of applicability. A detailed presentation of each model and CFD code related to gas explosions would not be feasible in the present report due to the vast amount of information available. However, the reader is directed to [18] for a very comprehensive overview of these models.

### A2.4.2 Damage probability by an explosion

Simple approaches to assess the damage to equipment caused by explosions exist in literature. A damage probability function based on the distance from the center of the explosion has been proposed [19]:

$$F_d = \left(1 - \frac{r}{r_{th}}\right)^2 \quad (\text{A2.19})$$



where  $F_d$  is the damage probability,  $r$  (m) is the distance from the explosion center and  $r_{th}$  (m) is the distance from the explosion center at which a threshold value of static overpressure is reached (36 kPa).

Another simplified model relating the equipment damage to the peak static overpressure has also been proposed [4]:

$$Y = a + b \times \ln(P^0) \quad (\text{A2. 20})$$

where  $Y$  is a probit function for equipment damage,  $P^0$  (Pa) is the peak static overpressure,  $a$  and  $b$  are the probit coefficients ( $a=-23.8$  and  $b=2.92$ ). Different sets of coefficients  $a$  and  $b$  have also been proposed considering the various categories of industrial equipment presented in Table A2.11:

**Table A2.11 Probit coefficients for different equipment categories [21].**

Equipment category	<i>a</i>	<i>b</i>	Threshold
Atmospheric vessels	-18.96	+2.44	22 kPa
Pressurized vessels	-42.44	+4.33	16 kPa
Elongated equipment	-28.07	+3.16	31 kPa
Small equipment	-17.79	+2.18	37 kPa

Apart from the above-mentioned models, different probit models exist in literature. An overview of such models along with a study on the validity of the probit models in scenarios involving cascading effects in chemical process equipment cause by overpressure can be found in [22].

#### A2.4.3 Peak overpressure in an explosion

The peak overpressure in an explosion can be calculated as [23]:

$$P^0(r) = \frac{1616 \left[ 1 + \left( \frac{z_e}{4.5} \right)^2 \right]}{\sqrt{1 + \left( \frac{z_e}{0.048} \right)^2} \cdot \sqrt{1 + \left( \frac{z_e}{0.32} \right)^2} \cdot \sqrt{1 + \left( \frac{z_e}{1.35} \right)^2}} \quad (\text{A2. 21})$$

where  $P^0(r)$  (kPa) is the peak overpressure and  $z_e$  (m/kg<sup>1/3</sup>) is a scaled distance. The scaled distance,  $z_e$ , is approximated as:

$$z_e = \frac{r}{m_{TNT}^{1/3}} \quad (\text{A2. 22})$$

where  $r$  is the distance from the center of the explosion and  $m_{TNT}$  (kg) is the equivalent mass of TNT. The scaled distance,  $z_e$ , can also be estimated by setting the threshold values of peak overpressure for the different equipment categories, previously presented in Table A2.10.

In accidents involving explosions,  $m_{TNT}$ , is used to evaluate the potential damage of a given fuel assuming that an exploding fuel mass behaves like an exploding TNT on equivalent energy basis. The equivalent mass of TNT can then be estimated as [24]:

$$m_{TNT} = \frac{\mu m \Delta H_c}{E_{TNT}} \quad (\text{A2. 23})$$



where  $\mu$  is the explosion efficiency (0.01 to 0.1),  $m$  (kg) is the mass of fuel involved in the explosion,  $\Delta H_c$  (MJ/kg) is the energy of explosion of the gas and  $E_{TNT}$  (MJ/kg) is the energy of explosion of TNT.

A peak overpressure of approximately 70 kPa is reported [23,25-26] to be enough to cause severe damage to process equipment and to trigger new events (cascading effects), either related to new explosions or new events involving fires. A list of the various effects caused by overpressure is given in Table A2.12.

**Table A2.12 Various effects of overpressure (Source: AIChE/CCPS, Guideline for chemical process quantitative risk analysis).**

Pressure (kPa)	Damage
0.14	Annoying noise (137 dB)
0.28	Loud noise (143 dB)
0.69	Breakage of small windows under strain
1.03	Typical pressure for glass breakage
3.4-6.9	Large and small window usually shattered; occasional damage to window frames.
4.8	Minor damage to house structure
6.9	Partial demolition of houses
9.0	Steel frame slightly distorted
13.8	Partial collapse of walls and roofs of house
17.2	50% destruction of brickwork of house
34.5	Damage to wooden poles
34.5-48.2	Complete destruction of houses
48.2	Loaded train wagon overturned
62.0	Loaded train boxes completely demolished
68.7	Total destruction of building, heavy machine tool, etc.

#### A2.4.4 BLEVEs

If a substance involved in a BLEVE is flammable, it is likely that the resulting cloud of the substance will ignite after the explosion has occurred, forming a fireball. Empirical correlations for the maximum diameter of the fireball,  $D_{max}$ , the duration of the BLEVE,  $t_{BLEVE}$ , and the distance between the fireball center and the ground,  $H_{BLEVE}$ , have been developed [27]:

$$D_{max} = 5.8M^{1/3} \quad (\text{A2. 24})$$

$$t_{BLEVE} = 2.6M^{1/6} \quad (\text{A2. 25})$$

$$H_{BLEVE} = 0.75D_{max} \quad (\text{A2. 26})$$

where  $M$  (kg) is the initial mass of the flammable material.

Fragments during a BLEVE explosion are usually not evenly distributed; the vessel's axial direction receives more fragments than the side directions. The total number of fragments is approximately a fraction of the vessel size and can be approximated as [28]:

$$N = -3.77 + 0.0096V \quad (\text{A2. 27})$$

where  $N$  is the number of fragments and  $V$  ( $\text{m}^3$ ) is the vessel capacity. It's important to note that this correlation is valid for vessel volumes of 700-2500  $\text{m}^3$ .

For pressurized vessels, the initial velocity of a fragment can be estimated as [29]:



$$u = 3.356 \sqrt{\frac{PD^3}{W}} \quad (\text{A2. 28})$$

where  $u$  (m/s) is the initial velocity of the fragment,  $P$  (Pa) the rapture pressure of the vessel,  $D$  (m) the fragment diameter and  $W$  (kg) the weight of the fragment.

The maximum distance a fragment will travel (at 45° angle) can be calculated as [30]:

$$r_{\max} = \frac{u^2}{g} \quad (\text{A2. 29})$$

where  $g$  is the gravitational acceleration ( $g = 9.81 \text{ m/s}^2$ ).

## A2.5 Verification of correlations

The experimental correlations reported in literature can be further verified by the use of CFD modelling. This way not only any uncertainties related to the derivation of such correlations are dismissed but then it is also validated that the results obtained with the numerical simulations are reliable. An example of such validation is given in Figures A2.8-A2.9, presenting a comparison of the predicted flame heights and centerline plume temperatures predicted by different CFD codes (FDS and FireFOAM) and the results obtained from some of the previously presented experimental correlations. The validation test case consists of 1 m in diameter CH<sub>4</sub> fire plumes of different heat release rate (1.59-2.61 MW). It can be seen that the numerical results agree very well with both the experimental data and the correlations available, proving that the use of CFD can be, if properly designed and performed, a reliable tool for modelling the physics.

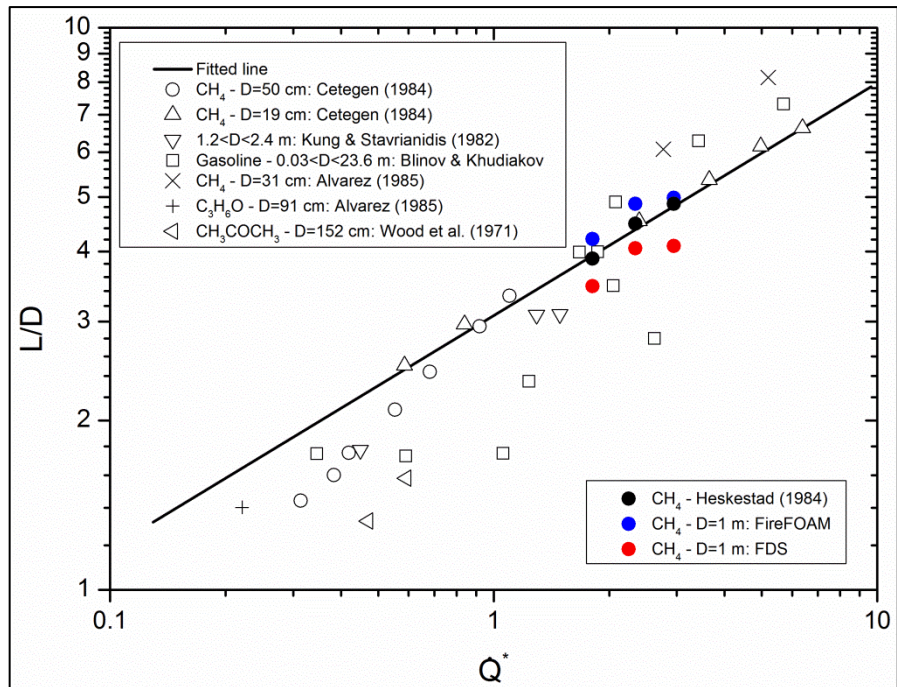
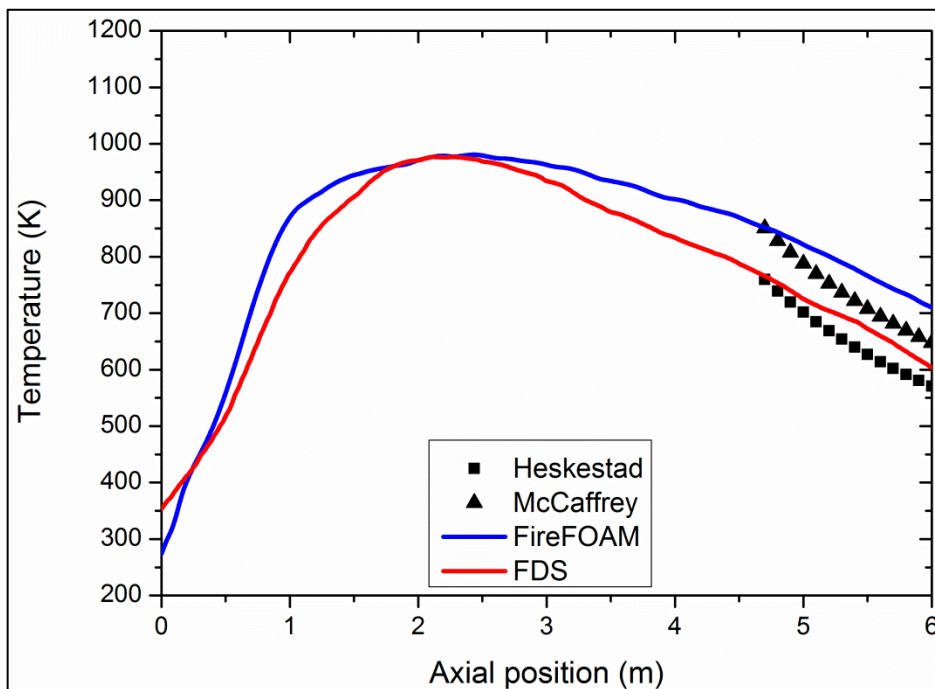


Figure A2.8 Comparison of the average flame heights predicted by CFD codes, experimental data and correlations.



**Figure A2.9 Comparison of the average centreline plume temperatures predicted by CFD codes and experimental correlations.**

## A2.6 References

- [1] SFPE Handbook of Fire Protection Engineering, 4th edition, National Fire Protection Association, Quincy, MA, 2008.
- [2] C. J. H. van der Bosch, R. A. P. M. Weterings, Methods for the Calculation of Physical Effects: Due to Releases of Hazardous Materials (liquids and Gases): Yellow Book, Directorate-General for Social Affairs and Employment, Committee for the Prevention of Disasters, 1997.
- [3] E.K. Budnick, D.D. Evans, H.E. Nelson, NFPA Fire Protection Handbook, Section 11, Chapter 10, National Fire Protection Association, Quincy, MA, 1997.
- [4] G. Heskestad, Virtual origins of fire plumes, *Fire Safety Journal*, 5:109-114 (1983).
- [5] D.G. Heskestad, Luminous heights of turbulent diffusion flames, *Fire Safety J.*, 5:109-114 (1983).
- [6] D. Drysdale, An Introduction to Fire Dynamics, 3rd Edition, John Wiley & Sons, England, 2011.
- [7] V. Cozzani, G. Antonioni, G. Spadoni, Quantitative assessment of domino scenarios by a GIS-based software tool *Journal of Loss Prevention in the Process Industries*, 19:463-477 (2006).
- [8] G. Landucci, G. Gubinelli, G. Antonioni, V. Cozzani, The assessment of the damage probability of storage tanks in domino events triggered by fire *Accident Analysis and Prevention*, 41:1206-1215 (2009).
- [9] F. Kadri, P. Lallement, E. Chatelet, The Quantitative Risk Assessment of domino effect on Industrial Plants Using Colored Stochastic Petri Nets, in: PSAM11 & ESREL Conference. Presented at the PSAM11 & ESREL Conference, Helsinki, Finland, p. 10, 2012.
- [10] B.J. McCaffrey, J.G. Quintiere, M.F. Harkleroad, Estimating room temperatures and the likelihood of flashover using fire test data correlations, *Fire Technology*, 17:98-119 (1981).

- [11] K.L. Foote, P.J. Pagni, N.J. Alvares, Temperature correlations for forced-ventilated compartment fires, Proceedings of the International Symposium, 1:139-148 (1986).
- [12] P.H. Thomas, Rates of Spread for Some Wind-Driven Fires, Forestry, XLIV, p. 2, 1971.
- [13] New Zealand Ministry for the Environment, Good Practice Guide for Atmospheric Dispersion Modelling. Ministry for the Environment, ME 522, ISBN 0-478-18941-9 (2004).
- [14] HSE, Indicative Human Vulnerability to the Hazardous Agents Present Offshore for Application in Risk Assessment Of Major Accidents, SPC/Tech/OSD/30, 2006.
- [15] P.A. Vesilind, J.J. Peirce, R.F. Weiner, Environmental Engineering, Butterworth Heinemann, 3rd edition, 1994.
- [16] [http://www.utexas.edu/research/ceer/che357/PDF/Lectures/gaussian\\_plume\\_modeling.pdf](http://www.utexas.edu/research/ceer/che357/PDF/Lectures/gaussian_plume_modeling.pdf)
- [17] D.B. Turner, Workbook of atmospheric dispersion estimates: an introduction to dispersion modeling (2nd Edition ed.), CRC Press, 1994.
- [18] C.J. Lea, H.S. Ledin, A Review of the State-of-the-Art in Gas Explosion Modelling, Health and Safety Laboratory Report HSL/2002/02, Fire and Explosion Group, Buxton, UK, 2002.
- [19] D.F. Bagster, R.M. Pitblado, The estimation of domino incident frequencies – an approach, Process Safety and Environment Protection, 69:195-199 (1991).
- [20] N.A. Eisenberg, C.J. Lynch, R.J. Breeding, Vulnerability Model: A Simulation System for Assessing Damage Resulting from Marine Spills, Report CG-D-136-75, Enviro Control Inc., Rockville, MD, 1975.
- [21] V. Cozzani, E. Salzano, The quantitative assessment of domino effects caused by overpressure Part I. Probit models Journal of Hazardous Materials, A107, 67-80 (2004).
- [22] D. Sun, G. Huang, J. Jiang, M. Zhang, Z. Wang, Study on the Rationality and Validity of Probit Models of Domino Effect to Chemical Process Equipment caused by Overpressure, Journal of Physics, 423:012002 (2013).
- [23] F. Kadri, E. Chatelet, P. Lallement, The Assessment of Risk Caused By Fire and Explosion in Chemical Process Industry: A Domino Effect-Based Study, Journal of Risk Analysis and Crisis Response, 3:66-76 (2013).
- [24] A.C. Daniel, J.F. Louvard, Chemical Process Safety: Fundamentals with Applications, Prentice Hall International Series in the Physical and Chemical Engineering Sciences, 2002.
- [25] F.I. Khan, S.A. Abbasi, An assessment of the likelihood of occurrence, and the damage potential of domino effect (chain of accidents) in a typical cluster of industries, Journal of Loss Prevention in the Process Industries, 14:283-306 (2001).
- [26] F.I. Khan, S.A. Abbasi, Estimation of probabilities and likely consequences of a chain of accidents (domino effect) in Manali Industrial Complex, Journal of Cleaner Production, 9:493-508 (2001).
- [27] AIChE/CCPS, Guideline for evaluating the characteristics of vapour cloud explosions, flash fire and BLEVE, New York, 1994.
- [28] T. Abbasi, S.A. Abbasi, The boiling liquid expanding vapor explosion (BLEVE): mechanism , consequence assessment, management, J. Haz. Mater., 141:489-519 (2007).
- [29] C.V. Moore, The design of barricades for hazardous pressure systems, Nuclear Engineering Design, 5:1550-1566 (1967).
- [30] M.R. Baum, J. Pressure Vessel Technology, 168-176 (1988).

